

AD-A165 688

CUMULATIVE DAMAGE MODEL FOR ADVANCED COMPOSITE  
MATERIALS(U) GENERAL DYNAMICS FORT WORTH TX FORT WORTH  
DIV H R MILLER ET AL. JUN 85 AFWAL-TR-85-4869

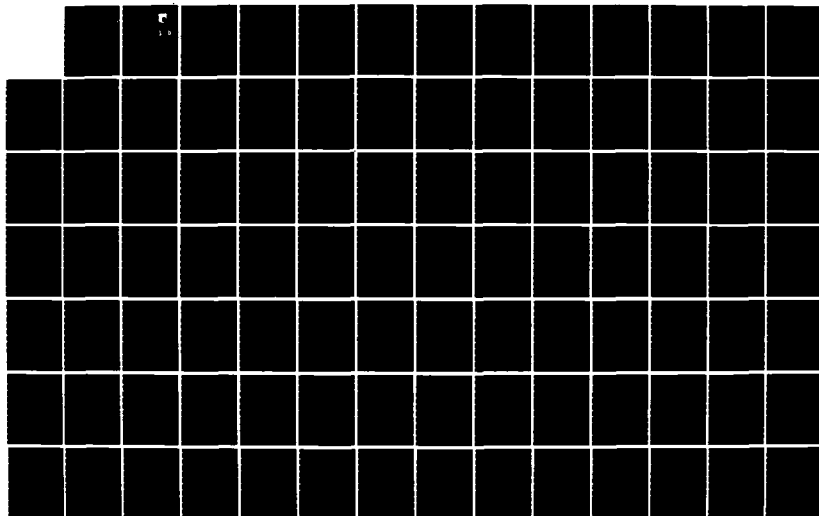
1/2

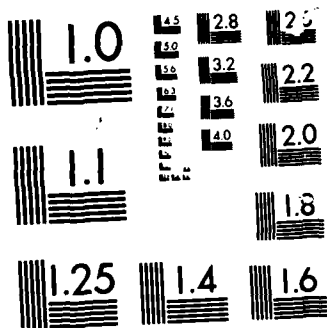
UNCLASSIFIED

F33615-81-C-5049

F/G 11/4

NL



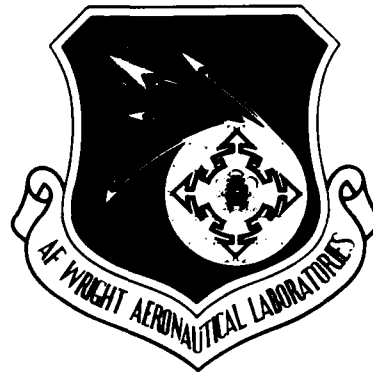


MICROCOPY RESOLUTION TEST CHART  
10X

12

AFWAL-TR-85-4069

CUMULATIVE DAMAGE MODEL FOR  
ADVANCED COMPOSITE MATERIALS



GENERAL DYNAMICS  
FORT WORTH DIVISION  
P.O. BOX 748  
FORT WORTH, TEXAS 76101

DTIC  
ELECTE  
MAR 20 1986  
S D

June 1985

Final Report for Period October 1983 - January 1985

Approved for public release; distribution unlimited.

DTIC FILE COPY

MATERIALS LABORATORY  
AIR FORCE WRIGHT AERONAUTICAL LABORATORIES  
AIR FORCE SYSTEMS COMMAND  
WRIGHT-PATTERSON AIR FORCE BASE, OHIO 45433

AD-A165 688

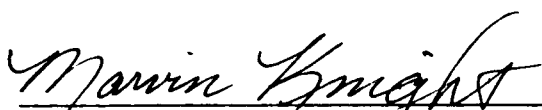
86 3 20 007

## NOTICE

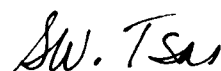
When Government drawings, specifications, or other data are used for any purpose other than in connection with a definitely related Government procurement operation, the United States Government thereby incurs no responsibility nor any obligation whatsoever; and the fact that the Government may have formulated, furnished, or in any way supplied the said drawings, specifications, or other data, is not to be regarded by implication or otherwise as in any manner licensing the holder or any other person or corporation, or conveying any rights or permission to manufacture, use, or sell any patented invention that may in any way be related thereto.

This report has been reviewed by the Office of Public Affairs (ASD/PA) and is releasable to the National Technical Information Service (NTIS). At NTIS, it will be available to the general public, including foreign nations.

This technical report has been reviewed and is approved for publication.



MARVIN KNIGHT, Project Engineer  
Mechanics & Surface Interactions Br  
Nonmetallic Materials Division



STEPHEN W. TSAI, Chief  
Mechanics & Surface Interactions Br  
Nonmetallic Materials Division

FOR THE COMMANDER



ROBERT L. RAPSON, Actg Chief  
Nonmetallic Materials Division

"If your address has changed, if you wish to be removed from our mailing list, or if the addressee is no longer employed by your organization please notify AFWAL/MLBM, W-PAFB, Ohio 45433 to help us maintain a current mailing list.

Copies of this report should not be returned unless return is required by security considerations, contractual obligations, or notice on a specific document.

Unclassified

SECURITY CLASSIFICATION OF THIS PAGE

AD-A165688

## REPORT DOCUMENTATION PAGE

1a. REPORT SECURITY CLASSIFICATION Unclassified			1b. RESTRICTIVE MARKINGS		
2a. SECURITY CLASSIFICATION AUTHORITY			3. DISTRIBUTION/AVAILABILITY OF REPORT Approved for public release; distribution unlimited.		
2b. DECLASSIFICATION/DOWNGRADING SCHEDULE					
4. PERFORMING ORGANIZATION REPORT NUMBER(S)			5. MONITORING ORGANIZATION REPORT NUMBER(S) AFWAL-TR-85-4069		
6a. NAME OF PERFORMING ORGANIZATION General Dynamics Corporation		6b. OFFICE SYMBOL (If applicable) N/A		7a. NAME OF MONITORING ORGANIZATION Materials Laboratory Mechanics & Surface Interactions Branch	
6c. ADDRESS (City, State and ZIP Code) Fort Worth Division Fort Worth, TX 76101		7b. ADDRESS (City, State and ZIP Code) AFWAL/MLBM WPAFB, OH 45433			
8a. NAME OF FUNDING/SPONSORING ORGANIZATION AFWAL/MLBM		8b. OFFICE SYMBOL (If applicable)		9. PROCUREMENT INSTRUMENT IDENTIFICATION NUMBER F33615-81-C-5049	
8c. ADDRESS (City, State and ZIP Code)		10. SOURCE OF FUNDING NOS.			
		PROGRAM ELEMENT NO.		PROJECT NO.	TASK NO.
		62102F		2419	03
11. TITLE (Include Security Classification) Cumulative Damage Model for Advanced Composite Materials		WORK UNIT NO. 27			
12. PERSONAL AUTHOR(S) H. R. Miller, K. L. Reifsnider, W. W. Stinchcomb, D. A. Ulman, R. D. Bruner					
13a. TYPE OF REPORT Final		13b. TIME COVERED FROM Oct '83 TO Jan '85		14. DATE OF REPORT (Yr., Mo., Day) June 1985	
				15. PAGE COUNT 168	
16. SUPPLEMENTARY NOTATION <i>... for ...</i>					
17. COSATI CODES			18. SUBJECT TERMS (Continue on reverse if necessary and identify by block number)		
FIELD	GROUP	SUB. GR.	Cumulative Damage, composite materials, stacking sequence, fatigue testing, multiple load histories, <del>MOE</del> , stiffness change, residual strength, <del>models</del> , property degradation		
11	04				
19. ABSTRACT (Continue on reverse if necessary and identify by block number) This report details the model verification activity of Phase III of this program and summarizes the modeling effort conducted over the entire program duration. In the Phase III effort, the model was used to predict the specimen response using four previously unstudied parameter variations. The variations consisted of introduction of a different specimen width than that used in Phase I and II, a new stacking sequence, new loading conditions applied to previously studied stacking sequence, and a different material system (T300/V378A as opposed to AS/3501 used throughout Phases I and II). In each case the model predictions were obtained prior to the specimen testing; in fact, the model was used to determine the load conditions used in the test program. In all cases, predicted lifetimes were within the same decade--indicating good agreement between the theory and experiment for fatigue analysis. <div style="text-align: right;">(Continued)</div>					
20. DISTRIBUTION/AVAILABILITY OF ABSTRACT UNCLASSIFIED/UNLIMITED <input checked="" type="checkbox"/> SAME AS RPT <input type="checkbox"/> DTIC USERS <input type="checkbox"/>			21. ABSTRACT SECURITY CLASSIFICATION Unclassified		
22a. NAME OF RESPONSIBLE INDIVIDUAL M. Knight			22b. TELEPHONE NUMBER (Include Area Code) (513) 255-7131		22c. OFFICE SYMBOL AFWAL/MLBM

Unclassified

SECURITY CLASSIFICATION OF THIS PAGE

19. ABSTRACT (Continued)

- Also discussed are the methodologies associated with applying the model in tension-tension, tension-compression, compression-compression, and mixed block loading situations. Sensitivity of the model to various parameters in these loading conditions is demonstrated.

Ko. 1. 1. 1.

FLD 18

Unclassified

SECURITY CLASSIFICATION OF THIS PAGE

## FOREWORD

The Cumulative Damage Model for Advanced Composite Materials program (F33615-81-C-5049) is sponsored by the Air Force Wright Aeronautical Laboratories, Materials Laboratory, Air Force Systems Command, Wright-Patterson Air Force Base, Ohio, 45433. Marvin Knight of AFWAL/MLBM is the Air Force Project Engineer.

The program has been performed jointly by the Structures and Design Department of General Dynamics, Fort Worth Division, and by the Materials Response Group at Virginia Polytechnic and State University. Harry R. Miller of the Composite Material and Process Engineering group is the General Dynamics Program Manager. Drs. K. L. Reifsnider, W. W. Stinchcomb, and E. G. Henneke are the principal investigators at VPI & SU.

Acknowledged for their contributions to this program are R. D. Bruner of the Composite Material and Process Engineering group, D. A. Ulman of the Fracture and Fatigue group, J. H. Fruit of the Materials and Processes Laboratory, and VPI research assistants R. Simonds and R. Schultz.

Accession For	
NTIS CRA&I	<input checked="checked" type="checkbox"/>
DTIC TAB	<input type="checkbox"/>
Unannounced	<input type="checkbox"/>
Justification	
By	
Distribution /	
Availability Codes	
Dist	Availability and/or Special
A-1	

## TABLE OF CONTENTS

<u>Section</u>	<u>Title</u>	<u>Page</u>
I	INTRODUCTION	1
II	CUMULATIVE DAMAGE MODEL AND IMPLEMENTATION	5
	1. MODEL CONCEPTS	5
	2. TENSION DOMINATED FAILURE	28
	3. COMPRESSION FAILURE	72
III	PHASE III PREDICTIONS AND RESULTS	113
	1. PREDICTIONS AND RESULTS	113
IV	SUMMARY AND CONCLUSIONS	143
	1. EXERIMENTAL PROCEDURES FOR CUMULATIVE DAMAGE MODEL INPUT	143
	A. SPECIMEN DESCRIPTION	144
	B. NONDESTRUCTIVE TEST TECHNIQUES	144
	C. TEST PROCEDURES	149
	1. MONOTONIC TENSION AND COMPRESSION	149
	2. QUASI-STATIC TENSION AND COMPRESSION	149
	3. FATIGUE TESTING	150
	2. CLOSURE	152
	REFERENCES	157



## LIST OF ILLUSTRATIONS

<u>No.</u>	<u>Title</u>	<u>Page</u>
1	Conceptual Flow Chart of "Critical Element Model"	8
2	Computational Flow Chart for Critical Element Model	12
3	Schematic Diagram of Laminate Strength Reduction-Life Relationship	14
4	Schematic Diagram of Critical Element Strength-Life Relationship	16
5	Schematic Diagram of Critical Element Strength-Life Relationship for Three-Dimensional Formulation	19
6	Damage Modes During Fatigue Loading of Composite Laminate	20
7	Longitudinal Young's Modulus Reduction for a [0/45/-45/0] <sub>s</sub> Graphite Epoxy Laminate Cycled at 0.85 of the Static Ultimate Strength, and a [0/90] <sub>s</sub> Glass Epoxy Specimen Cycled at 0.6 of the Static Ultimate Strength	22
8	Schematic Diagram of Regions of Damage Development for Composite Laminates	23
9	An Example of the Interpretation of Terms in the Summation Equation for Tension-Tension Constant Amplitude Loading	25
10	Crack Spacing in the -45 Ply of [0/90/45/-45] <sub>s</sub> Graphite Epoxy Laminates Under Cyclic and Quasi-Static Loading	32
11	Residual Strength and Life Predictions for Uncorrected Model, Showing Effects of Stress Redistribution	42
12	Predictions and Observations for Model in which $F_L$ , the Local Failure Function, Was Set Equal to the Ratio of Applied Stress to Undamaged Strength	44
13	Semi-log Plot of the Data in Figure 12 Showing Life Prediction for Specimen F4-6	46

# LIST OF ILLUSTRATIONS (CONTINUED)

<u>No.</u>	<u>Title</u>	<u>Page</u>
14	Predicted and Observed Data for Type F Laminates in T-T Loading for Model with Biaxial Correction	52
15	Illustration of the Influence of Various Model Parameters on Predicted Results	54
16	Curve Fit of Typical Stiffness Change Data for T-T Loading of Type D Specimens	60
17	Estimate of Local 0-Degree Ply Stress for Data in Figure 16	61
18	Predicted Variation of Residual Strength for a Type D Laminate	62
19	Change in Residual Strength for T-T Loading with a Maximum Strain Level of 5000 $\mu\epsilon$	63
20	Schematic of Geometry Used for Shear-lag Analysis in Type D Laminates	65
21	Cases of Crack Growth Analyzed for Type D Damage Analysis	67
22	Crack Face Opening Geometry Predicted from Shear-lag Analysis for a Long Coupled Crack in the Type D Laminate	68
23	Comparison of Calculated Stiffness Change and Change in Local Axial Stress in the 0-Degree Plies for Crack Coupling	69
24	Residual Strength Prediction and Typical Observation for a Shear-lag Refinement of Damage Accumulation Model	71
25	Stiffness Retention Fraction for Several C-C Tests of Type B Specimens	77
26	Summary of Predictions and Observations for C-C Loading of Type B Laminates	79
27	Fractional Stiffness Change Measured During T-C Loading of Type D Laminates	81

# LIST OF ILLUSTRATIONS (CONCLUDED)

<u>No.</u>	<u>Title</u>	<u>Page</u>
28	Summary of Observed and Predicted Data for T-C Loading of Type D Laminates Using Critical Stiffness Model	82
29	Parameter Study of the Power of the Delamination Growth Law	90
30	Predicted and Observed Life Data for T-C Model Which Uses Observed Stiffness Changes	98
31	Stiffness Change During Block Loading of Three Specimens	99
32	Fatigue Life Observations for Five Different R Values	103
33	Residual Strength Predictions for R=-1, Type C Specimen	106
34	Life Predictions and Observations for R=-0.5 Tests	107
35	Predicted and Observed Life for R=-2 Tests	109
36	Predicted and Observed Results for Two Inch Wide Specimens	118
37	Estimated Lives for Block Loading with Reversed Sequences	123
38	Predicted Life for Three Blocks of Widely Different Loading	126
39	Predicted Residual Strength and Life for Tension-Tension Loading Assuming Only Matrix Cracking	130
40	Results for Different Stacking Sequence under T-C Loading	135
41	Predictions and Data for Reversed Loading of Graphite BMI Specimens	139
42	Block Loading Results for Graphite BMI Specimens	141
43	Typical View of Damage State Using Edge Replica	146
44	Typical View of Damage State Using X-Radiography	148

# LIST OF TABLES

<u>No.</u>	<u>Title</u>	<u>Page</u>
1	Example: [0/90/45/-45] <sub>s</sub> T300-5208	35
2	Example: [0/90/45/-45/-45/45/90/0] <sub>3s</sub>	38
3	Stresses in 0-Degree Plies of Type F Laminates During Damage Development	50
4	Type C 7500 $\mu$ e Data	57
5	Results of Block Loading Tests and Predictions	92
6	Results of Block Loading Tests and Predictions	93
7	Summary Results for Variable R Series	110
8	Phase III Test Matrix	114
9	Cumulative Damage Model Phase III Results	117
10	Phase III Block Sequence Estimates	122
11	Lives Predicted Assuming Delamination Dominates E-Stack	131
12	E-Stack Calculations for $\pm 4000 \mu$ e	133
13	Block Loading of E-Stack for Severe Delamination	136

## SECTION I

### INTRODUCTION

The application of advanced composite materials as primary load carrying structures on Air Force weapons systems is increasing. These materials possess unique structural properties, such as high strength, high modulus, and low density, as compared to other material systems. Combined with the ease of manufacturing, they offer opportunities to fabricate low cost and high efficiency structures. However, the quantitative methodology to analytically predict the life of advanced composite laminates from the properties of the lamina and their stacking sequence is somewhat lacking. In the past, prediction of advanced composite materials' performance has been based on a limited understanding of fundamental failure modes and mechanisms.

This program was not intended to be another program to develop statistical , empirical effects of defect, nor strength reduction models. The intent of this program was to establish mechanistic methodologies to address cumulative damage mechanisms to make optimum use of the advanced composite properties in design applications of primary aircraft structures. In particular, the objectives of this program were to (1) develop a cumulative damage model for composite laminates which can be used to predict the strength, stiffness, and life for various load histories, and (2) establish the type of experimental test program that should be conducted in order to determine the parameters in the analytical model.

The program has been conducted in three phases. Phase I

incorporated the tasks of preliminary model development and evaluation. Phase II activity focused on refinement of the models developed in Phase I and on an extension of the data base through conducting tests with various load conditions, histories, and lamination sequences. In Phase III, the models developed and refined in the previous phases have been verified. These models address the effects of the damage modes that occur during either tensile or compressive loading. The mechanics principles on which the model is based provide a fundamental formulation through which refinements can be made as failure mechanisms are better identified. The model is based on stiffness change, a familiar observable which is directly related through continuous internal stress redistributions to residual strength and life. Physical reality is thus modelled with engineering accuracy with no distinction being made between laboratory coupons and structural laminates.

Both the analytical and experimental efforts involved in the Phase I model development and the Phase II models refinement tasks have been documented in the respective Phase Final Reports (References 1 and 2). The work of Phase III provides the proof that the model does accurately predict the effect of cumulative damage on advanced composite materials. This proof is in the form of a comparison between model predictions and experimental results where the model predictions have been obtained prior to performing the tests. Responses predicted include damage development, change in strength and modulus, and failure for each laminate/load history selected for study.

The Phase III research plan was formulated to provide a full

demonstration of the capabilities of the model as it has been developed and refined and to test the limits on the applicability of the model. Predictions and experimental data have been obtained for each of four major categories. One series of tests has been included specifically for the purpose of verifying the recent refinements of the model; one to study the ability to extend the model to other materials of engineering interest; one to verify the geometry independence of the model; and finally, one to demonstrate the model under complex, competing damage mode load conditions. The GD/VPI team believes that this test program, in conjunction with the independent exercising of the model to obtain the predicted responses, provides a comprehensive verification and demonstration of the model.

Rather than concentrating solely on the Phase III activity, this report will summarize both the experimental and analytical aspects of the effort conducted throughout the course of the program. The modeling concepts for both tension-dominated and compression-dominated failures will be discussed, including discussions on the sensitivities of the model predictions to input parameters. Results obtained from each of the six basic laminations used in the experimental program will be included as appropriate. For the sake of brevity, these laminations will be discussed in terms of letter designations, as detailed below:

Type A ---  $[(0/45/-45/90)_s]_{3s}$

Type B ---  $[(0/90/45/-45)_s]_{3s}$

Type C ---  $[(0/45/90/-45)_s]_{3s}$

Type D ---  $[(0/((45/-45/90)_s/90/90/45/-45/90)_s/0)]_s$

Type E ---  $[(0/45/0/-45)_s/(0/45/-45/90)_s/(0/45/-45/0)_s]_s$

Type F --- [(0/45/-45)<sub>s</sub>]<sub>4s</sub>.

The results from Phase III will be presented separately. Finally, a discussion of the experimental program and methodologies required to develop the necessary parameters used in the model will be discussed.



## SECTION II

### CUMULATIVE DAMAGE MODEL CONCEPTS AND IMPLEMENTATION

#### 1. MODEL CONCEPTS

In order to understand the approach that was taken to the modeling of cumulative damage in composite laminates, it is desirable to define precisely the problem that was addressed. The basic objective of the effort was to develop a mechanistic cumulative damage model that would have the capability of describing and predicting the strength and life of composite laminates during cyclic loading. The major point of departure of this research effort from prior modeling activities is the mechanistic approach. In fact, for the most part, the major thrust of the entire research program can be characterized as an attempt to make major step in philosophy from phenomenological descriptions of composite laminate fatigue behavior to mechanistic modeling based on the physics and mechanics of the details of laminate response during cyclic loading. A thorough discussion of the development of the model appears in Reference 2. In the pages which follow, we will only attempt to provide the basic elements and concepts, discuss implementation of the model, and present Phase III results.

The scope of the present effort was intentionally broad; it addressed the residual strength and life of several types of composite laminates in unnotched coupon (plate) specimen form subjected to tension-tension, compression-compression,

tension-compression, and spectral cyclic loading. The approach was to construct a framework, a lattice of rational rigor and sound physical philosophy, into which intricacies of precise representations, physical insights, and mathematical sophistication can be interwoven as understandings of the physical phenomena involved are developed and analytical representations achieved. The modeling effort described in the following pages is entirely a result of this commitment to a general approach. Since the scientific and engineering community is at a very early stage of development of an understanding of the behavior of composite laminates under cyclic loading, and a great number of questions regarding the strength, stiffness and life of laminates under those conditions are presently unanswered, the penalty of initial imprecision of such an approach will certainly be evident in our results. However, if we are successful in establishing a valid, general approach to the mechanistic description of cumulative damage under the arbitrary cyclic loading modes and loading histories mentioned above, then it is reasonable to expect that a sound foundation has been laid for the construction of a rigorous general philosophy for the anticipation of residual response of such laminates under a variety of practical situations with an acceptable amount of precision.

Hence, we concentrated our attention on an effort to develop an engineering model in such a way that a minimum amount of phenomenological characterization of material systems can be used to anticipate the behavior of various laminate configurations under arbitrary loading conditions. We

require that the model be based upon measurable parameters which can be used to characterize the development and current state of damage in a composite laminate so that an assessment of the current condition and anticipated behavior of a given specimen can be made based on measurements of immediate physical characteristics (in contrast to statistical predictions of group behavior based on statistical sample characterization). We further require that a definition of "equivalent damage states" be established so that cumulative damage under arbitrary load spectra can be correctly assessed. Finally, we require that the model provide a framework into which representations of individual events (damage modes, etc.) can be removed and inserted as understandings of those events allow, and that the framework be constructed in such a way that it can easily be translated into operational codes which allow engineers to use the philosophy in a direct and straightforward way for initial design and subsequent inspection interpretations.

To achieve these objectives, a new concept was introduced as basis for construction of the mechanistic model. The "critical element concept" and the resulting approach to model construction is illustrated in Figure 1. We make the claim that it is sufficient for the model to produce values of residual strength at any given number of cycles since the life of a laminate or component will be defined by the coincidence of that strength with the applied stress level. Hence, it is the objective of the model to achieve a calculation of strength given information about the laminate and the loading

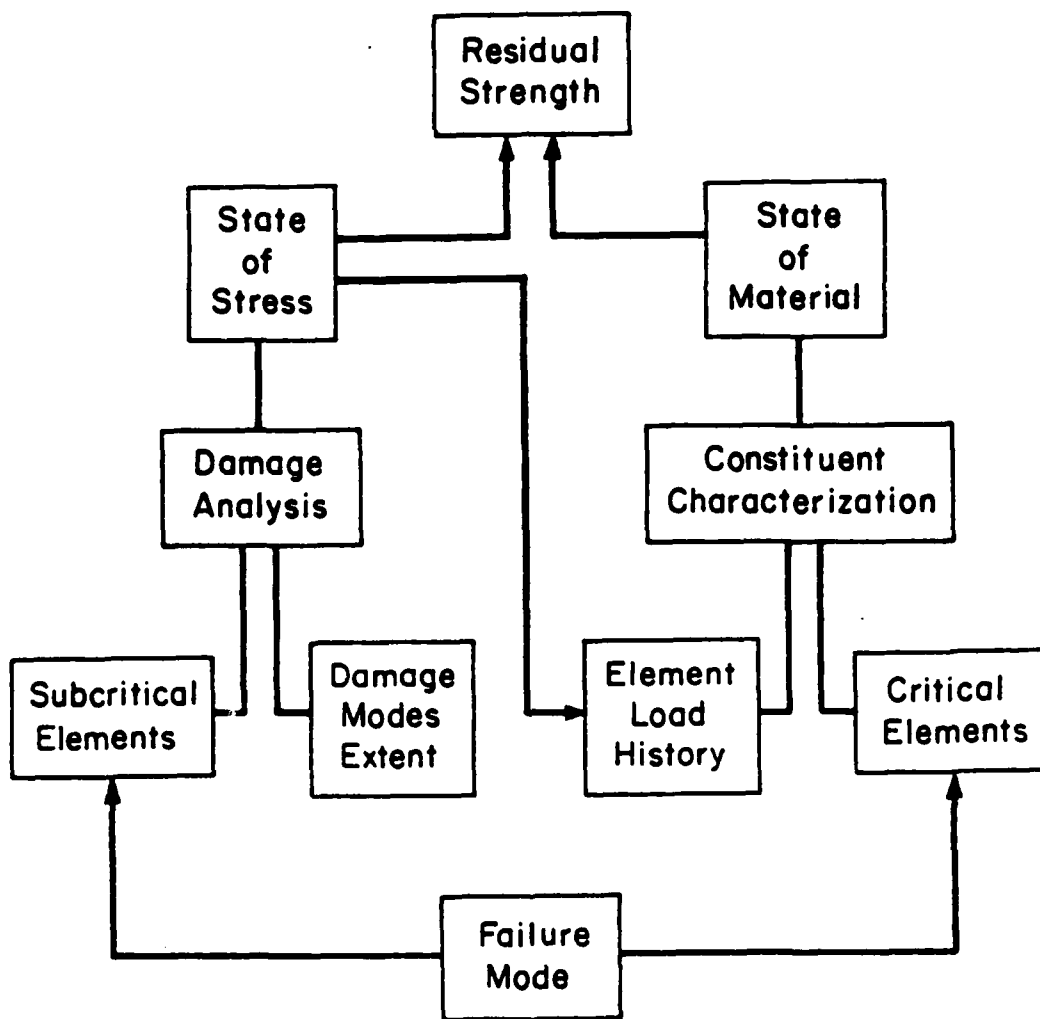


Figure 1. Conceptual Flow Chart of "Critical Element Model"

conditions. The manner in which that is done in the present case is illustrated by reading from the bottom to the top of Figure 1. One begins by answering the question "How does the component fail?" The failure mode can be established from quasi-static loading of the same type used for cyclic loading, by analytical computations or simulations, or by postulation based on experience. While the number of damage modes in composite materials is generally large, the number of failure modes is considerably smaller; hence, this task is usually feasible. Once the failure mode is established, the laminate is subdivided (in the analytical sense) into two types of elements, "critical elements" and "subcritical elements". These are defined on the basis of the failure mode. Critical elements are those parts of the laminate whose failure causes (and is coincident with) failure of the laminate or component. Since they are the last part of the laminate to fail, the strength of the laminate is defined by their resistance to failure and the stress state in which they operate. For tensile loading of a quasi-isotropic laminate, for example, the critical elements may be the zero degree plies, etc.

Subcritical elements are the parts of the laminate or component which sustain damage during the fatigue loading process, but which contribute to failure only in the sense that they contribute to a redistribution of internal stresses as a consequence of damage accumulation. For the tension example just mentioned, subcritical elements may be the off-axis plies in which matrix cracks cause reductions in stiffness and local stress concentrations. In

a very direct sense, the "fatigue effect" in composite materials is defined by the damage accumulation process in the subcritical elements.

The purpose of dividing the laminate into critical and subcritical elements is to facilitate the subsequent computation of residual strength. The activity of subcritical elements is handled by mechanics analysis, while the activity of the critical elements is represented by phenomenological (constituent) information. As shown in Figure 1, once the subcritical elements are defined, and information regarding the damage modes and the extent of damage is obtained, then a damage analysis can be conducted to establish the state of stress in the interior of the laminate as a function of the number of applied cycles, i.e., as a function of the amount of damage that has developed at any point in time. This state of stress is used in two ways. As shown in Figure 1, it is an input into the determination of the stress state in which the critical element must operate, the "element load history". The element load history for a given critical element can be used as input into equations which describe the constitutive behavior of the critical elements to establish the state of the material in those elements as a function of the number of cycles of applied load. For example, for the tension case described above, the constituent characterization for the critical elements may be a S-N curve for the unidirectional material loaded in the fiber direction. Then, the local stress state provided by the element load history, entered into such a relationship, would provide a current estimate of the life of the

element under those load conditions, an indication of the state of the material when combined with the number of cycles of loading that have been applied.

If the state of stress and the state of the material have been determined for the critical elements, then one should be able to use some strength philosophy to establish the residual strength of the critical elements and therefore the laminate or component. A particularly important aspect of the model is its generality. The approach suggested in Figure 1 does not depend on the specific inputs. Conversely, advancements in, say, damage analysis or constituent characterization can be used to improve the results of the model without major rearrangement of the computational scheme or philosophy. However, for computational purposes, a flow chart such as that shown in Figure 2 indicates the manner in which calculations are actually carried out. Beginning at the top of that figure, one begins by specifying a critical element as defined by the failure mode of the material under the stress state given. Then phenomenological data which characterizes the response of the critical element as determined from independent testing is provided to the model. This information will be used throughout the calculation to determine the state of the material in the critical element. Then the element stress state is determined from the applied stress, the details of the critical element, and information regarding the amount of damage development combined by well-set mechanics analysis of the damage state in which the critical element must operate. As indicated by Figure 2, information about the damage modes and

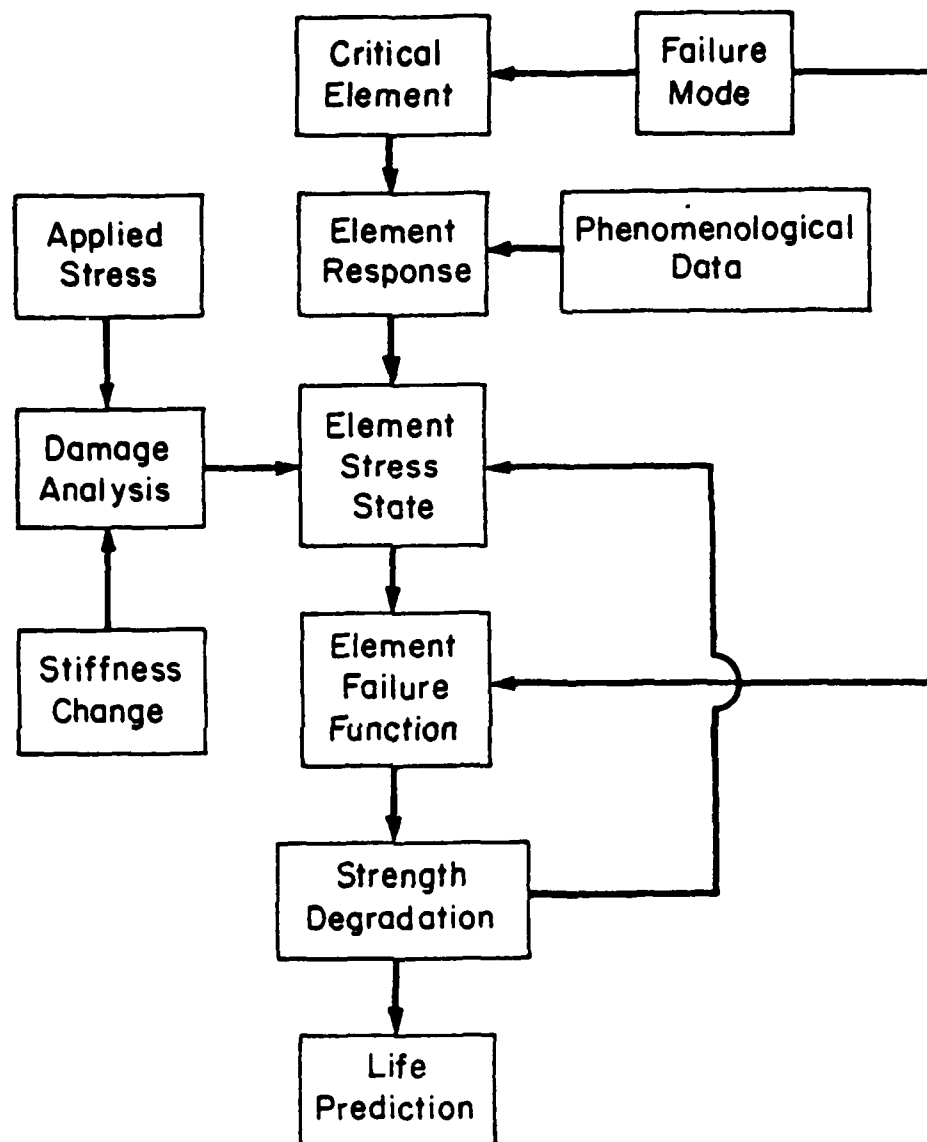


Figure 2. Computational Flow Chart for Critical Element Model



the extent of damage is provided in the present approach by measurements of stiffness change induced by damage development. Stiffness changes are nondestructive measurements which are directly related to the micro-damage and attendant reduction in residual strength in composite laminates. Furthermore, stiffness changes are directly related to internal stress redistributions since the same damage events produce both effects in proportion. Details and examples of stiffness change and stress redistribution due to the various damage modes observed in composite laminates are included in Reference 3. More will be said of this association later.

Continuing down Figure 2, once the state of material and state of stress in the critical element have been determined, it is necessary to interpret those results in terms of a failure function which accurately describes the resistance of the critical element to failure for the given failure mode known to occur. This failure function may be something as simple as a maximum strain criterion or other failure criteria. Then this information is combined into a calculation of the remaining strength of the laminate for a given number of cycles. That calculation is made through the use of an integral equation that was postulated by the authors based on the following rationale.

Consider Figure 3, which is a schematic representation of some of the basic relationships for laminate fatigue behavior. For the present we imagine that this representation is essentially one-dimensional, i. e., that the residual strength,  $S_n$ , and the life locus represent laminate values

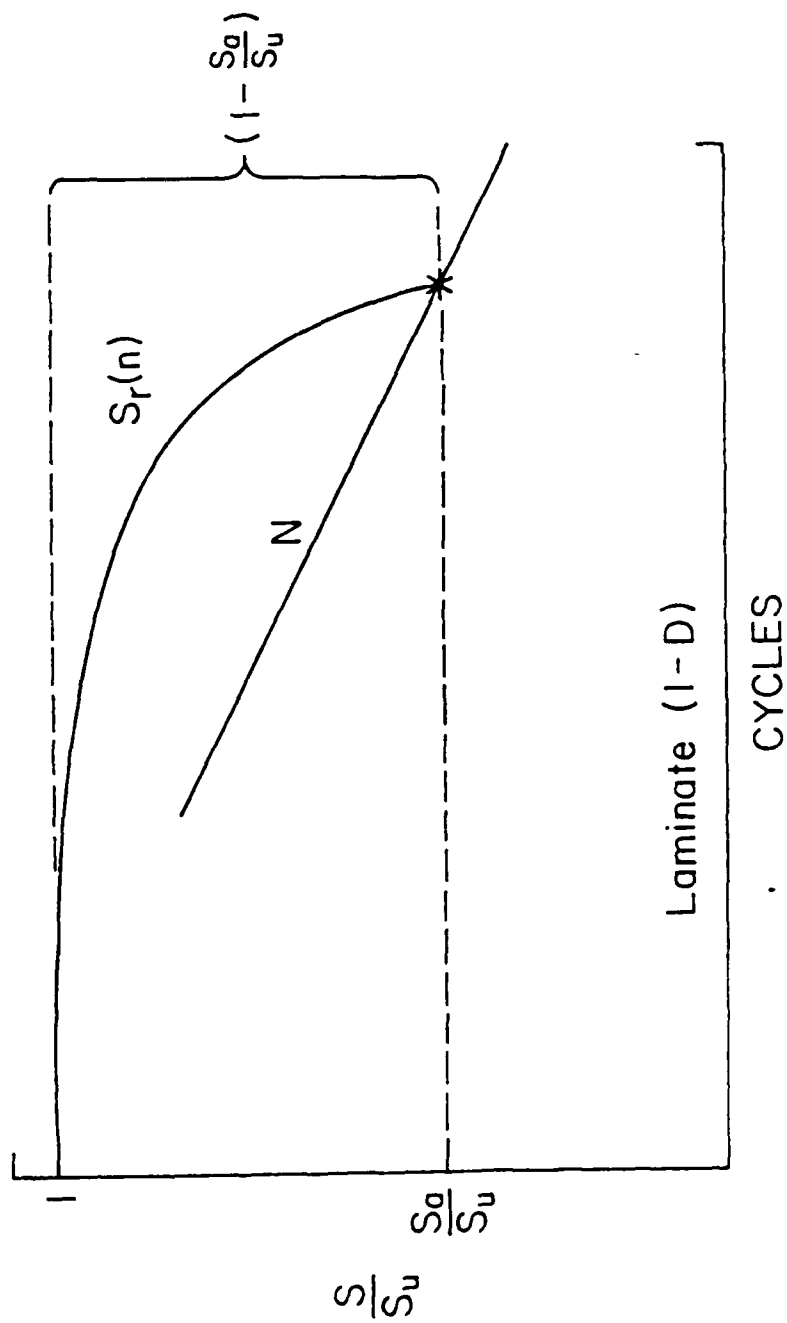


Figure 3. Schematic Diagram of Laminate Strength Reduction-Life Relationship.

determined from unidirectional loading. The residual strength curve can be written in terms of the applied stress,  $S_a$ , as shown in Equation (1) where  $i$  is a parameter introduced to accommodate the nonlinearity in the residual strength reduction curve. It is

$$S_r(n) = 1 - \left(1 - \frac{S_a}{S_u}\right) \left(\frac{n}{N}\right)^i \quad (1)$$

where  $\frac{n}{N}$  = life fraction

further assumed that the applied stress amplitude,  $S_a$ , is constant throughout the test. The residual strength,  $S_n$ , is a function of the number of applied cycles.

We have indicated that the modeling approach that we have taken is based on a phenomenological characterization of the critical elements in the laminate, and not on the laminate itself. Hence, the next step in the construction of our generalized summation equation is to consider the fatigue behavior of the critical elements, as schematically indicated in Figure 4. Since these critical elements are imbedded within a laminate, and since, as we have emphasized, the internal stress state is constantly changing as damage develops in the subcritical elements causing internal stress redistribution, the applied stress,  $S_a$ , is no longer constant as a function of the number of cycles. Since it is variable, we cannot simply multiply all of our terms in a degradation equation by the ratio of applied cycles to life, the so-called life fraction. Instead, an equation such as Equation 2 is more appropriate. Here it should be noted that the integrand is a

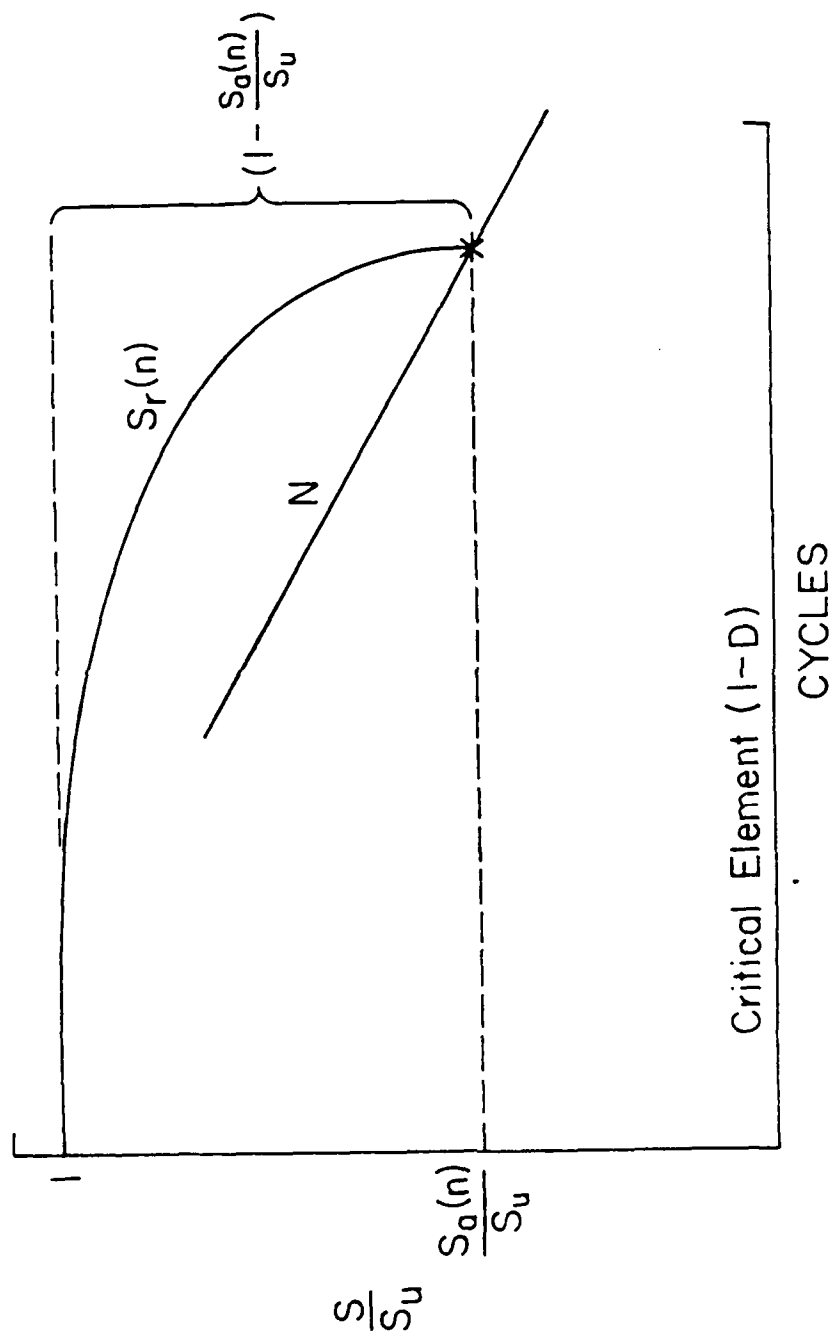


Figure 4. Schematic Diagram of Critical-Element Strength-Life Relationship.

function of the number of applied cycles, not only because of the

$$S_r(n) = 1 - \int_0^{\gamma} \left(1 - \frac{S_a(n)}{S_u}\right) \left(\frac{n}{N(n)}\right)^{\gamma-1} d\left(\frac{n}{N(n)}\right) \quad (2)$$

where  $\gamma$  = specific value of  $\frac{n}{N}$

variation of the applied stress on the critical element,  $S_a$ , but also because of the fact that the life that is calculated from a given applied stress (from the equation which fits the phenomenological data for the critical element) is also a function of the number of applied cycles, i. e.,  $N$  is a function of  $n$ .

The last major item to be added to our formulation incorporates the reality that the stress state of the critical element is almost never one-dimensional. Since it is imbedded in a laminate, the internal stresses are generally predominantly two-dimensional, and occasionally three-dimensional. In order to correct our model for that fact, we introduce a local failure function,  $F_L$ , to replace the local applied stress ratio,  $S/S_u$ . This local failure function is unspecified at this point, except to the extent that it must represent the tendency for the internal stress state in the critical elements to cause failure of those elements in a manner consistent with the observed failure mode and established mechanisms. There is an obvious relationship between the concept behind the local failure function and the familiar "failure theories" introduced by a variety of investigators such as Tsai-Hill, Tsai-Wu, and others. For this

refinement, Equation 2 becomes Equation 3, the final form of our residual strength equation.

$$\Delta S(n) = \int_0^Y (1 - F_L(n)) i \left( \frac{n}{N(n)} \right)^{i-1} d \left( \frac{n}{N(n)} \right) \quad (3)$$

This equation functions by producing a normalized residual strength estimate (a fraction of the static ultimate strength) as a continuous function of loading history indicated by the number of cycles of load application,  $n$  (Figure 5). The equation produces that estimate by integrating and convoluting the influence of two fundamental types of microdamage development consequences, changes in the state of stress and state of the material. This formulation reflects the opinion of the investigators that fatigue damage in composite laminates can generally be discussed in terms of microevents which occur in "non-critical" elements of the laminate (events that influence the degradation of the laminate primarily by internal stress redistribution and adjustment of geometry), and microevents which act directly on "critical elements" (elements which control the final fracture of the laminate).

Some of the damage modes which can be observed during the fatigue loading of a laminate with off-axis plies are illustrated in Figure 6. The slope of the representative damage curve is the damage rate. There are numerous damage modes which develop in a multitude of combinations depending upon loading level and mode, orientation of plies

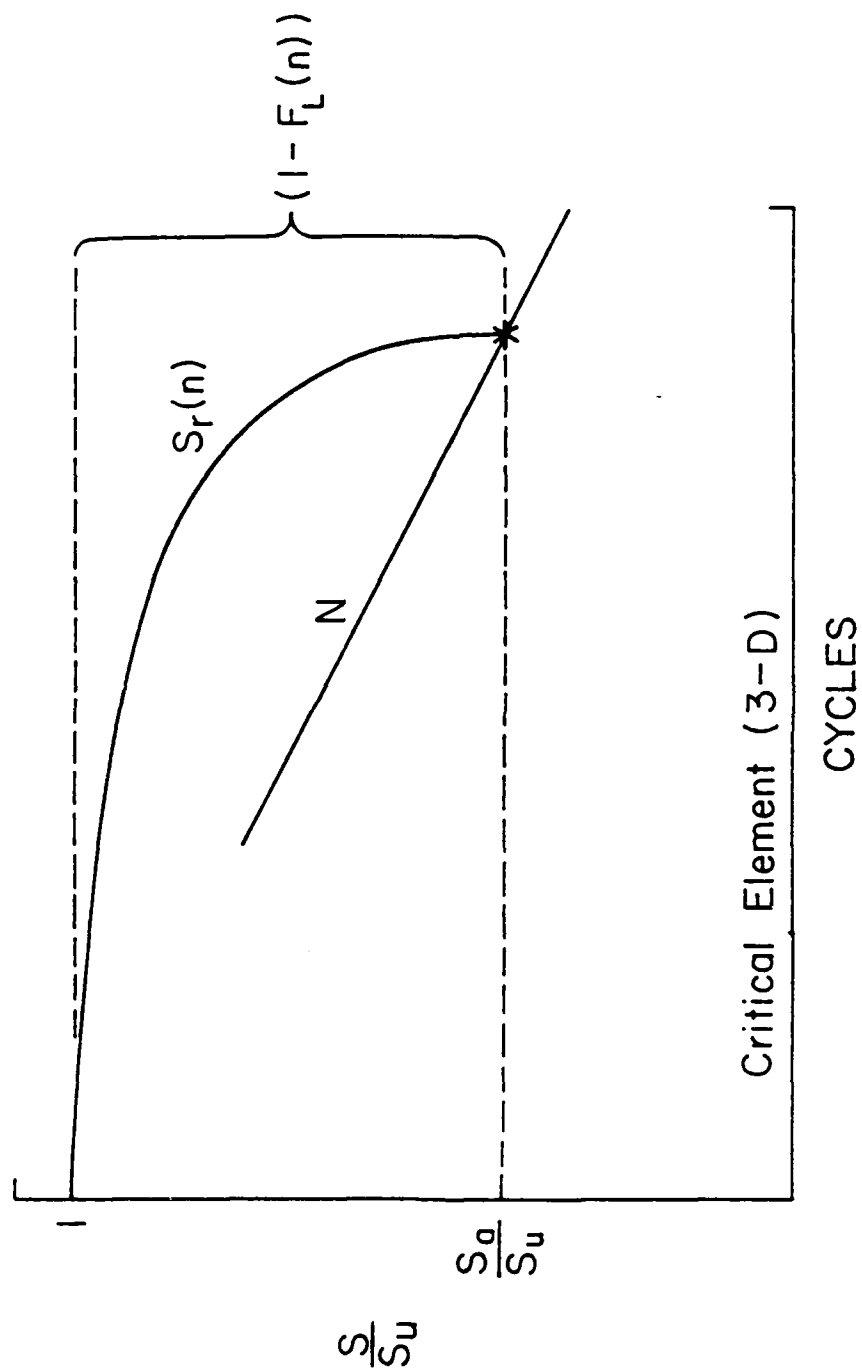


Figure 5. Schematic Diagram of Critical Element Strength-Life Relationship for Three-Dimensional Formulation.

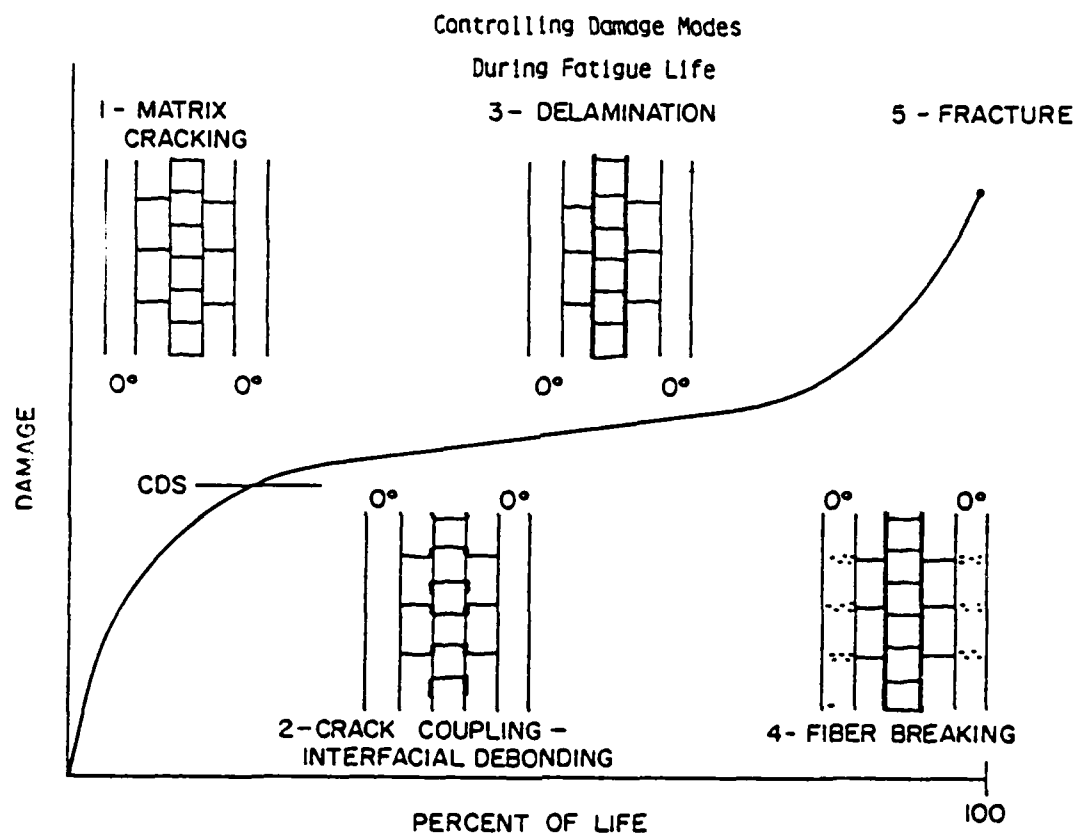


Figure 6. Damage Modes During Fatigue Loading of Composite Laminates.



in the laminate, and specimen or component geometry. Since the engineer will not, in general, wish to make laboratory investigations of micro-damage in each component in order to establish residual properties, it is necessary to establish some means of nondestructively measuring the degree of damage development in an arbitrary laminate for which the applied load history is unknown. Change in stiffness is used for that purpose in the model. The association between damage, stiffness change, and residual strength is illustrated in Figures 7 and 8 for laminates under tension-tension fatigue. Experimental observations show that matrix cracks develop in off-axis plies early in the loading history (stage I) accompanied by an initial but small change in laminate stiffness and strength. Fiber fractures also develop near the matrix cracks in stage I but they are thought to be inconsequential to our modeling process. As the cracks couple along ply interfaces to form delaminations (stage II), stiffness and strength change only slightly. As advanced damage states develop (stage III), and large delaminations and interfacial cracks form throughout the laminate, the rate of stiffness change and strength degradation increases markedly.

A great deal of work has been done and reported in the literature which has provided a foundation for understanding many of the details of tension-induced damage development (c.f. Reference 4). The Materials Response Group at Virginia Tech has identified generic patterns of damage which are well defined "characteristic damage states" for a given laminate and loading condition, References 5-8. These patterns form the

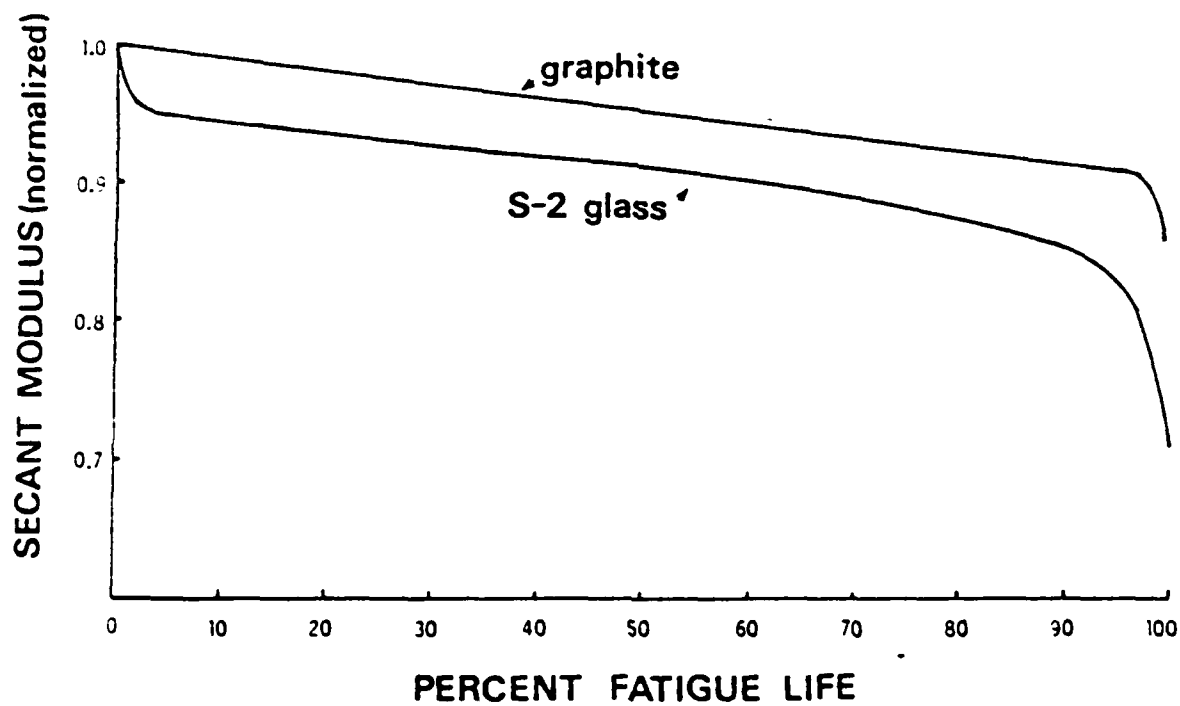


Figure 7. Longitudinal Young's Modulus Reduction for a  $[0/\pm 45/0]_s$  Graphite Epoxy Laminate Cycled at 0.85 of the Static Ultimate Strength, and a  $[0/90_2]_s$  Glass Epoxy Specimen Cycled at 0.6 of the Static Ultimate Strength.

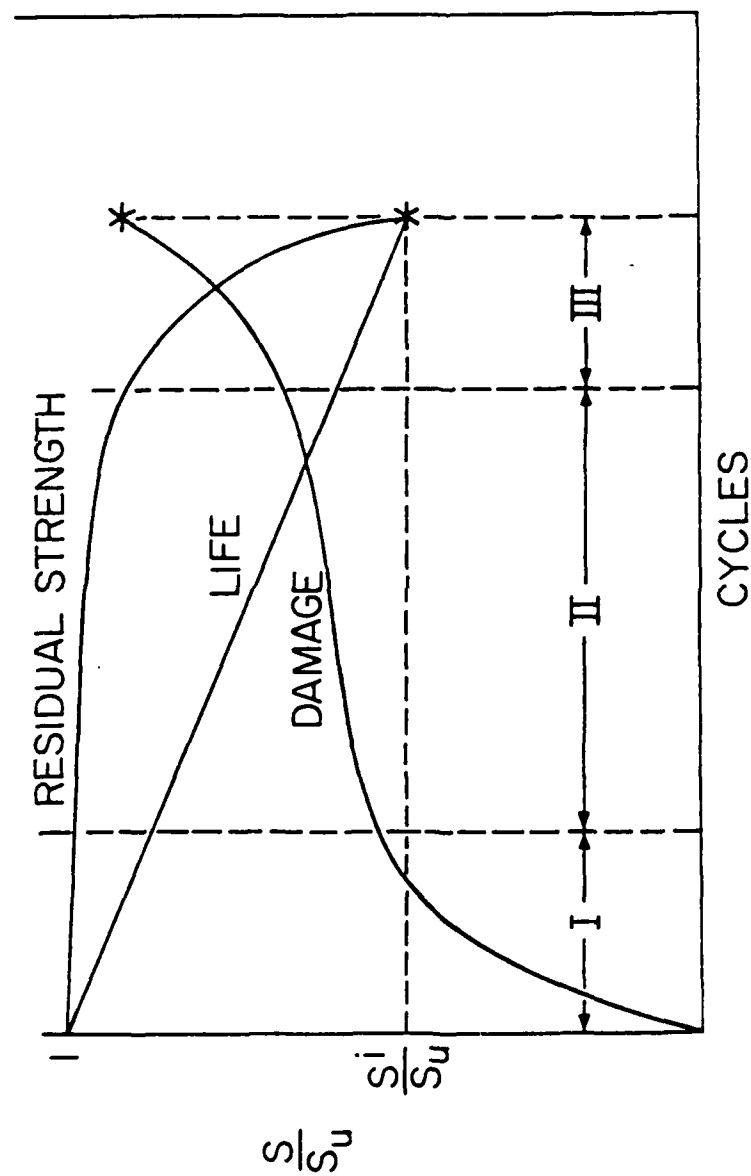


Figure 8. Schematic Diagram of Regions of Damage Development for Composite Laminates.

basis for well-set mechanics analysis of the local stress states associated with the collective damage state rather than individual damage events.

In contrast to the complexity of the damage modes, there are relatively few failure modes. For example, under tensile loading, the zero degree plies (or nearest on-axis plies) are responsible for the residual strength and life of composite laminates regardless of the complexity of damage that develops in the off-axis plies during fatigue loading. Although one may change the stacking sequence and, therefore, the general nature of matrix cracking, delamination, and debonding throughout a fatigue test, the final fracture event is still controlled by the zero degree plies. In this case, the failure can be modeled using an appropriate failure theory, such as the familiar Tsai-Hill postulate, applied to the zero degree plies.

For the tensile failure mode, the various terms in Equation 3 are identified in Figure 9. We will discuss the figure from right to left. The life locus described by the function  $N$  is a phenomenological representation of the life of the critical element, taken to be the 0 degree plies in this case. The equation is written as a function of the applied unidirectional stress,  $S(n)$ , normalized by the ultimate strength of the element,  $S_u$ . The material constants,  $A$ ,  $B$ , and  $x$ , are determined by fitting the data obtained from fatigue testing of unidirectional material of the type from which the laminate was constructed. Since, in this case, we are concerned only with the unidirectional performance of the 0

# Tension-Tension

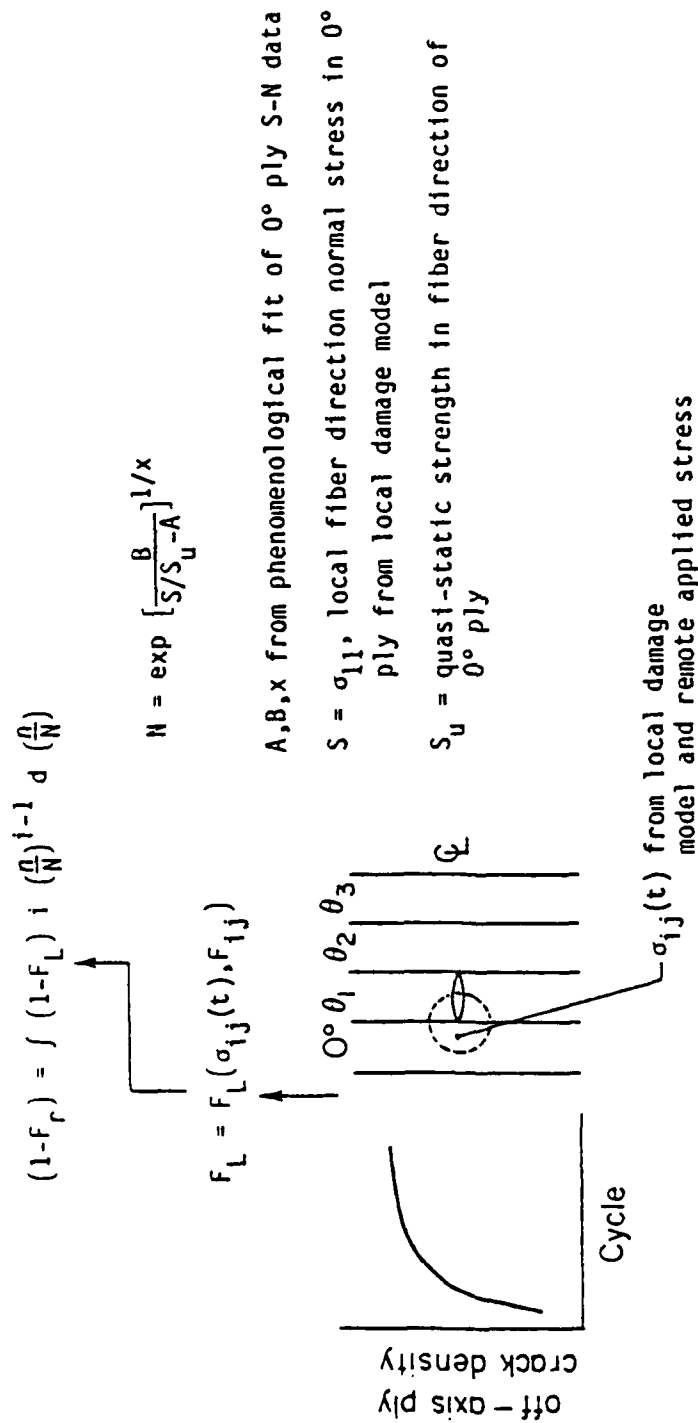


Figure 9. An Example of the Interpretation of Terms in the Summation Equation for Tension-Tension Constant Amplitude Loading.

degree plies, (the critical elements) one such relationship will suffice for all laminates regardless of their construction (stacking sequence, etc.). Since it is recognized that the 0 degree plies in the laminate may carry different amounts of the total load as the damage development in noncritical elements redistributes stress and alters internal geometry, the applied stress on the critical element,  $S(n)$ , is stated as a continuous function of the number of applied cycles,  $n$ . It should also be mentioned that the local internal applied stress,  $S(n)$ , can be determined from measurements of changes in laminate stiffness.

The choice of variable of integration,  $n/N$ , is important since that variable is a continuous function, even in circumstances when the applied loading spectrum is continuously varying in time. Hence, the residual strength Equation 3 can be used to determine the effect of cumulative damage under spectrum loading. The parameter  $i$  in Equation 3 is a material parameter which is associated with the nonlinearity of degradation (sometimes referred to as a tendency for sudden death) in composite laminates, and is also obtained from curve fitting of data. However, that constant generally has a value close to unity and does not appear, at this writing, to be a function of the construction of the laminate.

Continuing to move to the left in Figure 9, the term in parentheses determines the total amplitude of allowable strength reduction, in the sense that the laminate is expected to fail when the laminate strength (determined from the computation achieved by the equation) is reduced to the level

of the normalized failure function,  $F_L(n)$ . The failure function for the critical element, the 0-degree plies in this case, can be taken to be any of the typical phenomenological characterizations of strength computed at the cyclic load level. However, it is especially important that the stresses that enter into such an equation may be functions of  $n$  since internal stress redistribution will generally change the local stresses that cause failure of the critical element. Hence, the first term in parentheses in Equation 3 is also altered by the microdamage that occurs in subcritical elements causing internal stress redistributions and changes in internal geometry. Those changes are, as mentioned earlier, detected and interpreted based on stiffness changes in the scenario described. The choice of the failure function (and indeed a choice of the critical element) is dependent upon an anticipated failure mode of the laminate itself. This anticipation must be based on prior experience or guiding experiments. When the integral is performed, a normalized change in residual strength is produced as a function of the applied cycles,  $n$ , as indicated on the left of the equation shown in Figure 9.

In the pages that follow, an implementation example will be given for tension-tension, tension-compression, and compression-compression loading. Additional examples will be used to demonstrate the sensitivity of the model to various physical parameters and inputs. The reader is referred to References 1 and 2 for more complete descriptions of the results of application of the model to six different laminates and comparison with over 270 experimental results.

Only demonstrative examples of those results will be given here.

## 2. TENSION DOMINATED FAILURE

We begin with tension-dominated failure, and assign example values to the terms in Equation 3 as follows. As mentioned earlier, the power of the degradation ratio,  $i$ , is a parameter which is determined by the laminate tendency to demonstrate "sudden death", a behavior whereby the residual strength remains unchanged through a large fraction of the total life of the specimen and drops precipitously just prior to fracture. While some variations in that parameter will be introduced for demonstration purposes, it should be mentioned that ultimately a constant value of  $i$  equal to 1.2 was used throughout this entire research program for all computations.

It is assumed in Figure 1 that the critical elements which define the residual life and strength of the laminates to be considered are the zero degree plies, since that was in fact the case for all six laminates considered in this program. Hence, the phenomenological characterization of S-N behavior used in Equation 3 is taken to be a somewhat idealized form of the fatigue behavior of the zero degree plies. Actually, this characterization of fatigue behavior should be obtained under the two- or three-dimensional stress state that is appropriate for each of the laminates in which the zero degree plies are tested. However, since recovering such data would essentially require testing all laminates, and such a practice would preclude any predictive information obtained



from the model, a single one-dimensional phenomenological characterization was assumed to be adequate for all cases. Hence, it is only necessary to establish that single relationship for the zero degree plies in order to predict the residual strength and life for all laminates made from that material for which the critical elements are zero degree plies. Moreover, since the object of this research project was to establish a philosophy rather than become engrossed in the nuances of data representation, a further simplification of the phenomenological representation was introduced; it was assumed that the parameter A was equal to unity, an assumption that is equivalent to requiring that the half cycle residual strength be equal to the ultimate strength of the zero degree plies. It was further assumed that the power,  $x$ , was equal to -1, so that the only variable to be considered was the constant, B. Hence, one test of the applicability and validity of the present model is the extent to which the value of the constant, B, is the same for all laminates tested and modeled when reasonable agreement between the observations and predictions are obtained. Variations of B will be introduced for demonstration purposes and illustration of its influence, but ultimately a value of 0.07 was used for all data predictions. To that extent, the model appears to have been very self-consistent.

The value of the local stress,  $S$ , in the zero degree plies is obtained from models of local damage that is known to occur and from measurable damage parameter which indicates the extent of damage development; the change in longitudinal

stiffness was used as a damage parameter in the present case. We will provide more discussion of the local stress concepts below. At this point, it should be noted that the local stress which is used as an input to the phenomenological equation to calculate the expected life,  $N$ , becomes a function of the number of applied cycles, since the progressive development of damage has the effect of changing the local stress values which control the rate of degradation of the critical elements (the zero degree plies in this case) as cyclic damage develops. This local stress redistribution is due to the release of load in the plies (or regions of plies) which crack or break, and possibly also due to local stress concentrations caused by the internal geometry of cracks that form in the off-axis plies, between plies, and between matrix and fiber phases. These local redistributed stresses also enter into the computation of the local failure function,  $F_L$ , which appears in the integrand of the damage summation equation.

This stress redistribution concept is perhaps the most important central feature of the mechanics of the present modeling philosophy. The modeling of these local stress redistributions controls the accuracy with which we are able to make predictions of strength and life. The generality of the model is greatly enhanced by the fact that all damage events beyond (the phenomenological representation of) the degradation of the critical plies for all of the complex damage modes that occur in all possible laminates are handled by stress redistribution modeling. Of course, this continues to be an area of fertile and vigorous research activity. As our understandings of the nature and

consequence of local damage events improve with time, these representations will improve correspondingly. In the next few paragraphs we introduce a discussion of how these local stresses are computed based on laminate analysis as a starting point for more sophisticated treatments mentioned later.

As suggested earlier, there is an early "stage of adjustment" to tensile cyclic loading which is characterized by a rapid (and rapidly decreasing) rate of damage development. For laminates which have off-axis plies, such as the common quasi-isotropic stacking sequences, this early stage involves matrix cracking, usually by the formation of matrix cracks through the thickness of the off-axis (90,+45,-45 degree) plies parallel to the fibers and perpendicular (at least in transverse projection) to the dominant load axis (the 0 degree direction). This type of transverse crack formation has received a great deal of attention and is, by comparison to other micro-events, fairly well described and understood. Formation of the cracks can be anticipated reasonably well by laminate analysis coupled with a common "failure theory" such as the maximum strain, Tsai-Wu or Tsai-Hill concepts. The prediction of the occurrence (or absence) of such cracks is, however, of relatively little consequence in the engineering sense. It is possible, however, to anticipate the number and arrangement of such cracks, information which can be used for subsequent analysis of behavior.

Figure 10 shows the spacing between cracks in a -45 degree ply in a Type B laminate as a function of quasi-static load level and cycles of loading at about two-thirds of the ultimate

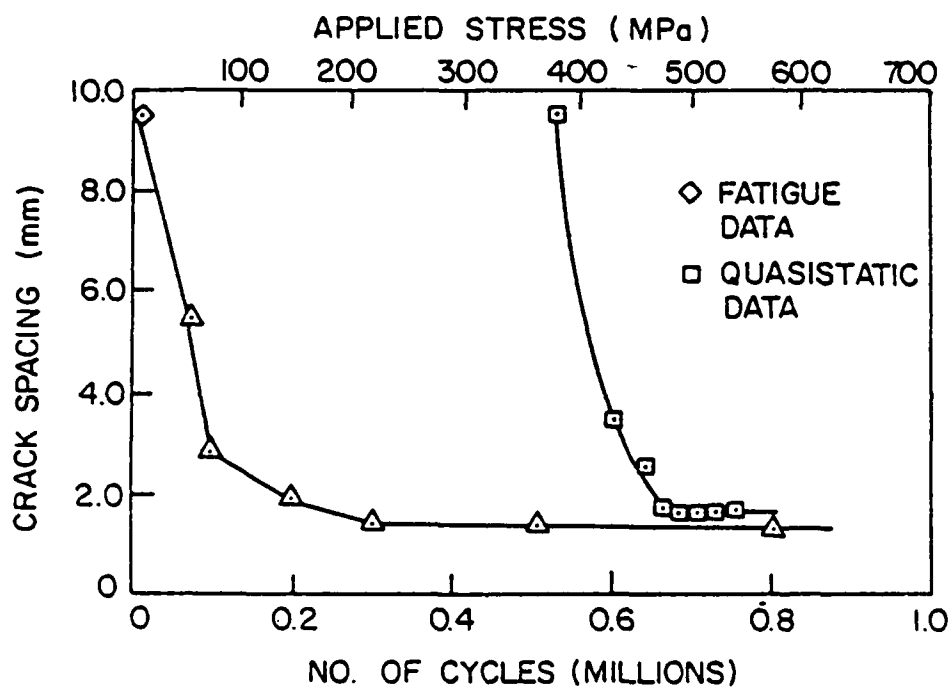


Figure 10. Crack Spacing in -45 Ply of  $[0/90/+45]_s$  Graphite Epoxy Laminates Under Cyclic and Quasi-static Loading.

strength ( $R=0.1$ ). As one can see, cracks develop quite early in the life and quickly stabilize to a very nearly constant pattern with a fixed spacing. The same behavior occurs for quasi-static loading, in the sense that crack development occurs over a small range of load and quickly stabilizes into a pattern which has the same spacing as the fatigue crack pattern. In fact, the two patterns are essentially identical regular crack arrays in that ply regardless of load history. Similar behavior is observed for the other off-axis plies and in other laminates. We have named these crack patterns "characteristic damage states" (CDS for short) for matrix cracking in laminates having off-axis plies. The CDS is a laminate property, i.e. it is completely defined by the properties of the individual plies, their thickness, and the stacking sequence of the variously oriented plies. The CDS is independent of extensive variables such as load history and environment (except as the ply properties are altered) and internal affairs such as residual or moisture related stresses. A more thorough discussion of the CDS can be found in References 3, 5, 6, and 7-12.

The stability of the off-axis crack pattern, the CDS, is the reason for the sudden decrease in damage rate between regions I and II in Figure 8 and also accounts for the relatively flat nature of the damage development curve in region II. The regular crack patterns can be predicted with engineering accuracy as we show in the references just noted, and the stress state in the neighborhood of such cracks can be accurately anticipated (Reference 3). Using these predicted crack densities,

the corresponding stiffness changes can be calculated. Such calculations have been made by the authors, and reasonable agreement with measured changes has been obtained (Reference 3).

The model for residual strength (and life) for cyclic tensile loading is based on the local stress state near the matrix cracks discussed above. A net section strength concept is also used based on the following argument.

When calculating the quasi-static strength of an unnotched laminate, the common scheme is to calculate the ply stresses using laminate analysis, invoke some failure criterion to predict first ply failure (usually matrix cracking), reduce the moduli in the broken ply (usually  $E_2$  perpendicular to the fibers and the in-plane shear stiffness  $G$ ), recalculate ply stresses, test for second ply failure, etc. until "last ply failure" is predicted. This scheme, commonly referred to as the ply discount method, has been widely used over period of at least fifteen years and is known to provide good engineering estimates of laminate strength when edge effects do not dominate the failure process. Table 1 shows the stresses in the individual plies of an example laminate before and after matrix cracks form in the 90 degree and  $\pm 45$  degree plies (for which  $E_2$  and  $G$  are then set equal to zero). The stress in the fiber direction of the 0 degree plies (which control final fracture) is increased from 2631 to 2993 MPa, a jump of 14% which is then used in a failure analysis of some type to predict the "correct" strength (if both off-axis plies fail before laminate failure). In general, failure of the off-axis plies will cause stress redistribu-

TABLE 1.

EXAMPLE:  $[0,90,\pm45]_s$  T300-5208Applied stress  $\sigma = 1000$  units

Ply	$\sigma_x$		$\sigma_y$		$\sigma_{xy}$	
	Before	After	Before	After	Before	After
0	2631	2993	- 2.3	- 4.7	0	0
90	167	0	-796	-1000	0	0
+45	600	503	400	503	417	503
-45	600	503	400	503	-417	-503

tion of this type which, based on some 15 years of literature, must be properly accounted for to predict "good" values of laminate strength.

It is easy to forget, however, that these stress redistributions (and the stiffness reductions that caused them) are not, in reality, uniform. They exist only near the matrix cracks in the off-axis plies. The first direct proof of that (to our knowledge) was provided by Highsmith and Jamison (References 13,14) who (with the able help of Prof. Post at Virginia Tech) constructed a very high resolution moire diffraction device which was used to resolve strain distributions in the 0 degree ply of several different laminates in regions near cracks in adjacent off-axis plies during quasi-static loading.

Recent results have shown that the tensile failure mode is probably controlled by a region of concentrated damage that forms near the intersection of primary matrix cracks (discussed above) and secondary matrix cracks which form in plies adjacent to those which form primary cracks due to the tensile stress field at the tip of the primary cracks. Secondary cracks generally extend only short distances into the adjacent plies, but the local stress field at the ply interfaces where primary and secondary cracks cross is significantly elevated. Highsmith has conducted a three-dimensional stress analysis of that situation and checked his results with experimental measurements of the local stress fields (Reference 15). While these results were available too late to include in the model, their incorporation will contribute to increased accuracy when they are included.



The average net section stress in the fiber direction of the zero degree plies can be recovered from laminate analysis. For demonstration purposes, the simplest possible interpretation of the fatigue behavior of those plies would be to claim that the fatigue behavior of any laminate can be predicted by calculating the fiber-direction stress for that laminate and estimating the resulting fatigue life from the curve that fits the data for one-dimensional fatigue behavior of that zero degree ply. When matrix cracking is the damage mode which is causing the local stress redistributions, we can calculate approximate values for the increased local stresses by the discount scheme described above.

However, when a specimen is actually tested, it must be determined to what extent the cracking in various plies develops so that the proper amount of local stress redistribution can be assigned. As we have suggested earlier, we have chosen (measured or predicted) stiffness changes as the damage parameter which allows us to monitor damage development and interpret that development in terms of internal stress redistributions. (In a sense, these stiffness changes replace the measurable crack length in a comparable fracture mechanics treatment in homogeneous materials.) Another positive consequence of this choice is the fact that axial stiffness changes are almost identical to local axial stress changes in the zero degree plies in a laminate. Such a relationship is demonstrated for quasi-isotropic stacking sequences by the information shown in Table 2. It is shown there for a Type B laminate that the axial fiber direction stress (calculated from laminate analysis)

TABLE 2.

EXAMPLE:  $[0,90,\pm 45,\mp 45,90,0]_{3s}$ Applied Stress  $\sigma = 1000$  units

Cracked Plies	$\sigma_x$ in 0° plies	$\Delta\sigma_x$ due to ply cracking (%)	$\Delta E$ due to ply cracking (%)
none	2540	----	----
all 90's	2646	4.2	4.1
all 90's and 45's	2992	18	15.3

is 2.54 times as great as the applied stress when no other plies are broken in that laminate. When the 90 degree plies are cracked, however, the local axial stress in the zero degree plies increases to 2.64 times the applied value, an increase of 4.2%. The corresponding decrease in the stiffness of the total laminate is 4.1%, a nearly identical figure. When all of the 90 degree plies and all of the 45 degree plies are cracked, the discount scheme suggests that the local applied stress in the zero degree plies is 2.99 times the laminate applied stress, an increase of about 18% over the original value in that ply. The corresponding decrease in stiffness for that case is 15.3%, a very similar number. These computations have been made for literally dozens of laminates, with similar results. Hence, for our starting point, we make the assumption that the local axial stress in the fiber direction in the zero degree plies can be estimated from an initial calculation of that stress using laminate analysis and knowledge of the stiffness change measured in a given specimen which can, in turn, be interpreted directly as percentage increases in the local stress that controls the rate of degradation of those zero degree plies.

In the instance that stiffness change observations are not available, it is possible to anticipate and estimate those changes for a given laminate and a given amplitude of applied load in tension. That estimation can be made by using any common failure theory (such as the Tsai-Hill or Tsai-Wu concepts) to estimate which off-axis plies will crack for a given maximum applied cyclic stress. The corresponding laminate stiffness change can be calculated from laminate analysis

using the discount method and a corresponding local stress change can then be estimated. Of course, more sophisticated concepts and analyses can be used for these purposes, and we will demonstrate the use of several of those including shear lag schemes and finite difference as well as finite element analyses in a later section.

Hence, we have identified the source of all inputs to the model. The S-N curve for unidirectional material can be obtained from pilot tests or by estimating the values of A, B, x in the idealized equation as discussed. (The same set of values was used throughout this entire program.) The local stress ratio in the critical elements is obtained from stress analysis of the controlling damage mode; as a first approximation it can be set equal to the laminate analysis ply stresses associated with the discount method and proportioned by the crack density based on observed or estimated stiffness changes. The local failure function can be any of the "failure theories" with the local stress as an input. As a first approximation it can be set equal to the local fiber direction stress normalized by the ultimate strength. Both the failure function and the local stress ratio (which is an input to the S-N characterization and the failure function) are functions of the number of cycles as determined from interpretations of stiffness changes.

We will consider a few examples below to demonstrate the tensile failure mode model sensitivity to several factors of importance to the response of a laminate or component.

We consider the Type F laminate which has a stacking sequence of  $[(0, \pm 45)_s]_{4s}$ . This laminate has a very high loading

of zero degree plies and is very strong under axial and shear loading. The quasi-static properties are given in References 1 and 2. Initially, the ratio of axial normal stress in the fiber direction of the zero degree plies to the applied stress on the laminate in that direction is 2.3. If the discount method is used, when the -45 degree plies crack the ratio changes to a value of 2.5, a 10.5% change. When the +45 degree plies also crack the ratio changes to 2.87, a total change of about 25%. Generally, during the fatigue testing of these laminates, the stiffness changes were rarely more than 10 to 15%. We note in passing that the calculated strength of the Type F laminate using the discount method was 81 ksi compared to an average value for the quasi-static tests of this laminate of about 80 ksi. (A Tsai-Hill theory of failure was used.) For the purpose of demonstration, a second interpretation of the local failure function,  $F_L$  was introduced. In some of our calculations that function had been taken to be equal to the local stress ratio in the zero degree plies. When that interpretation is used to predict the residual strength reduction for specimen F2-2, which was cycled with a maximum stress of 71 ksi, a life of about 14,000 cycles is predicted as shown in Figure 11, compared to an observed life of about 21,000 cycles. At 10,000 cycles the residual strength is predicted to have been reduced to a normalized value of 0.88. Specimen F5-5, run at essentially identical stress levels, had a strength retention of 0.97 which compares reasonably with the predicted number. Also shown in Figure 11 is a curve of predicted residual strength which ends in a life prediction of over 60,000 cycles. That

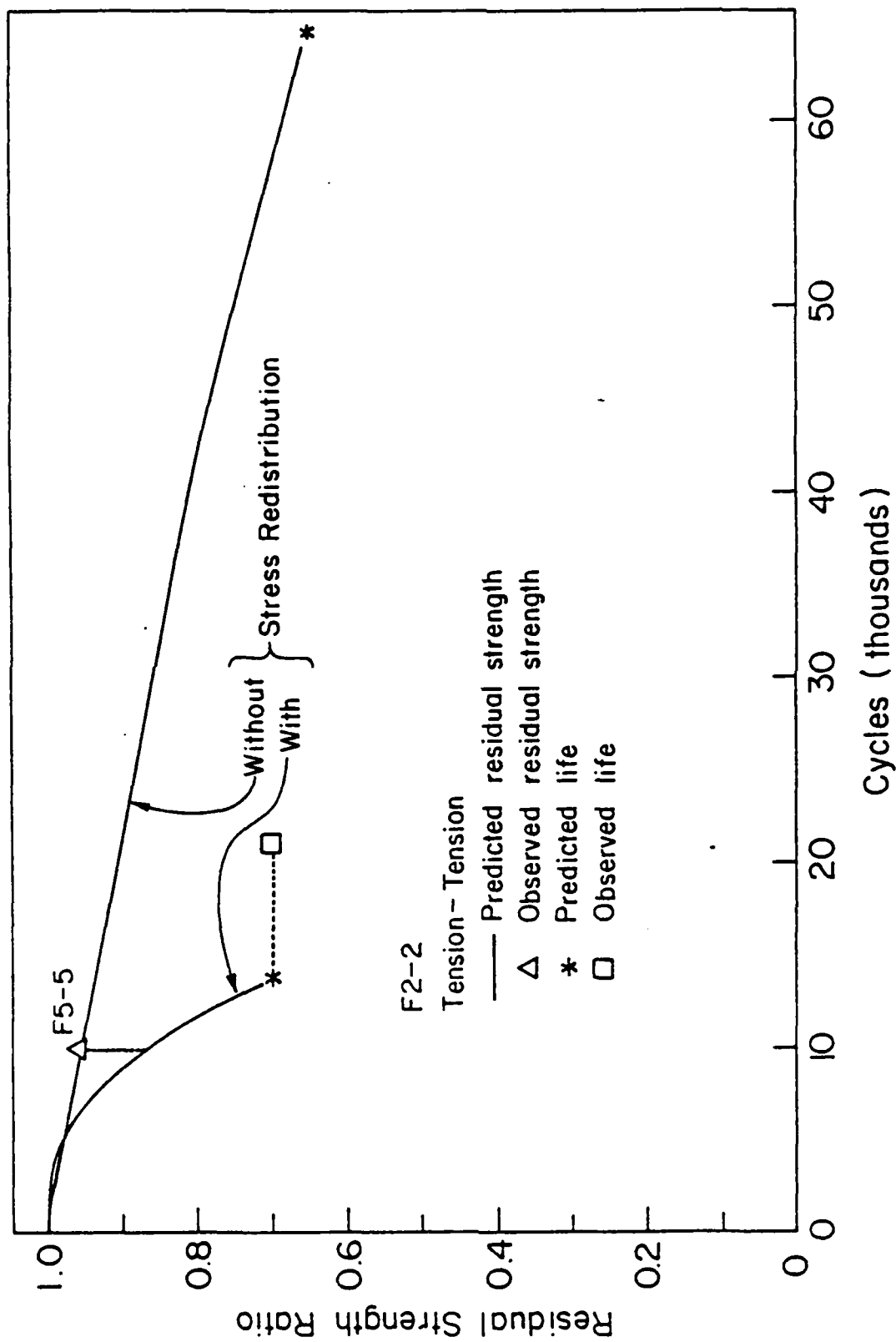
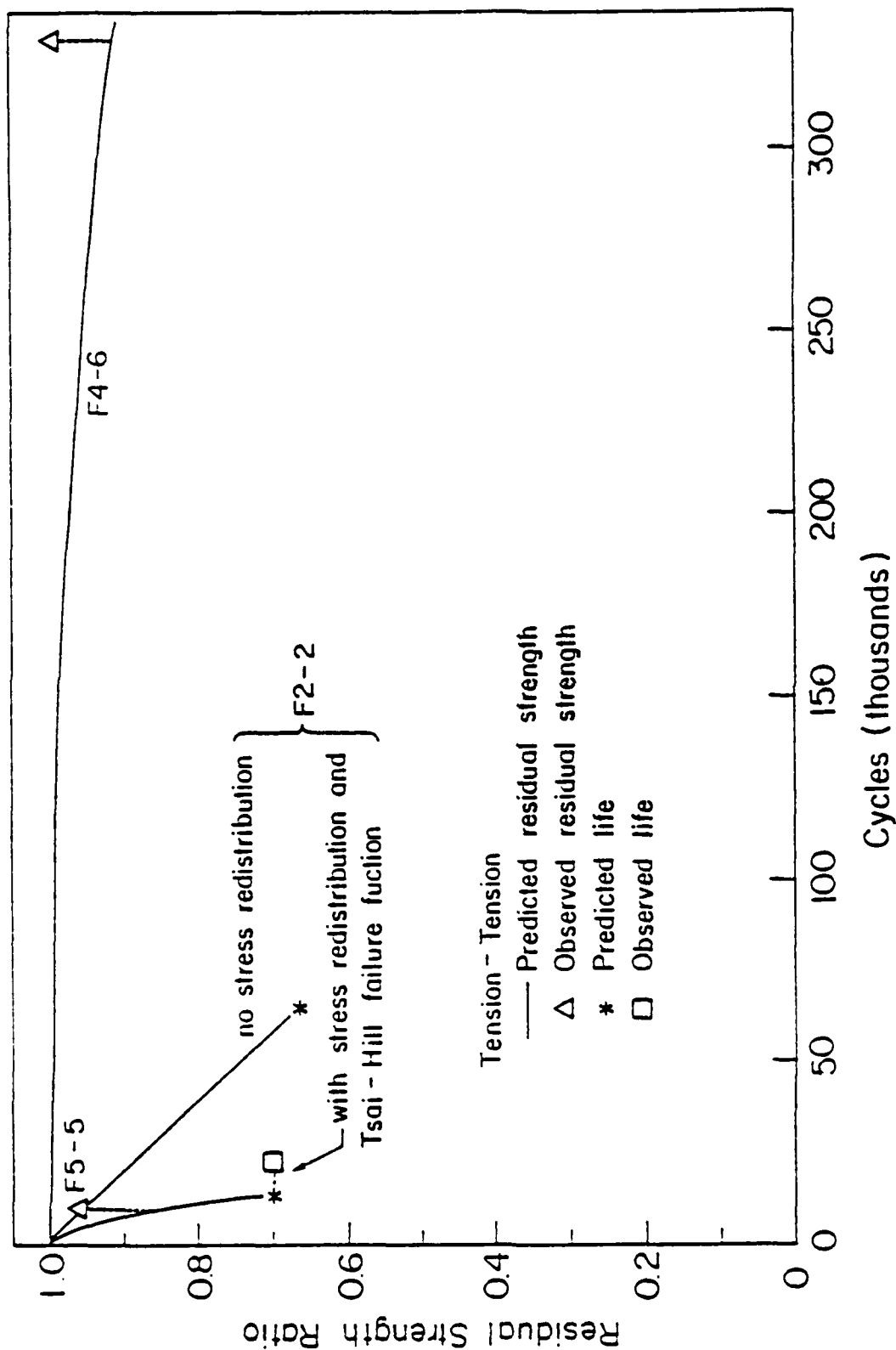


Figure 11. Residual Strength and Life Predictions for Uncorrected Model, Showing Effect of Stress Redistribution.

curve corresponds to the same cumulative damage model when stress redistribution is ignored. It is clear that the influence of stress redistribution is extremely great in this highly fiber-dominated laminate. The predictions of this model would make no sense at all if the internal stress redistribution due to damage development were ignored.

As we mentioned above, the local failure function,  $F_L$ , was reinterpreted in this series of tests. Figure 12 illustrates some of the results of that variation. It was decided to consider the case when the local failure function was set equal to the ratio of the applied laminate stress to the predicted laminate undamaged strength from the Tsai-Hill criterion used in the laminate analysis mentioned earlier. The predicted undamaged strength is used since the applied stress is thought to cause damage in the laminate in proportion to the strength of the laminate before damage occurs, rather than to the measured strength of the laminate after damage has occurred due to the increase in stress beyond the level of maximum stress during cyclic loading, i.e., the final quasi-static strength. Hence, for specimen F2-2 the initial value of the local failure function was taken to be  $71.2 / 104.42$  or a ratio of 0.683. The 10% modulus change and corresponding increase in laminate strain was assumed to cause an increase in that ratio of about 10% as well over the period of the test. The results of that computation are shown on the left-hand side of Figure 11, again for a calculation for which the stress redistribution was considered and for which it was ignored. The corrected calculation of life for specimen F2-2 is shown as a prediction "with stress redis-





tribution and Tsai-Hill failure function" and compares quite well with the observed life of that specimen. Again, the predictions which ignore stress redistribution are widely different from the observed data. A similar computation is shown for specimen F4-6. The maximum stress for that specimen was 57.1 ksi. Hence, the initial value of the failure function was 0.55 increasing by about 8% (corresponding to an 8% change in stiffness) to about 0.6. The local stress in the zero degree plies for that case begins at a stress ratio of about 0.53 and increases to about 0.575. The estimated life for that case is about 550,000 cycles. The predicted residual strength retention at 330,000 cycles was 0.93. The measured strength retention at that number of cycles for specimen F4-6 was essentially 1.0.

Specimen F1-9 was also modeled, and represents an intermediate loading level. The maximum stress in that test was about 63.8 ksi. The specimen demonstrated approximately a 10% stiffness change at about 250,000 cycles and failed at 290,000 cycles. However, the predicted life for that specimen was 150,000 cycles and the predicted residual strength reduction was too great. Figure 13 shows the data indicated in Figure 12 on a semi-logarithmic scale which allows the life prediction to be indicated. The figure also serves to illustrate the "exaggeration" of the nonlinearity in the residual strength reductions caused by the plotting procedure as noted earlier.

At this point, another model sensitivity will be discussed based on the biaxiality of the stress in the zero degree plies in this particular laminate. The data in Table 3 illustrates this biaxiality. That table presents the stresses in the zero degree

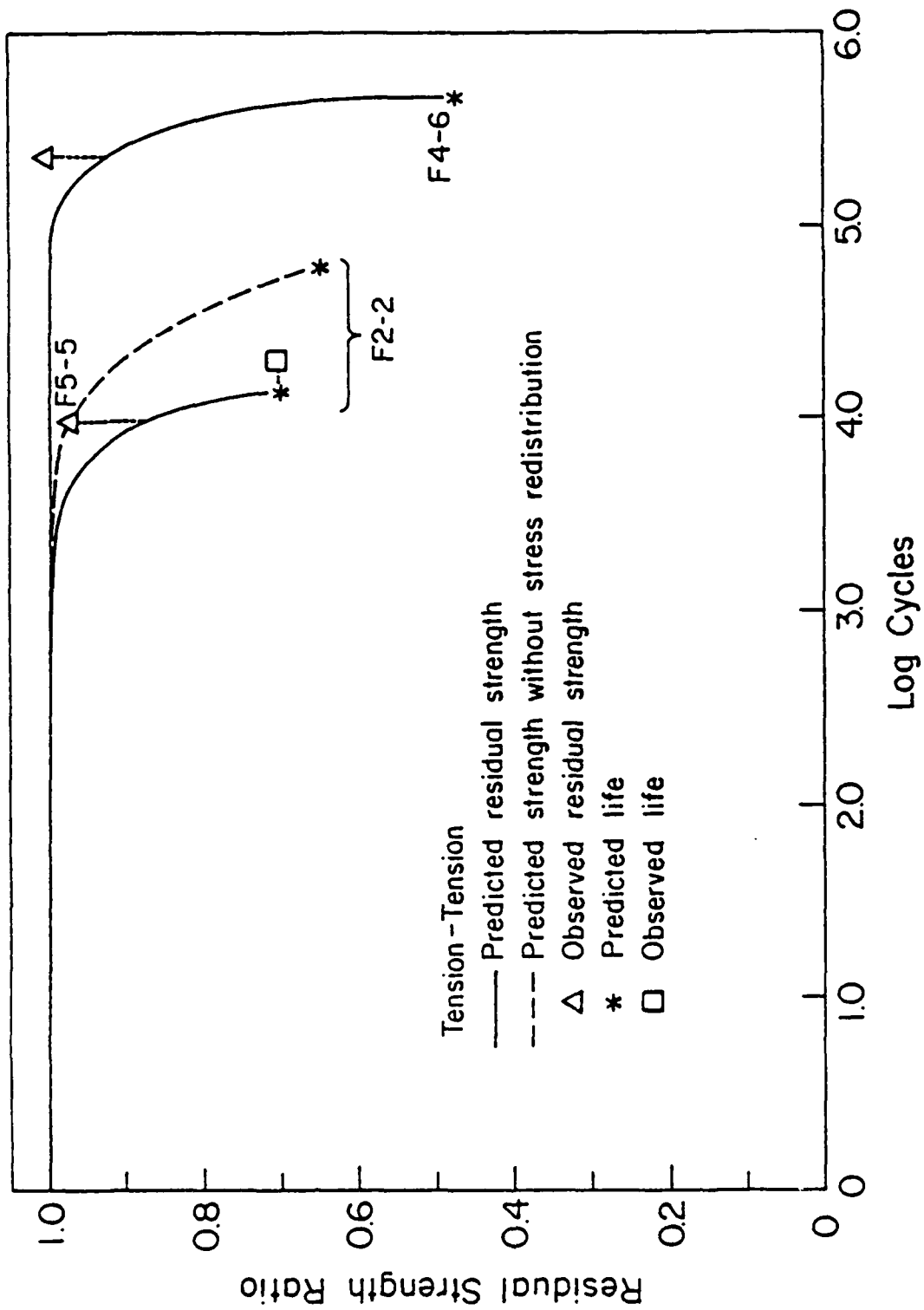


Figure 13. Semi-log Plot of Data in Figure 12 Showing Life Prediction for Specimen F4-6.

plies of a Type F laminate during damage development as determined from laminate analysis using the discount method described earlier. The stress in the zero degree plies for both a Type F and a Type C laminate are shown for comparison purposes. The last column of that table shows the computed value of the first term of the Tsai-Hill failure function (which corresponds to the normalized axial stress in the zero degree plies in the fiber direction) for the situations described. In the Type F laminate (for an applied stress of 1,000 units) the axial normal stress in the two laminates begins at a similar value. However, the transverse normal stress is compressive in the Type F laminate and tensile in the Type C laminate. Moreover, that transverse normal stress in the zero degree plies is more than 60 times as large in magnitude in the Type F laminate as it is for Type C specimens. The initial failure function is 0.94 for Type F and 1.0 for Type C. As damage develops, an even greater contrast develops between the types of laminates. The fiber-direction normal stress in both laminates increases, to 2,536 units in the case of Type F and to 2,646 units in the case of Type C. However, the transverse normal stress increases in the case of the Type F laminate and decreases in the case of the Type C laminate. When all of the off-axis plies are cracked, the axial normal stress in the zero degree plies is 2,873 units for Type F and 2,993 units for the Type C laminate. However, the transverse normal stress in the Type C laminate has passed through zero and has become slightly compressive, but still small in magnitude. The transverse normal stress in the Type F laminate has gained another order of magnitude to

reach a compressive value of 126.9 units. This increase in biaxiality for the Type F laminate is also illustrated by the progression of the failure function values from 0.94 to 0.92 to 0.89. In the case of the Type C laminate the values of the failure function remain very close to unity beginning at a value of 1.0, changing to 0.998, and ending up at 0.994. Hence, we have a situation where the internal stress redistribution is increasing the biaxiality of the internal state of stress and is influencing the rate of degradation in the zero degree plies. The reader may recall that one of the justifications for choosing a one-dimensional characterization of the internal stress in the zero degree plies and of the change in that stress with internal redistribution is the fact that, for most common laminates, the state of stress in the zero degree plies becomes more uniaxial as damage develops in the other off-axis plies. The Type F laminate is a distinct (and intentional) exception to that generality.

An experienced experimentalist might be quick to point out that the large values of transverse compressive stress (only one order of magnitude smaller than the axial normal stress) in the zero degree plies might produce a reduction in the rate of degradation of the zero degree plies by helping to prevent longitudinal cracking and related types of damage in those plies. Such an observation is certainly consistent with the fact that the model overestimates the degradation of these materials when only one-dimensional stresses are considered. With those observations as a starting premise, we pose the critical question. How is it possible to incorporate the "positive" aspect of the "negative"

transverse normal stress in the zero degree plies into our phenomenological representation of the S-N behavior of those plies? A relationship such as Equation 4 could be solved for the number of cycles to failure for an arbitrary biaxial stress state as in Equation 5, if all of the parameters in that equation were known.

$$\left(\frac{n}{N_1(\sigma_1)}\right)^2 + \left(\frac{n}{N_2(\sigma_2)}\right)^2 - \frac{n^2}{N_1(\sigma_1)N_2(\sigma_2)} + \left(\frac{n}{N_s(\sigma_{12})}\right)^2 = 1 \quad (4)$$

$$n = \frac{1}{\frac{1}{N_1(\sigma_1)^2} + \frac{1}{N_2(\sigma_2)^2} - \frac{1}{N_1(\sigma_1)N_2(\sigma_2)} + \frac{1}{(N_s(\sigma_{12}))^2}}^{1/2} \quad (5)$$

That would require characterization of the zero degree plies under fiber direction normal stress (to produce  $N_1$ ), under transverse normal stress (to determine  $N_2$ ), and under shear stress (to determine  $N_s$ ) with sufficient data base to establish Equation 4. That information was not (and generally is not) available.

To demonstrate the effect of this factor, we postulate that the local fiber direction stress is diminished in its influence on the degradation of that ply by an amount which is proportional to the absolute value of the first term in the Tsai-Hill failure function, according to the data presented in Table 3. Hence, if half of the 45 degree plies crack in that laminate, the local fiber stress ratio would be multiplied by 0.92 to account for the fact that the compressive normal stress in the transverse direction is diminishing the effect

TABLE 3.

STRESSES IN 0° PLIES OF TYPE F LAMINATES DURING DAMAGE DEVELOPMENT  
(APPLIED STRESS = 1000 UNITS)

	$\sigma_x$	$\sigma_y$	$\tau_{xy}$	f.f.(1)
Type F Laminate:				
Undamaged	2295	- 65.9	0	0.94
One 45° ply cracked	2536	- 90.2	0	0.92
Two 45° plies cracked	2873	-126.9	0	0.89
Type C Laminate:				
Undamaged	2541	1.2	0	1.00
90° plies cracked	2646	3.9	0	0.998
All off-axis plies cracked	2993	- 5	0	0.994

Note (1) first term of the Tsai-Hill failure function,  $(\sigma_x/X)^2$

of the increased axial normal stress in the fiber direction. While this refinement is somewhat artificial, it is at least rational. Using that refinement, and the refinement of the local failure function mentioned earlier, all of the data predictions were recalculated and plotted in Figure 14. The predictions are seen to agree surprisingly well with the experimental data for both residual strength and life. For specimen F2-2, for example, the predicted life is about 27,000 cycles compared to the observed life of about 20,000. The predicted residual strength retention at 10,000 cycles is about 0.98, which compares nicely with the experimental data for specimen F5-5 which was 0.97. For specimen F4-6, the predicted life becomes 800,000 cycles and the residual strength retention at 330,000 cycles is predicted to be 0.98, which compares well with the measured value of about 1.0. The life prediction for specimen F1-9 is virtually coincident with the observed data. The residual strength retention for that load level is considerably less than the experimental observation for specimen F3-1, but that value is certainly suspect since it is nearly 115% of the average quasi-static measured value. In general, the biaxial correction appears to be reasonable.

It should be mentioned that this biaxial correction scheme cannot be extrapolated. In the limit, it predicts the ridiculous result that an infinitely large compressive normal stress in the transverse direction in the zero degree plies would completely suppress the degradation of those plies! In reality, of course, no such "huge" values are observed. And, the correction scheme should be interpreted more in the sense of

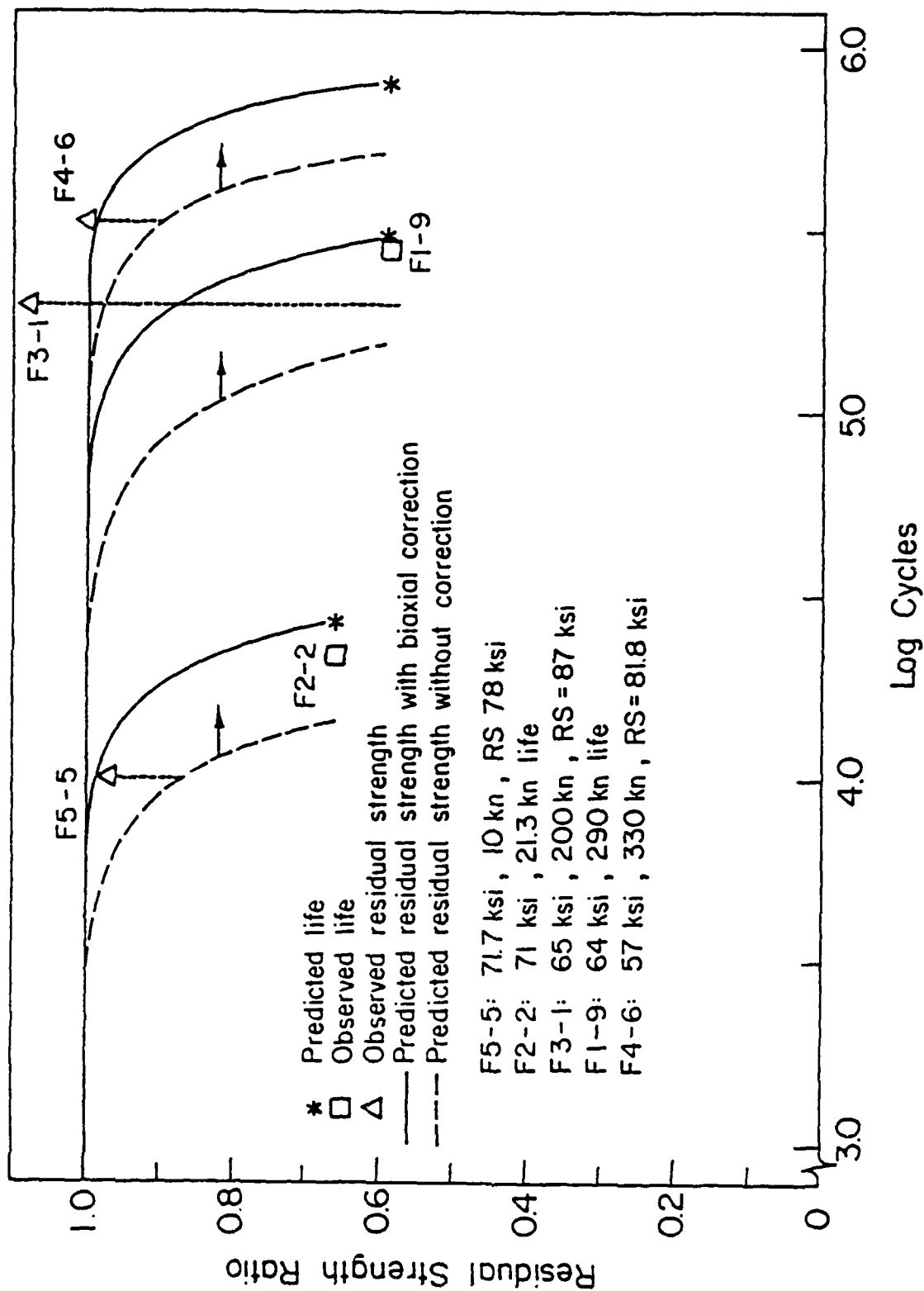


Figure 14. Predicted and Observed Data for Type F Laminates in T-T Loading for Model with Biaxial Correction.



having the degradation of the zero degree plies suppressed in deference to another damage mode or simply suppressed altogether. It is also possible that one could discuss this behavior in terms of stress interaction concepts. These points cannot be resolved without substantive further physical information and considerable amount of basic research effort. However, the present discussion indicates the nature of this situation, the sensitivity of the model to it, and an interim method of dealing with it.

We will continue our discussion of sensitivity with some comparisons for a different laminate. Figure 15 shows a variety of predictions (in a range of observed data for tension-tension fatigue testing of Type B laminates at about 6,000 ue) which illustrate the influence of two of the parameters which enter into the damage accumulation model, the slope of the phenomenological fatigue characterization of the zero degree plies,  $B$ , and the power of the degradation ratio " $i$ " in Equation 3. It also illustrates the influence of internal stress redistribution for this case where changes in stiffness (and internal stress) are small, of the order of about 5 to 6%. Curves A and B show that internal stress redistribution contributes significantly to the nonlinearity of the residual strength degradation curve, especially near the end of the specimen life. While the predictions through the early part of the fatigue life for those two cases are relatively similar, the residual strength and especially the life predictions of those two approaches to modeling can be radically different, even for relatively small amounts

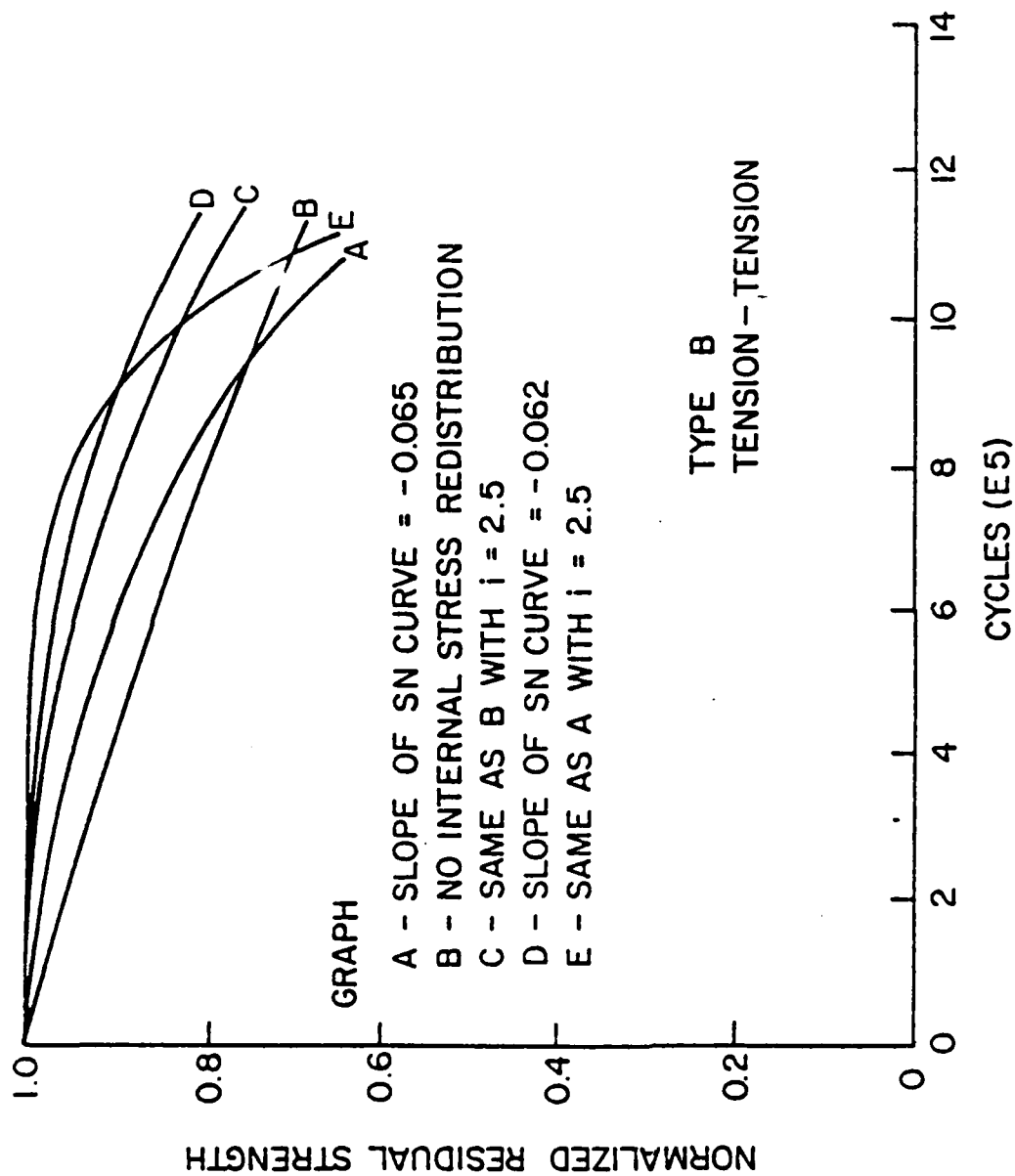


Figure 15. Illustration of the Influence of Various Model Parameters on Predicted Results.

of damage development and rather long life situations. The power of the degradation ratio,  $i$ , is equal to 1.2 for curves A and B. If that power is changed to 2.5, one obtains the curve shown in C instead of the curve shown in B (both of which include no stress redistribution). One can see that the otherwise-straight curve B does become more curved with an increase in that power as would be expected. It should also be noted, however, that curve C is considerably higher (less residual strength reduction) in the early part of the fatigue life of the specimen than is curve B. Mathematically, this is a result of the fact that the small damage ratios in Equation 3 experienced in the early part of the fatigue life are raised to a higher power, making them smaller fractions during that period.

Curve D in Figure 15 represents the predictions of residual strength when the degradation slope is equal to  $-0.062$  and the power of the degradation ratio is equal to 1.2. Hence, that curve can be compared with curve A which differs from it only in the value of the degradation slope. Curve E is also similar to curve A except for a change in the power of the degradation ratio. The nonlinearity is very obvious in that curve and shows that relatively small changes in that power can make large differences in the strength predictions for a given specimen. Although it isn't obvious from the figure, several hundred calculations with the model suggest that the influence of the power on life is minor by comparison to the influence of the degradation slope, B.

Another important sensitivity of the mechanistic model is

demonstrated by the following discussion. Table 4 presents a sample of experimental data for Type C specimens subjected to essentially identical test conditions at a maximum strain amplitude of about 7,500  $\mu\epsilon$ . The maximum stress for each specimen is listed along with the life that was observed or the residual strength if the test was terminated before failure. It can be seen that one specimen failed after about 32,000 cycles of loading while two specimens went beyond one million cycles without failure. In fact, one of the specimens which went more than a million cycles without failure was subsequently tested and found to have a residual strength which was 9% greater than the average value determined from the quasi-static tests for that laminate. It can also be observed that the largest stiffness change did not correspond to the shortest specimen life although on the average it is true that the largest stiffness changes occurred in the specimens which failed after the smallest number of cycles of loading. The reader who is experienced in the field of fatigue will recognize that this variation in behavior is not unusual, nor is it peculiar to composite materials. From the standpoint of modeling, however, it does present a particular challenge, especially if one chooses to construct a model which is sensitive to the peculiarities of damage development in a given specimen and which is also capable of producing useful and representative behavior of laminates in general. The authors regard one of the particularly important strengths of the present model to be its capability to account for specimen differences because of its sensitivity to stiffness changes if they are available as

TABLE 4.

TYPE C 7500  $\mu\epsilon$  DATA  
R = 0.1

Specimen	Max. Stress (ksi)	Observed Life( $10^3$ )	Predicted Life( $10^3$ )	Observed	
				Change in Stiffness(%)	Change in Strength(%)
C7-3	53.8	58.9	---	22.6	---
C5-7	53.6	81.5	35	17.6	
C5-5	54.2	32.2	30	6	
C6-4	54.0	10+	---	5.1	-2.2
C7-11	54.2	1000+	---	6	-6.7
C8-4	53.4	1000+	440	5.4	+9

inputs to the model. For example, in Table 4 three predicted lives for widely different test data are shown for illustration. For specimen C5-5, the observed stiffness change in about 30,000 cycles was only 6%. The predicted life for that specimen was about 30,000 cycles compared to the observed life of about 32,200 cycles. For specimen C5-7 the stiffness change in 80,000 cycles was about 17% with a somewhat slower rate of stiffness change in the early part of the test than was observed for specimen C5-5. The corresponding life prediction was 35,000 cycles compared to about 81,000 for the observed test. If we then consider specimen C8-4 which had a stiffness change in one million cycles of only 5.4% we see that the model predicts a life of about 440,000 cycles which is an order of magnitude greater than the predictions for specimens C5-5 and C5-7 which were subjected to nominally identical test conditions. This sensitivity to degradation rates in individual specimens could not have been obtained from any other modeling approach which does not consider internal stress redistribution. From the standpoint of the practicing engineer, it means that the residual strength and life of individual specimens or engineering structural components can be anticipated by a model which is sensitive to the actual degradation that has occurred in that structure or specimen. This is believed to be critically important point since the load history of many structures is not generally known or cannot be anticipated precisely. The present model, however, could be used to predict the residual strength and life of such structures or components based on the results of periodic inspection.

We continue our sensitivity discussion by considering the tension-tension behavior of the Type D laminates which illustrate the sensitivity of the model to the accuracy of the determination of the local stress in the critical elements. These laminates are peculiar and special in the sense that only 10% of the laminates are zero degree plies, 45% are 45 degree plies and 45% are 90 degree plies. The stacking sequence was indicated earlier; the zero degree plies are on the exterior surfaces and on either side of the center line of the laminates. This particular stacking sequence was picked purely for its potential to create an extreme which would give us an opportunity to examine the limitations of our modeling procedure. The testing of specimens from that laminate produced exactly that kind of challenge. Figures 16, 17, and 18 illustrate typical results for an application of the model in the form described in the previous stages. A degradation slope of  $B = -0.07$  was used for those computations. The total amount of stiffness change observed for the data modeled in those figures was only about 8%. Figure 18 indicates that the strength reduction at one million cycles is predicted to be virtually zero. Figure 19 however, indicates that the residual strength reduction for one million cycles is typically about 6 or 7%. These results are typical of our attempts to apply the unrefined model to the Type D laminate. It is clear that the situation is characterized by strength reductions which exceed by considerable amounts the predicted strength reductions based on the observed stiffness changes and the local stress redistribution calculated from laminate analysis.

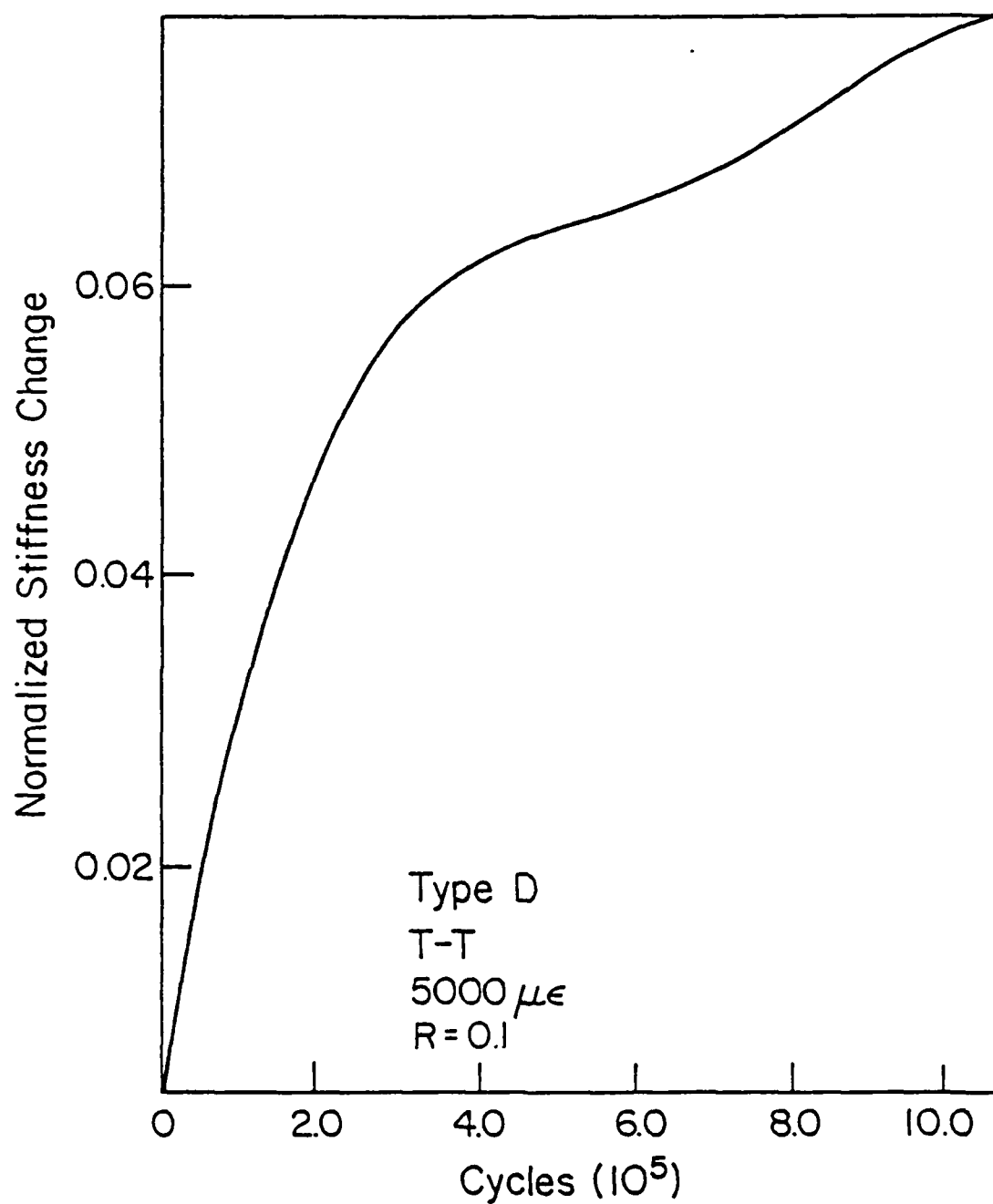


Figure 16. Curve Fit of Typical Stiffness Change Data for T-T Loading of Type D Specimens.



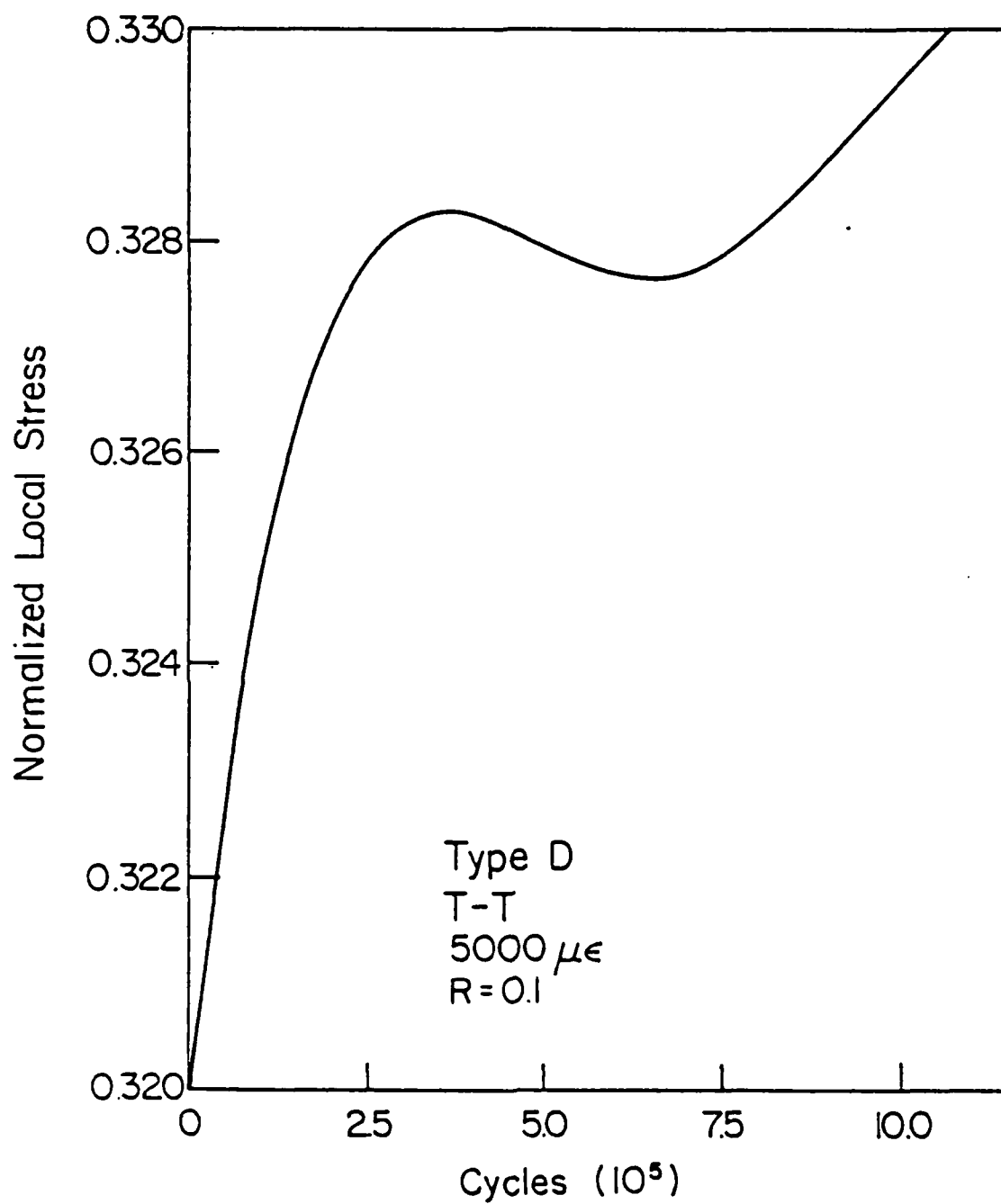


Figure 17. Estimate of Local  $0^\circ$  Ply Stress for Data in Figure 16.

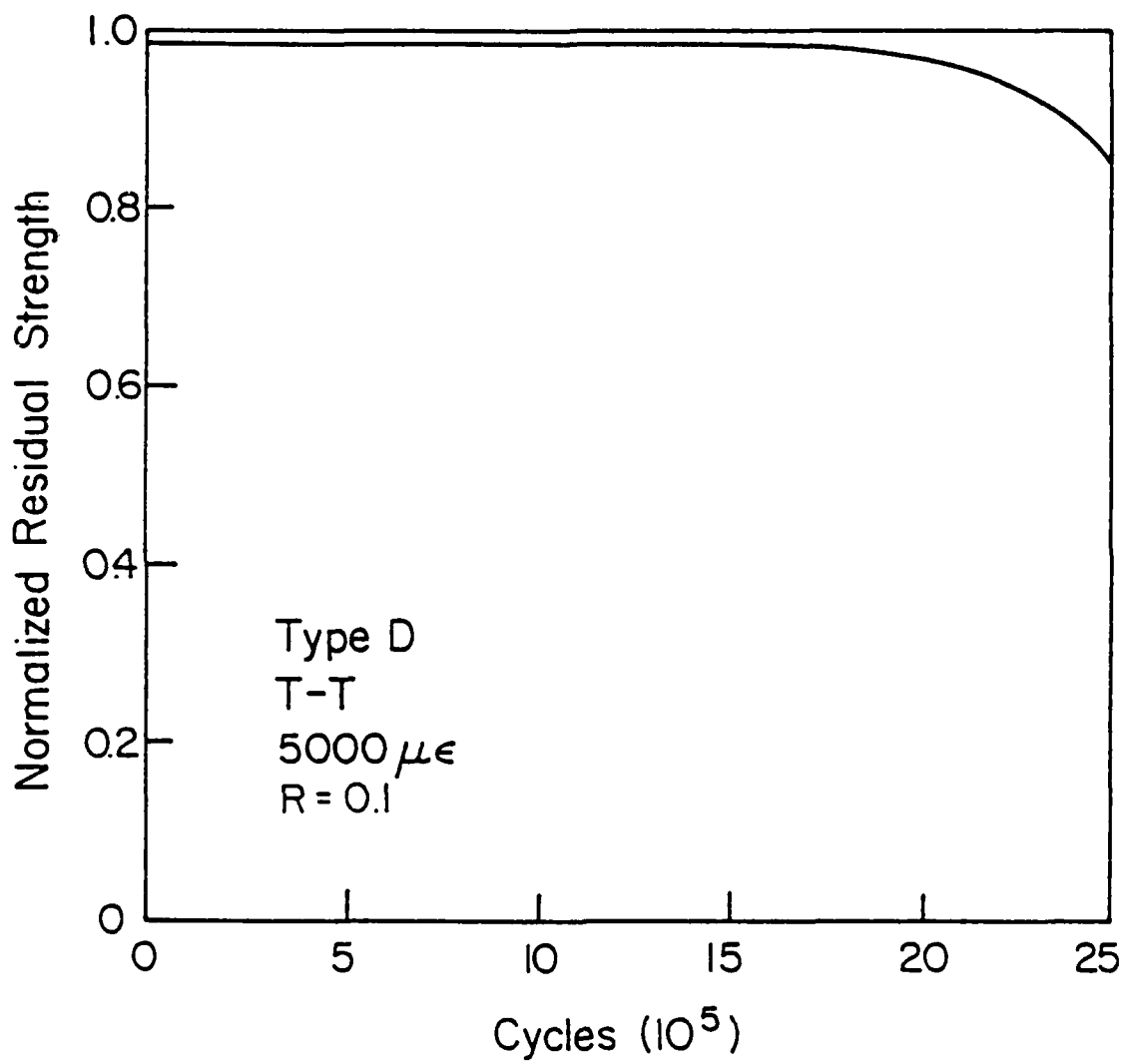


Figure 18. Predicted Variation of Residual Strength for a Type D Laminate.

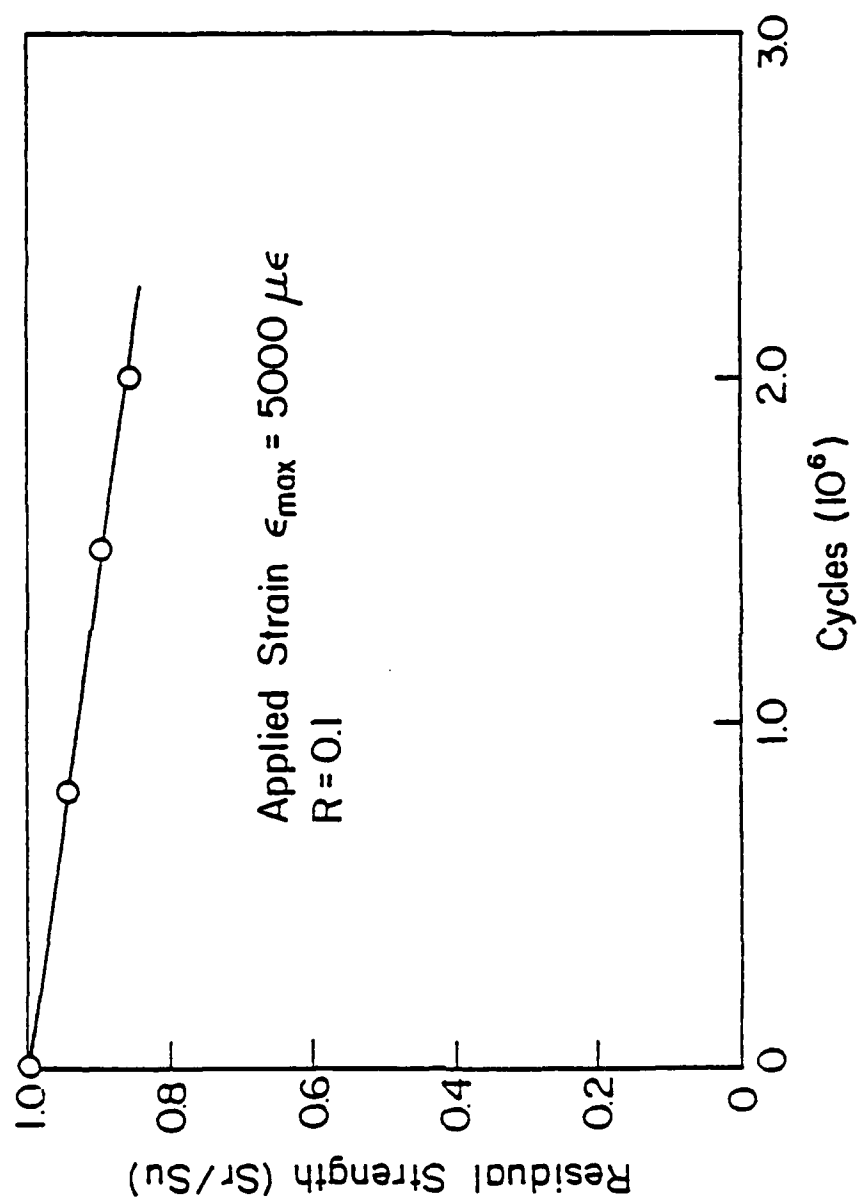


Figure 19. Change in Residual Strength for T-T Loading with a Maximum Strain Level of 5000 ue

Experimental observations during the testing of these laminates indicated that the cracks that formed in the off-axis plies (which are grouped in the sections between the 0 degree plies) had a strong tendency to couple together at a given cross-sectional position during the course of fatigue loading. It was hypothesized that this coupling process created a local geometry which resembled a crack having a total length equal to the combined length of the matrix cracks that coupled together, at least to the extent that they exerted a stress concentration on the remaining zero degree plies on the exterior and near the center-line. In order to estimate the resultant zero degree ply stresses which were caused by this process of coupling, it was decided to apply a shear-lag model to the local stress computation problem. However, it was important to recall that the geometry that is used for analysis must include the effect of the characteristic spacing of matrix cracks described earlier. That is, it is necessary to analyze the stresses in the zero degree plies when cracks forming in all of the off-axis plies couple together, but it is also essential to include in the problem the presence of a similar crack (or extended crack) at a distance which corresponds to the characteristic spacing of cracks in those off-axis plies that form a stable pattern with regular spacing, the so-called characteristic damage state. A shear-lag analysis (described in Reference 8) which was generated by Highsmith, et al., was chosen for this problem. Figure 20 shows a schematic of the geometry used for the analysis. The problem was formulated by considering an element of material between

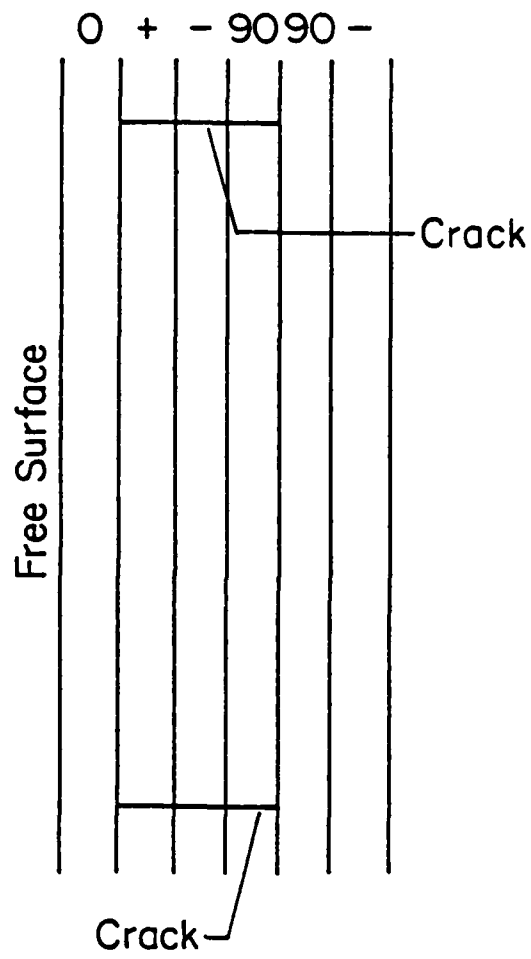


Figure 20. Schematic of Geometry Used for Shear-lag Analysis in Type D Laminates.

two cracks having a spacing corresponding to the equilibrium spacing measured (and predicted) for this laminate. Free surfaces at the crack faces and at the exterior surface of the zero degree ply in the laminate were required. Figure 21 shows the cases that were actually analyzed. Progressive crack growth from the first +45 degree plies through the subsequent -45,90,90,-45,+45,90,90 degree and remaining +45 degree plies were considered successively. Figure 22 indicates the crack opening displacement of the crack face for the longest crack considered as predicted from the analysis for a crack spacing of 0.035 inches. (The absolute amount of displacement is arbitrary.) It should be remembered that the shear-lag analysis is a net-section analysis in the sense that only one displacement function is used for each ply, so that the points in Figure 22 are really computed average values of the displacement in each of the plies indicated.

Figure 23 shows the results of the predictions of local stress using that analysis compared to the changes in stiffness which are also calculated from that analysis. If we were determining these quantities from a laminate analysis using the discount scheme, as indicated earlier, there would be a direct proportionality between the percent change in stress and the percent change in laminate modulus, as indicated by the diagonal trend line in Figure 23. The calculations, indicated by the curved line in that figure, show clearly that the local stress increases at a more rapid rate than the change in laminate modulus. For example, a change of 3% in the modulus yields a 12% local change in the axial normal stress in the zero

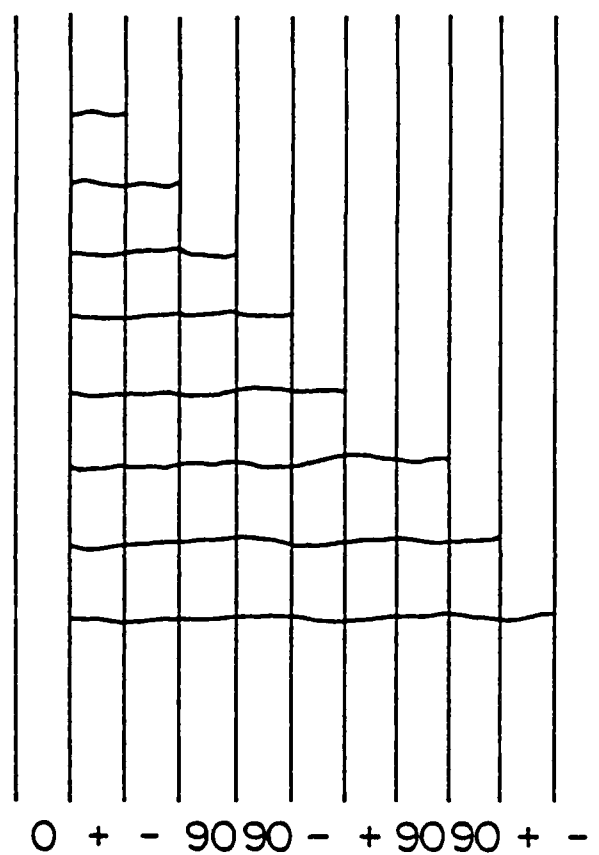


Figure 21. Cases of Crack Growth Analyzed for Type D Damage Analysis.

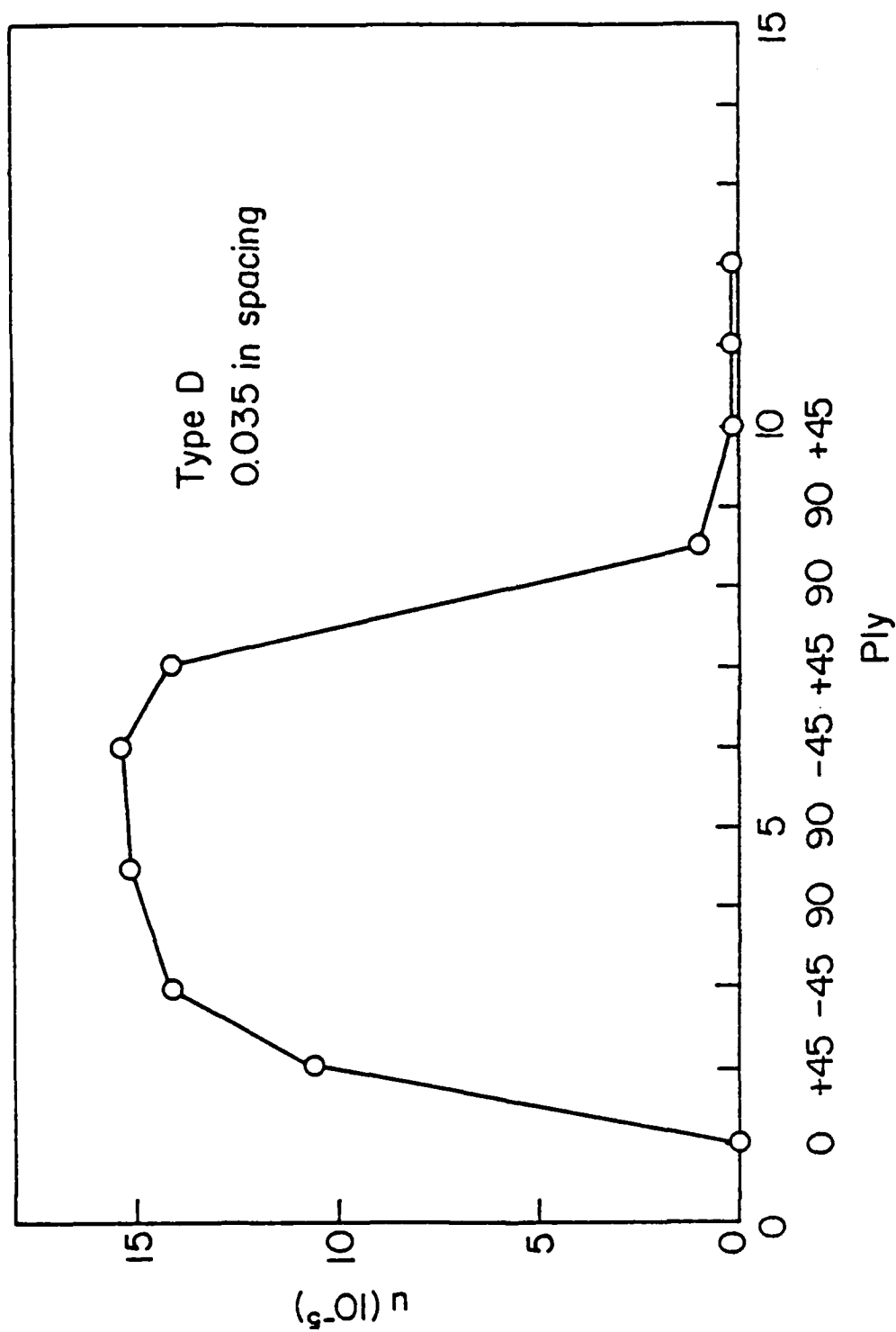


Figure 22. Crack Face Opening Geometry Predicted from Shear-lag Analysis for a Long Coupled Crack in the Type D Laminate.



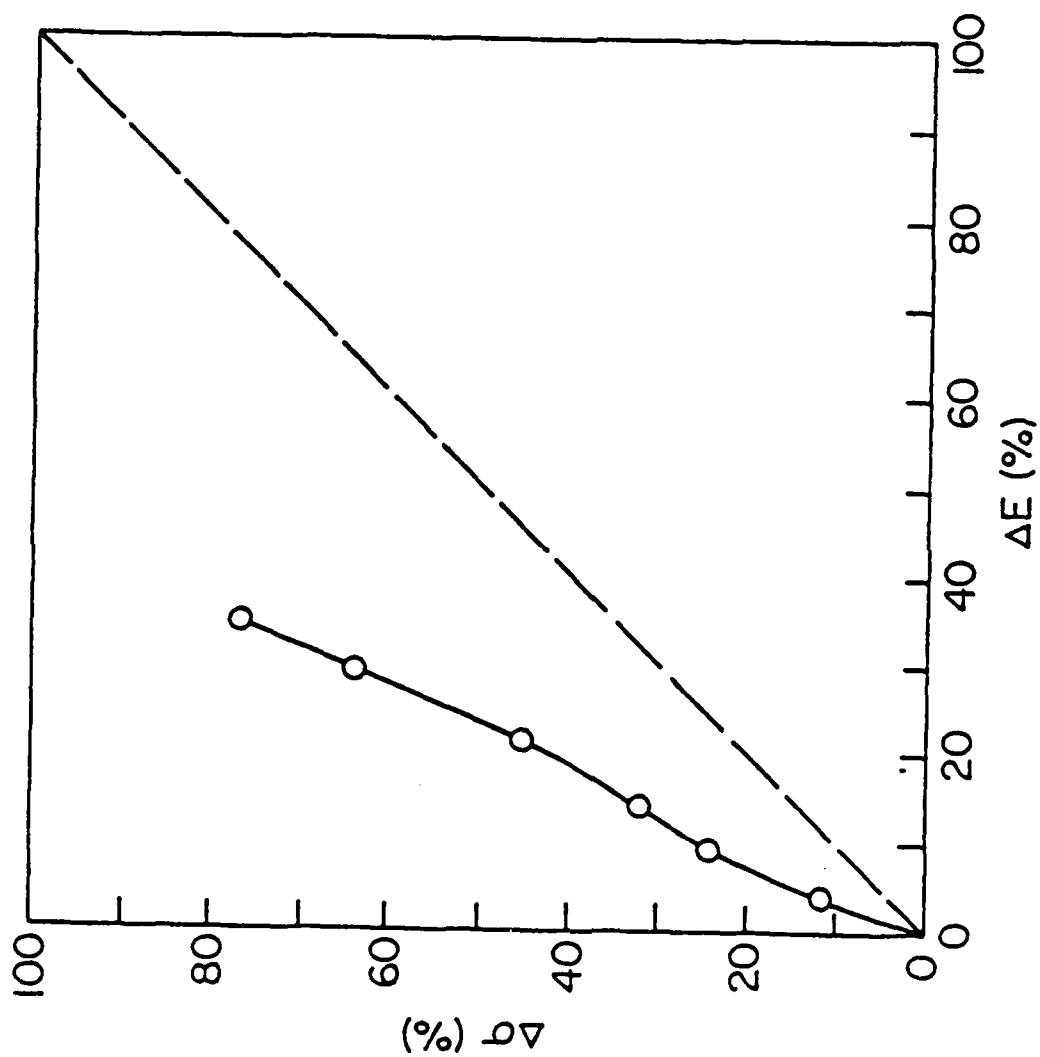


Figure 23. Comparison of Calculated Stiffness Change and Change in Local Axial Stress in the  $0^\circ$  Plies for Crack Coupling.

degree plies, corresponding to the crack formation in the 45 degree plies next to them. When both 45 degree plies and one 90 degree ply have cracked, the change in axial modulus is 13%, but the local stress changes by 32%. If the crack coupling extends throughout all of the off-axis plies indicated in Figure 21, a 34% modulus change should be observed and a 77% increase in the local stress is predicted.

In order to apply this to our cumulative damage model, we consider the test results for specimens D1-5, D2-10, and D2-12 which are observed to have a stiffness change of about 10% during tension-tension loading. According to our calculation, that stiffness change corresponds to a 26% change in local stress. Initially, the laminate applied stress is 21.4 ksi for those tests, which produces an axial normal stress in the 0 degree plies of 90.61 ksi calculated from laminate analysis. At one million cycles, after a 10% stiffness change and 26% local stress change, the stress in the zero degree plies is 113.3 ksi. If the strength of those zero degree plies is 230 ksi, the local stress ratio begins at a value of 0.394 and rises to a value of 0.492 (which equals  $113.3/230$ ) during the test. If a linear interpretation of that change is used in the cumulative damage model as described earlier, the predicted residual strength change shown in Figure 24 is obtained. A typical data point for the residual strength of 1.4 million cycles is also shown in that figure. It can be seen that the predictions are much more closely aligned with the observation. Comparison with the predictions in Figure 24 with the observations in Figure 19 confirm that in general the predictions are brought

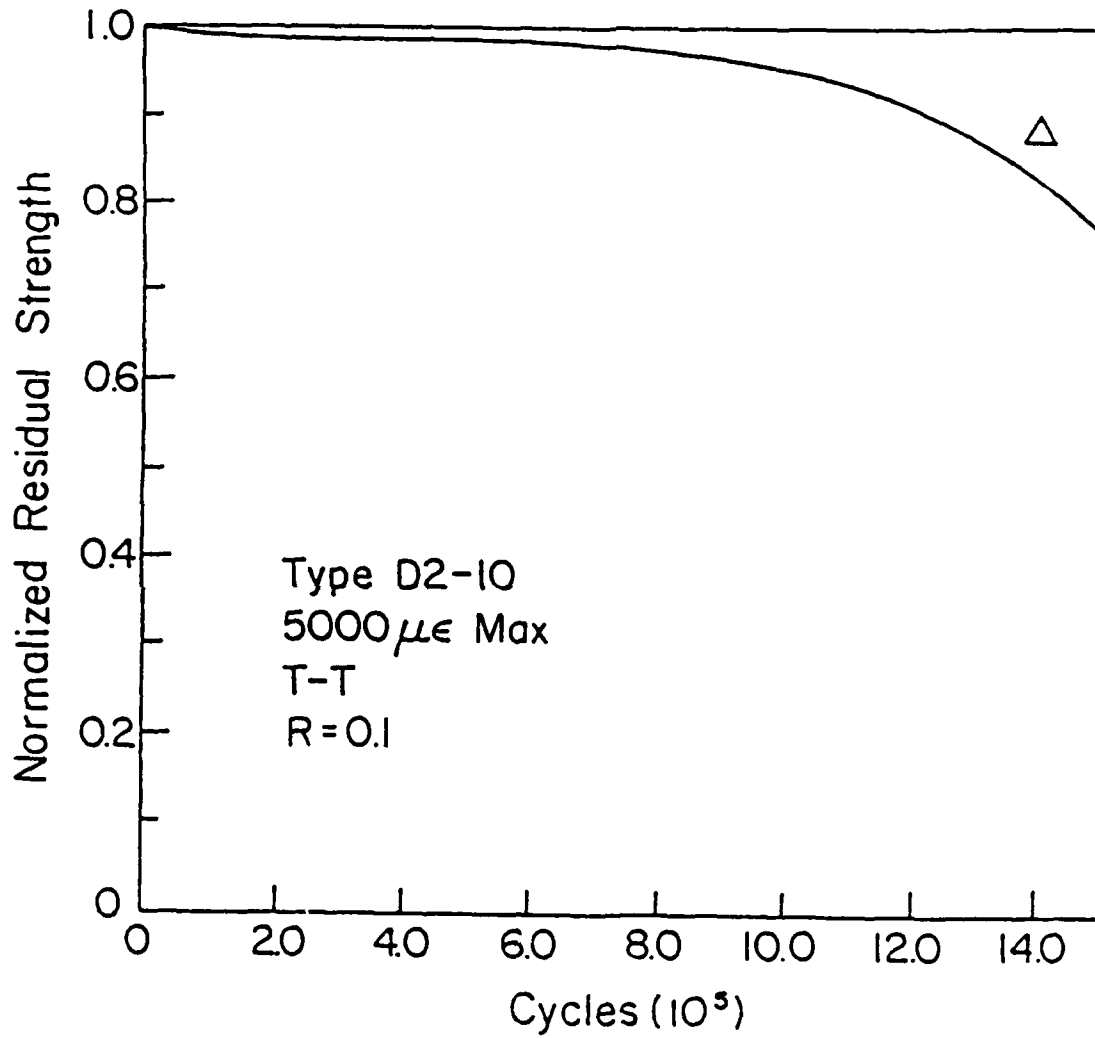


Figure 24. Residual Strength Prediction (Curve) and Typical Observation (Triangle) for a Shear-lag Refinement of Damage Accumulation Model.

into much better agreement with the data for this extreme case of stress redistribution. It is also possible to infer that better estimates of the local stresses in the zero degree plies obtained from more precise analyses, as they become available, can be used to obtain further improvements in the predictions of the model. It is important to note that local stress redistribution is an absolutely essential element of the correct modeling of cumulative damage in this laminate under fatigue loading. Finally, it is well to mention that the basic structure of the model was not altered to account for this extreme case; it was only necessary to improve the micromechanics (or minimechanics) models that are used to obtain the stress state in the critical elements.

This completes our discussion of the tension failure mode version of the model. We now examine the model for compression failure modes, and concentrate on demonstrative examples that demonstrate sensitivity as before.

### 3. COMPRESSION FAILURE

We now consider fatigue failure modes dominated by compression behavior. For this case the modeling of fatigue degradation, especially for the purpose of determining residual strength and life, is greatly complicated by a number of factors. Perhaps the most important of these is the fact that failure in compression loading is usually a stability problem, at least when the specimen is not side-supported as was the case in the present experiments. Parenthetically, it should be noted that for most applica-

tions in practical situations for which composite materials are commonly used, compressive failure usually involves macro-or micro-buckling of some type. The presence of buckling seriously constrains and complicates the interpretation of test data and the generality of any model of that behavior. Factors such as the precision with which the specimens are made, the degree to which the alignment of the specimen in the test machine is perfect, the accuracy with which the specimens are cut from the original plates, the absolute repeatability of all testing conditions, the degree of identity between the internal microstructure of each of the laminate specimens tested, and a variety of other realities contribute to an apparent variability in behavior which can be a serious obstacle to rational modeling.

We will examine two approaches to this problem attempted in the present investigation which appeared to have considerable utility. The first is a stiffness-based stability scheme and the other is based on critical delamination length. More complete discussions can be found in Reference 2.

One of the ideas which seemed to produce interesting modeling results was the use of a critical stiffness concept. The basis of this idea really lies within the association between stiffness and buckling. One possible scenario for the present objectives, based on that association, can be demonstrated by considering Equation 6,

$$\sigma_c = \frac{\pi^2 EI}{l^2 A} + \epsilon_c = \frac{\sigma_c}{E} = \frac{\pi^2 I}{l^2 A} \quad (6)$$

which is the familiar Euler Buckling Formula for a simple column. When that formula is rearranged in such a way that it describes a critical strain value, the remaining terms on the right-hand side of the equation are geometric (or other) constants. It is possible, then, to make the premise that buckling failure in compression loading occurs when the stiffness of the laminate (specimen) is reduced to the point where the critical strain is realized in the specimen for a given applied load, as suggested by Equation 7.

$$\epsilon_c = \frac{\sigma \text{ (applied, constant)}}{E(n) \text{ (measured, cycle dependent)}} \quad (7)$$

It is also possible to associate these concepts with the terms that one finds in Equation 3. One way of doing that is to associate the compressive aspects of damage development with edge delamination, an idea that is strongly supported by physical observations. Let us say, for example, that the stiffness reduction of the specimen during cyclic compressive loading corresponds to the stiffness reduction predicted by a linear relationship first stated by O'Brien as given in Equation 8.

$$E(n) = E_L + (E^* - E_L) \frac{a}{b} \quad (8)$$

In that equation,  $E_L$  is the initial modulus of the laminate,  $E^*$  is the completely delaminated modulus of the laminate,  $a$  is the length of the delamination growth, and  $b$  is the half-width of the specimen which is delaminating. Hence, The equation states that

as the delamination grows across a fraction of the width of the specimen given by  $a/b$ , the modulus of the laminate will be reduced to the value given by Equation 8 as a function of the number of cycles of loading. If one now combines Equations 7 and 8, and solves for the critical crack length,  $a_c$ , which corresponds to a critical reduction in stiffness, one obtains the expression given in relationship 9.

$$a_c = \frac{b(\sigma^0/\epsilon_c - E_L)}{E^* - E_L} \quad (9)$$

The stress entered in Equation 9 is the maximum absolute value of the applied stress in compression, a constant. Then in Equation 3, we take the ratio of the number of applied cycles to the total life of the specimen to be equal to the ratio of the current crack length to the critical crack length for buckling of the specimen as shown in Equation 10.

$$\frac{n}{N} + \frac{a}{a_c} = \frac{\sigma^0/\epsilon(n) - E_L}{\sigma^0/\epsilon_c - E_L} = \frac{E(n) - E_L}{\sigma^0/\epsilon_c - E_L} \quad (10)$$

As the equation shows, it is apparent that such a ratio is equal to the current change in stiffness divided by the critical change in stiffness. In order to maintain our normalized form of all the quantities to be entered into Equation 3, and to make our data interpretation scheme simpler, the final ratio to be used is expressed in normalized form as shown in Equation 11.

$$\frac{n}{N} = \frac{\Delta E(n)/E_L}{\Delta E_C/E_L} \quad (11)$$

Hence, Equation 3 takes the form shown in Equation 12.

$$\Delta S(n) = \int (1 - F_L(n)) \left( \frac{\Delta E(n)/E_L}{\Delta E_C/E_L} \right)^{i-1} d \left( \frac{\Delta E(n)/E_L}{\Delta E_C/E_L} \right) \quad (12)$$

We will examine the results obtained for two choices of the local failure function,  $F_L$ . In one case, that function was set equal to the critical value of the change in stiffness divided by the initial laminate stiffness. In the second case, that function was set equal to the simple ratio of the laminate applied stress to the buckling stress of the laminate measured in quasi-static compression. Similar results were obtained for the two situations. We will examine some typical examples of those results below, for compression-compression loading.

Stiffness changes observed during cyclic compression-compression (C-C) loading were large. An example of those changes is shown in Figure 25 for four levels of cyclic loading corresponding to the microstrain ranges indicated in that figure on each of the curves. Fifty percent reductions in (compressive) stiffness were common. In order to enter those changes into Equation 12, the fractional stiffness change as a function of cycles is needed. Curves were fitted to the data for those fractional stiffness changes. These fractional stiffness changes were entered into Equation 12 as described earlier, and the local failure function,  $F_L$ , was set equal to the ratio of the applied



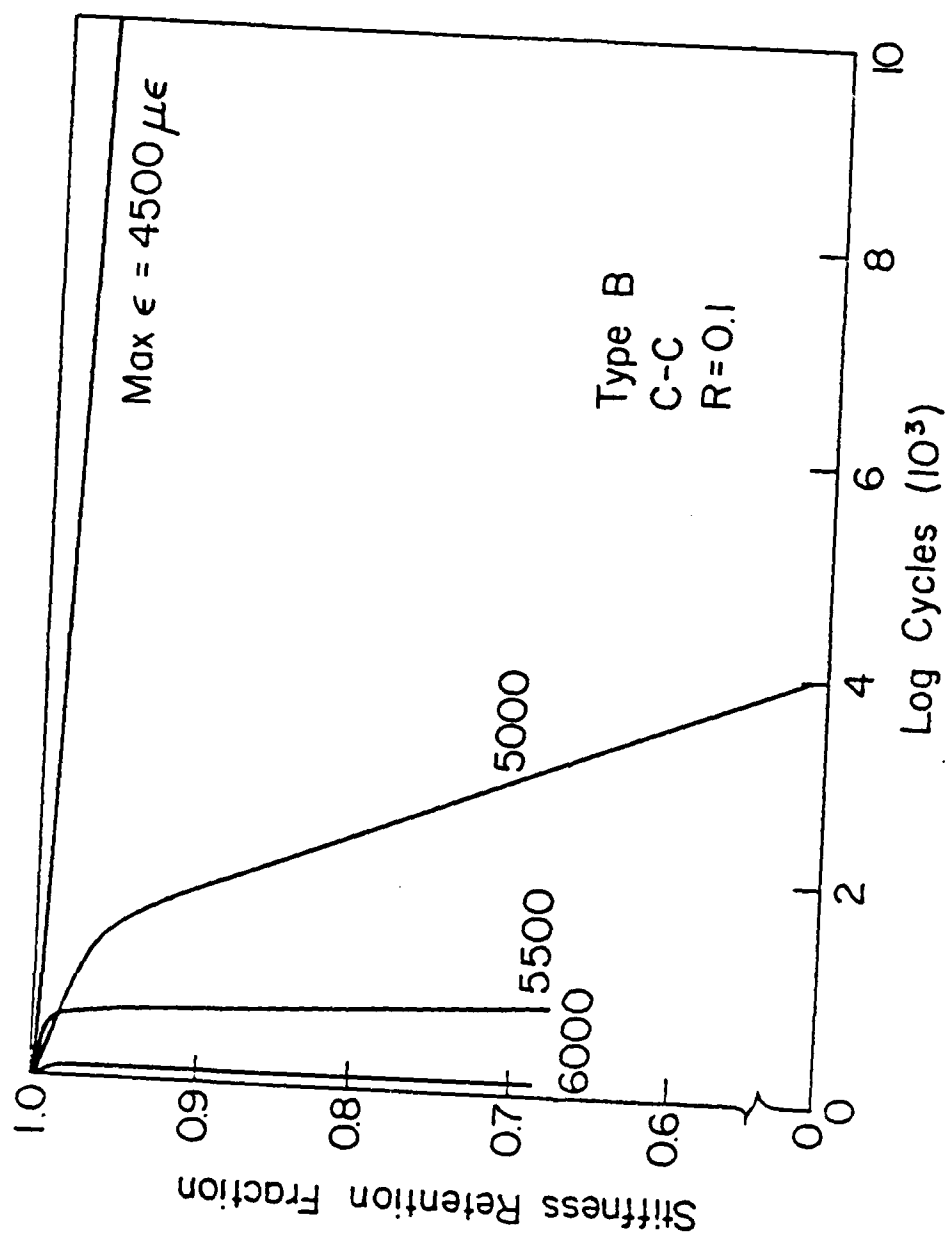


Figure 25. Stiffness Retention Fraction for Several C-C Tests of Type B Specimens.

strain level to the critical strain level for buckling, a ratio which is equivalent to the ratio of applied to ultimate stress. However, it was found that the buckling strain under quasi-static loading was not appropriate as a critical (normalizing) strain for the ratio to be used for  $F_L$ . It should be remembered that failure under C-C loading was controlled not only by the buckling of the specimen, but by the dynamic response of the test system including the test machine and the specimen itself. Failure was actually defined under cyclic loading as that point at which the specimen became so compliant that the test machine was unable to cycle over the compressive stress range that had been set as a required constant. Such a situation can hardly be ascribed the significance of a material constant! It was found that the critical dynamic strain for buckling under cyclic loading was about 12,400  $\mu\epsilon$ . That quantity was used in the denominator of the ratio  $F_L$ . The applied strain range was the numerator.

The resulting calculations of residual strength and life are shown in summary form in Figure 26. The corresponding maximum compressive stress ranges are also indicated on that figure. The data in that figure indicated that the agreement between the cumulative damage model and the experimental information is reasonably good. It is important to recall, however, that the model in this form includes relatively little information about the specific degradation mechanisms that are responsible for the fatigue performance in compression loading. Only the concepts of stiffness reduction and critical strain to failure have been used. Although edge delamination was mentioned and used to establish a model for the stiffness reduction, strictly speaking no

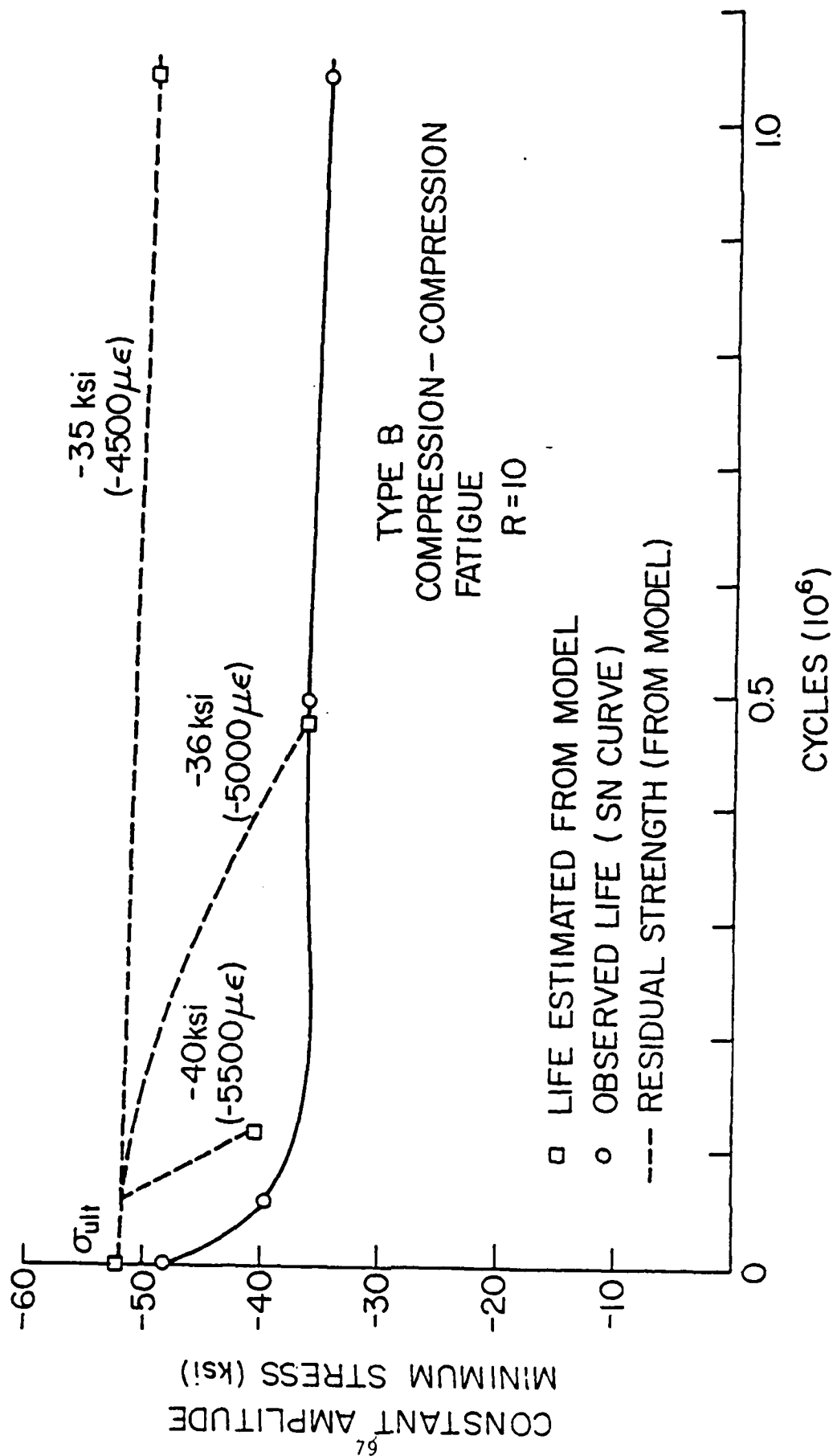


Figure 26. Summary of Predictions and Observations for C-C Loading of Type B Laminates.

specific information from the delamination concept is used in this form of the model. To examine the results of the second scheme of this type, we consider the tension-compression loading of Type D specimens.

A typical set of stiffness retention curves measured from specimens tested at several stress amplitudes (the corresponding strain amplitudes are indicated in the figure) are shown in Figure 27. However, the specimens did not fail at the point which corresponds to the last measurement of stiffness change that could be made before the specimen failed. Specimen D2-5 failed at 440,000 cycles, and specimen D2-8 failed at about 110,000 cycles, for example. From a variety of these kinds of observations, it was decided to attempt to extrapolate the stiffness retention curves to the number of cycles at failure to estimate the critical stiffness change for these laminates. The value obtained from that procedure for several widely different test conditions was surprisingly similar and was averaged to obtain a critical stiffness change fraction of about 0.27. That critical fraction was used as the normalizing denominator in Equation 12 for the calculations for the Type D laminates. The local failure function,  $F_L$ , was taken to be simply the strain amplitude divided by the critical strain amplitude for buckling determined from the quasi-static tests for each case. The fractional stiffness change for the tests shown in Figure 27 were put into the resulting model. A summary of some of the predicted and observed results is shown in Figure 28. The predictions of life are virtually coincident with the observations for the two lower 5,000  $\mu$ e are also quite close together. Hence, this interpretation of the model

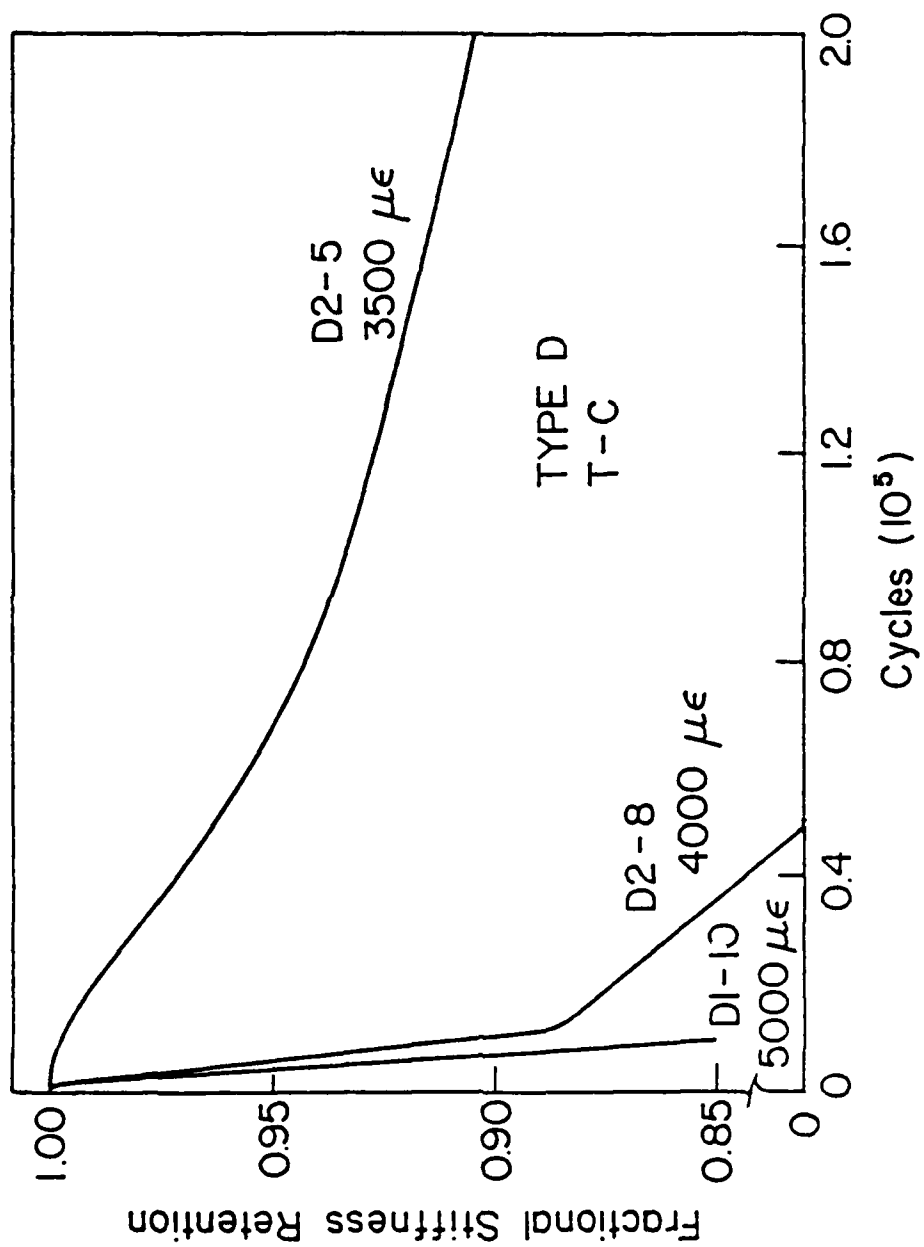


Figure 27. Fractional Stiffness Change Measured During T-C Loading of Type D Laminates.

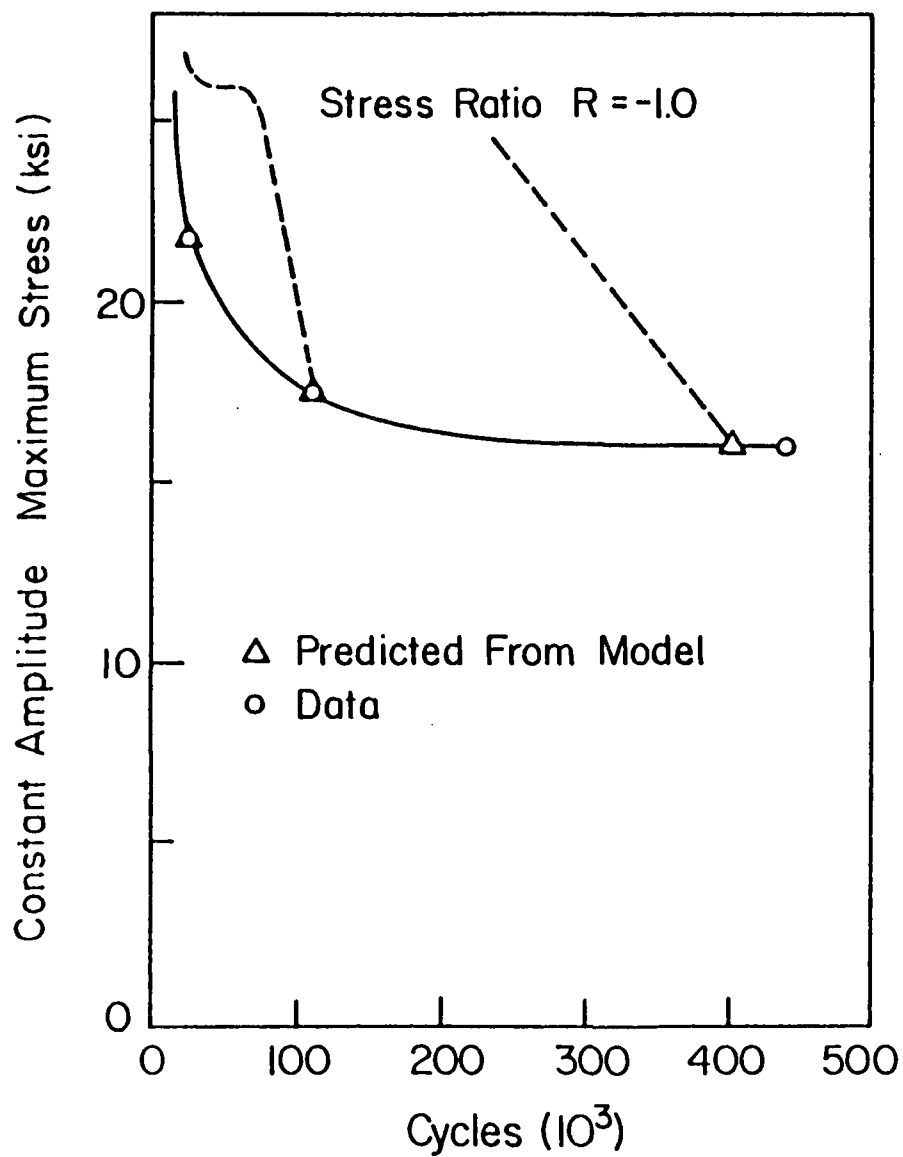


Figure 28. Summary of Observed and Predicted Data for T-C Loading of Type D Laminates Using Critical Stiffness Model.

appears to produce reasonable results.

We have mentioned earlier that the experimental behavior of the coupon specimens tested from the six laminates considered in this program was greatly affected by combined tension-compression loading in comparison to tensile or compressive loading alone. The experimental observations indicate that a very complex pattern of damage develops in that situation. One major aspect of that damage development is the influence and interaction of the transverse matrix cracks that form in tension with the edge delamination that forms and propagates predominantly during compressive load excursions. This interaction appears to be synergistic in the sense that the rate of delamination growth appears to be greatly enhanced by the presence of the matrix cracks. This is not surprising in view of the fact that large interlaminar stresses are known to occur at the tip of the transverse matrix cracks, stresses which certainly contribute to the tendency for the interface between the plies to separate. There is a great need for a vigorous research program to determine the details of this highly complex process. Some basic investigations are presently under way at Virginia Tech. It was not possible to resolve these issues during the course of the present investigation.

In an effort to include some aspects of the mechanisms involved, the cumulative damage model for T-C loading was altered to include the edge delamination mechanism. The form of the damage summation equation used for that purpose is given in Equation 13.

$$\Delta S(n) = (1 - F_r(n)) = \int (1 - E^*/E_L) d\left(\frac{a}{b}\right) \quad (13)$$

All of the quantities in that equation have been introduced earlier. The reader will recall that  $E^*$  is the longitudinal stiffness of a laminate which has completely delaminated along a given interface. The ratio  $a/b$  is the length of the delamination compared to the width of the specimen. Based on considerable evidence in the literature, we make the assumption that the crack length,  $a$ , is determined from the integral of a power law relationship between the rate of crack propagation and the strain energy release rate,  $G$ , as indicated in Equation 14.

$$a = a(n) = \alpha \int \mathcal{L}^\beta dn \quad (14)$$

The quantities  $\alpha$  and  $\beta$  in that equation are constants (References 16 and 17). If we assume that the strain energy release rate includes all modes of crack propagation, then we can use an expression introduced by O'Brien (Reference 16) to write

$$\mathcal{L} = \mathcal{L}(n) = \frac{\epsilon^2 t}{2} (E_L - E^*) \quad (15)$$

where  $\epsilon$  is the applied laminate strain,  $t$  is the laminate thickness and the other quantities have the values introduced earlier. We can also use an expression introduced by O'Brien for the



laminates stiffness as a function of the length of the delamination to write the laminate strain as a function of the number of applied cycles for a fixed value of applied stress,  $\sigma^a$ .

$$\epsilon = \epsilon(n) = \frac{\sigma^a}{(E^* - E_L) \frac{a}{b} + E_L} \quad (16)$$

Hence, the model can be used if the constants  $\alpha$  and  $\beta$  are known and if the value of the laminate stiffness for complete delamination,  $E^*$ , has been calculated.

The form of Equation 13 was chosen based on the following rationale. Equation 13 can be written in the following form:

$$(1 - F_r) = (1 - \sigma_r/\sigma_u) = (1 - E^*/E_L) \frac{a}{b} \quad (17)$$

If we assume that stress redistribution is to be ignored, so that all of the quantities in that equation and the Equations 15 and 16 mentioned above become independent of the number of cycles of load application,  $n$ , then we can also write

$$\sigma_r/\sigma_u = (E^*/E_L - 1) \frac{a}{b} + 1 = \frac{[(E^* - E_L) \frac{a}{b} + E_L] \epsilon_c}{E_L \epsilon_c} \quad (18)$$

where the propagation length,  $a$ , can be determined by integration by quadratures of Equation 14. The critical strain,  $\epsilon_c$ , in Equation 18 can be regarded as the critical strain to failure in a quasi-static test. Equation 18 can be rearranged as shown in

Equation 19.

$$\sigma^r = [(E^* - E_L) \frac{a}{b} + E_L] \epsilon_c \quad (19)$$

That equation can be read as stating that the residual strength of a laminate which is delaminating is equal to the reduced stiffness times the critical strain of that laminate measured from a quasi-static test. O'Brien has reached a conclusion of this type in an earlier investigation (Reference 18).

In order to apply this model, it is necessary to anticipate or to observe the delamination interfaces in a given laminate. From that information a laminate analysis can be used to estimate the completely delaminated modulus,  $E^*$ , from which the stiffness for a given crack length can be determined, and from which the strain and strain energy release rate can be determined using Equations 16 and 15. Then Equation 14 will yield a crack length (or an increment of crack length) and Equation 13 can be used to determine the amount of incremental change in residual strength. The process can then be iterated, the crack length increased by some increment, Equation 16 applied to find the strain, Equation 15 applied to find the strain energy release rate, and a new increment of crack length found from (a numerical integration of) Equation 14. We will look at a variety of calculations of this type. However, a second scenario is also possible. If the stiffness change of the specimen has been measured, or is otherwise available, one can use the measured stiffness change as

AD-A165 688

CUMULATIVE DAMAGE MODEL FOR ADVANCED COMPOSITE  
MATERIALS(U) GENERAL DYNAMICS FORT WORTH TX FORT WORTH  
DIV H R MILLER ET AL. JUN 85 AFWL-TR-85-4069

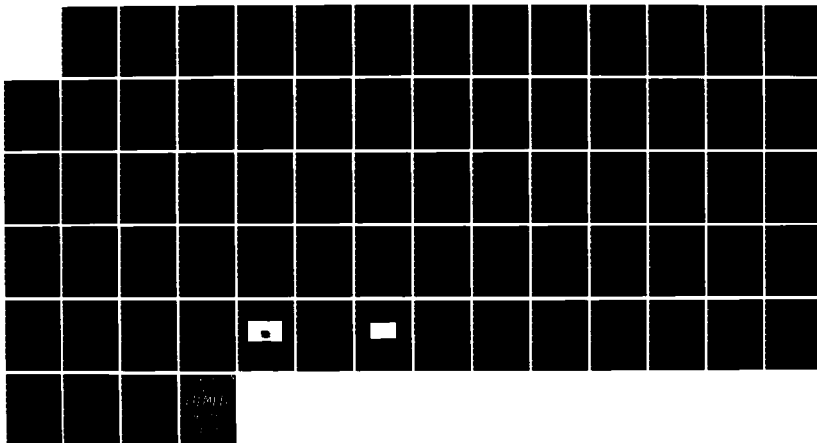
2/2

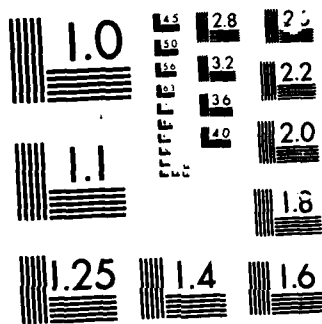
UNCLASSIFIED

F33615-81-C-5049

F/G 11/4

NL





MICROCOPY RESOLUTION TEST CHART

applied stress level to determine the laminate strain,  $\epsilon$ , and then proceed to Equations 15, 14, and 13. This interpretation will also be demonstrated in the following paragraphs, and the two approaches will be compared.

We begin by considering the application of this model to the Type C laminate. The reader will recall that the Type C laminate is a quasi-isotropic stacking sequence with the 90 degree plies interspersed between the 45 degree plies in the laminate. The experimental data indicates that delamination is likely to occur in that laminate at two different types of interfaces, the 0/+45 and the +45/90 interfaces. The Poisson mismatch for delamination along the 0/+45 interface is essentially zero since the transverse Poisson's ratio of the zero degree ply is about 0.31 which is essentially the same as the rest of the laminate. Hence, the calculation of the delaminated modulus,  $E^*$ , was done assuming that the +45/90 interface delaminates. The calculation was conducted by considering the stiffness of a 0,+45 degree sublaminates and 90,-45,-45,90,+45,0 degree sublaminates. Following the suggestion of O'Brien, (Reference 16) the delaminated modulus was calculated using a rule of mixtures concept, i.e., the delaminated modulus was set equal to the summation of the products of the moduli of the sublaminates times the number of plies in each of those sublaminates divided by the total number of plies in the total laminate. Hence, the delaminated modulus for Type C material was calculated as shown in Equation 20.

$$E^* = \frac{2(11.569) + 6(6.4) + 2(8)7.844}{24} = 7.793 \quad (20)$$

In that equation, the stiffness of the first sublamine mentioned above is 11.569 msi, the stiffness of the second sublamine mentioned is 6.4, and the stiffness of the remaining (undelaminated) laminate is 7.844. Hence, for a single delaminated interface, the delaminated modulus is 7.793 msi. These values are calculated from laminate analysis using the stiffnesses of the single plies tested in the quasi-static baseline series mentioned earlier. The actual value of the measured modulus of this laminate was 7.31 msi. Hence, it was assumed that the delaminated modulus was 7.26 msi when a single interface delaminates on each side of the centerline of the specimen. It should be mentioned that the experimental observations suggest that delamination begins at the interface in the sublamine that is closest to the outside surface of the laminate. As the damage develops, delaminations initiate at the same type of interface in sublamines which are further from the surface in the thickness direction. Hence, the initiation process is progressive beginning at the exterior surfaces of the specimens and progressing toward the interior centerline of the laminates. Based on these observations, it was decided to postulate that laminate failure was controlled by the initiation and propagation of the outermost delamination, and that failure was defined by the incidence of that delamination progressing across the total width of the specimen. Hence, in the computer code used for the computation of the residual strength degradation, an undelaminated value of the laminate stiffness of 7.31 was used and a completely delaminated value of 7.262 ksi was used.

The next matter of substance that needs to be considered to

apply the model was the power law that characterizes the rate of delamination propagation in terms of the strain energy release rate,  $G$ . The most fundamental question involving that power law is the interpretation of the strain energy release rate. Depending upon the laminate type and stacking sequence, and upon the interface which delaminates, various modes of crack growth may be appropriate (crack opening mode, shear mode, etc.). If we assume that a shear mode is dominating the process for our situation, then one might be tempted to use values quoted in the literature which suggest that the coefficient of the power law should be something like 0.016 and the power should be something like 7.218 in English units (Reference 17). However, it was found that in order to match the data for the Type C laminate, a value of the coefficient of about .016 was appropriate, but a power of about 10.7 was a better fit. Since we did not have the opportunity to conduct the basic studies necessary to establish the appropriate analytical or experimental form of that equation by other means, a set of values for the power and coefficient were determined from an initial fit of one set of data, after which those quantities were held constant for all other predictions. However, it should be mentioned that this choice of power in the propagation rate equation greatly influences the delamination length at a given number of applied cycles. This is illustrated by the information shown in Figure 29 which portrays the delamination length calculated for a given coefficient and three different powers of the strain energy release rate quantity. There is a substantial need for greater understanding of this sensitivity.

To indicate the applicability (or at least the internal

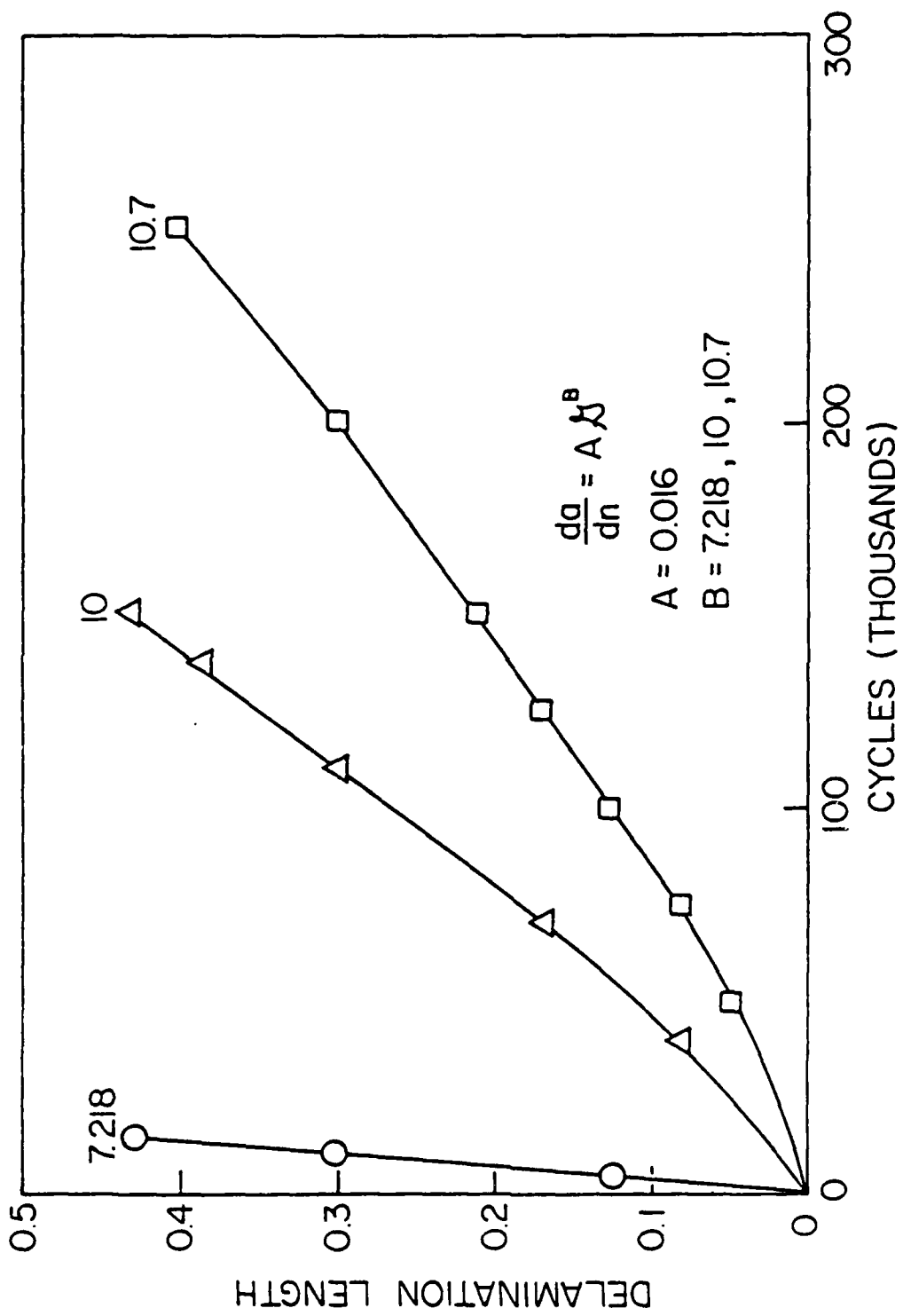


Figure 29. Parameter Study of the Power of the Delamination Growth Law.



consistency) of this delamination model, we will consider the block loading results discussed in the data section. Two sets of the block loading will be discussed, set 2 and set 3. The set 2 consisted of one block of loading of 150,000 cycles with a fully reversed strain amplitude of 3,500  $\mu\epsilon$ , followed by a second block of fully reversed loading at 4,500  $\mu\epsilon$  until failure occurred. Table 6 shows some typical results of that type of loading. For the three tests indicated in that table, the average life observed for set 2 loading was 183,000 cycles. Set 3 loading consisted of a block of tension-tension loading with an R value of 0.1 having a maximum strain level of 4,000  $\mu\epsilon$  for 150,000 cycles followed by fully reversed tension-compression loading at a strain amplitude of 4,000  $\mu\epsilon$ . Table 5 indicates that the average life for the three tests shown there was 474,000 cycles.

The delamination propagation model described above was applied to these block loading situations. The initial value of the strain energy release rate,  $G$ , was calculated from the initial strain (determined by dividing the applied stress by the initial modulus), the laminate thickness, and the difference between the fully delaminated modulus and the initial modulus of the laminate as indicated in Equation 15. Thereafter, as the number of cycles was incremented, the strain was increased according to Equation 16 based on the calculations of current crack length from Equation 14. The summation of the change in residual strength was determined from Equation 13 using an appropriate computer code. Equation 14 was integrated numerically. The results of those calculations are also shown in Table 5. For set 2 loading, the predicted life is about 173,000 cycles compared with the observed

TABLE 5.  
RESULTS OF BLOCK LOADING TESTS AND PREDICTIONS

<u>Set</u>	<u>Specimen</u>	<u>Block</u>	<u>Cycles (thousands)</u>	<u>Average Life (thousands)</u>	<u>Predicted Life<sup>1</sup> (thousands)</u>	<u>Percent Error</u>
2	5-6	1	150	183	173	5.4
		2	57			
	7-6	1	150			
		2	32			
	8-7	1	150			
		2	11			
3	8-5	1	150	474	451	4.8
		2	327			
	7-4	1	150			
		2	313			
	7-8	1	150			
		2	232			

<sup>1</sup> delamination law driven calculation

TABLE 6.  
RESULTS OF BLOCK LOADING TESTS AND PREDICTIONS

<u>Set</u>	<u>Specimen</u>	<u>Block</u>	<u>Cycles (thousands)</u>	<u>Average Life (thousands)</u>	<u>Predicted Life (thousands)</u>	<u>Percent Error</u>
2	5-6	1	150	183	173 <sup>1</sup> 195 <sup>2</sup>	5.4 7
		2	57			
	7-6	1	150			
		2	32			
	8-7	1	150	(250) <sup>3</sup>	(222) <sup>3</sup>	11
		2	11			
	8-5	1	150	474	451 <sup>1</sup> 486 <sup>2</sup>	4.8 3
		2	327			
3	7-4	1	150			
		2	313			
	7-8	1	150			
		2	232	(600) <sup>3</sup>	(490) <sup>2</sup>	18

<sup>1</sup> delamination law driven calculation

<sup>2</sup> measured stiffness change driven calculation

<sup>3</sup> block 2 without previous block 1; calculation using estimates of stiffness change data

average life of 183,000. The difference of 5.4% is certainly tolerable. For Block 3 loading, the calculated life of 451,000 cycles compares well with the observed average life of 474,000 cycles, a difference of 4.8%. Hence, based on these limited results, the model appears to be self-consistent and to produce reasonable predictions, even for block loading situations.

Two very important points should be made here. First of all, the value of strain used in Equation 15 to calculate the strain energy release rate is the total strain range, not the strain amplitude. One can justify this choice on the basis of a variety of philosophies. The principal motivation for the authors was provided by the apparent importance of the shear stresses in the delamination process. If the interlaminar shear stresses are, indeed, a major part of the driving force for the delamination propagation, then a strain range (or stress range) is a more appropriate quantity to use in the propagation equation than a strain (or stress) amplitude, since the sign of the shear stress is immaterial to the process. Ultimately, the most convincing argument for the use of the strain range is the success and utility of the idea.

The second important matter to be mentioned is that the block loading was handled in the calculations mentioned above by using the delaminated crack length obtained in the first block of loading as a starting point for the second block of loading, an initial crack length concept. While this is consistent with the physical idea of the mechanism involved, a variety of other choices are certainly possible.

During the course of these computations it became apparent

that another possible interpretation of the damage model described above would be useful. The reader will recall that the computed value of laminate strain as a function of the number of applied cycles was determined from Equation 16 using the constant applied stress amplitude,  $\sigma^a$ , divided by the current laminate modulus, determined from an equation which estimates that value based on the amount of delaminated fractional width and the difference between the undelaminated and delaminated modulus. Hence, the model actually produces a predicted stiffness change as a function of cycles which, in turn, is used to estimate the current laminate strain. A comparison of these calculated changes in laminate stiffness with the observed values indicated that the stiffness changes were being underestimated by the model. One simple remedy for this situation is to use the measured values of stiffness change to compute the strain range as a function of the number of applied cycles and to enter that value into the calculation of the strain energy release rate according to the Equation 15. While it is true that this approach depends upon having measured values of stiffness change or upon having a method of estimating those changes, it was decided that such a model should be examined since it has the capability of incorporating more of the reality of the tests. Hence, a refined version of the model was programmed and a number of calculations made. A representative group of those calculations will be described below.

We will begin by considering the Type C laminate. We use an initial data set to "calibrate" the model as we have done earlier. For that purpose we analyze specimen C5-11 which has a stiffness change throughout the test of about 13%. We mention in

passing that these large stiffness changes exceed the values calculated from delamination concepts, at least in part because of the contribution of transverse cracking and the coupling between transverse cracking and delamination which is not accounted for in the earlier delamination model. As one would expect, this significant decrease in the modulus tends to increase the laminate strain by a comparable amount, and since the strain energy release rate depends on the square of that quantity, the crack propagation rate is accelerated greatly. Hence, it is not too surprising that the coefficient of the power law becomes 0.008 and the power of that propagation relationship becomes about 15 in order to obtain a match between the model and the data for that specimen. For that choice, there is essentially an identity between the predicted life of 77,000 and the observed life of about that value. However, while the strain energy release rate,  $G$ , was virtually constant during the delamination process in the previous model, it changes dramatically during the process modeled by this form of the equations. Hence, the integrations in Equations 18 and 19 perform a very necessary function since the arguments become strongly dependent upon the number of cycles,  $n$ . The cyclic stress amplitude for specimen C5-11 is 32.1 ksi which corresponds to a strain amplitude of about 3,900  $\mu\epsilon$ . The total strain range was used in the model as before. The values of the delaminated and undelaminated moduli for the Type C specimens calculated earlier were also used for this computation.

Having indicated how to select the parameters in the model, we attempted to predict the results for other specimens. Specimen C7-1 was oscillated at a stress amplitude of about 35.7 ksi.

A stiffness change of about 6% was observed for that test. The calculated life for that specimen was about 12,500 cycles compared to an observed life of about 18,000 cycles. Specimen C8-8 was cycled at a stress amplitude of about 28.6 ksi which corresponds to a total strain range of about 7,820  $\mu\epsilon$ . A stiffness change of about 8% was observed during that test. The calculated life for that situation was 325,000 cycles compared to an observed life of about 328,000 cycles. Data for specimen C6-2 at the intermediate strain level is also shown on Figure 30. Agreement between predicted and observed results is excellent. Of course, we must remember that the model was set up to match one of these data points precisely, and we should also remember that the measured stiffness changes have a very strong influence on the accuracy of the model. To test the strength of this modeling concept, other situations should be examined.

We return now to the block loading results described earlier, and examine our predictions using this second form of our compression failure mode model. For the purpose of our computations, we require that stiffness changes be used. For that purpose we consider the data in Figure 31 collected during the typical tests indicated there. We consider the Set 2 sequence and observe that during Block 1 loading stiffness change of 1.5% is observed. A polynomial is fit to the resulting specimen axial strain over the course of  $4 \times 10^5$  cycles of loading and used as input to the model. Block 1 of Set 2 loading consists of fully reversed cycling at a strain amplitude of about 3,500  $\mu\epsilon$  for 150,000 cycles. That computation produces a predicted delaminated crack length of about  $6.2 \times 10^{-5}$  inches. While it is true that this

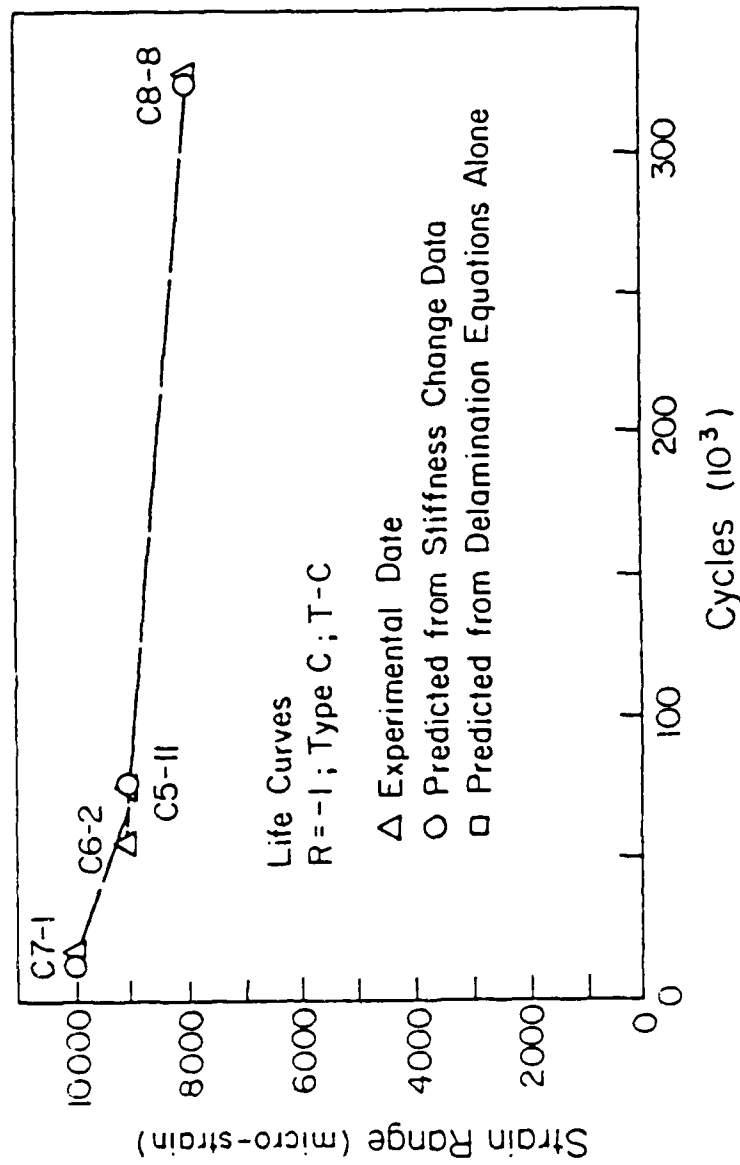


Figure 30. Predicted (Circles) and Observed (Triangles) Life Data for T-C Model Which Uses Observed Stiffness Changes.



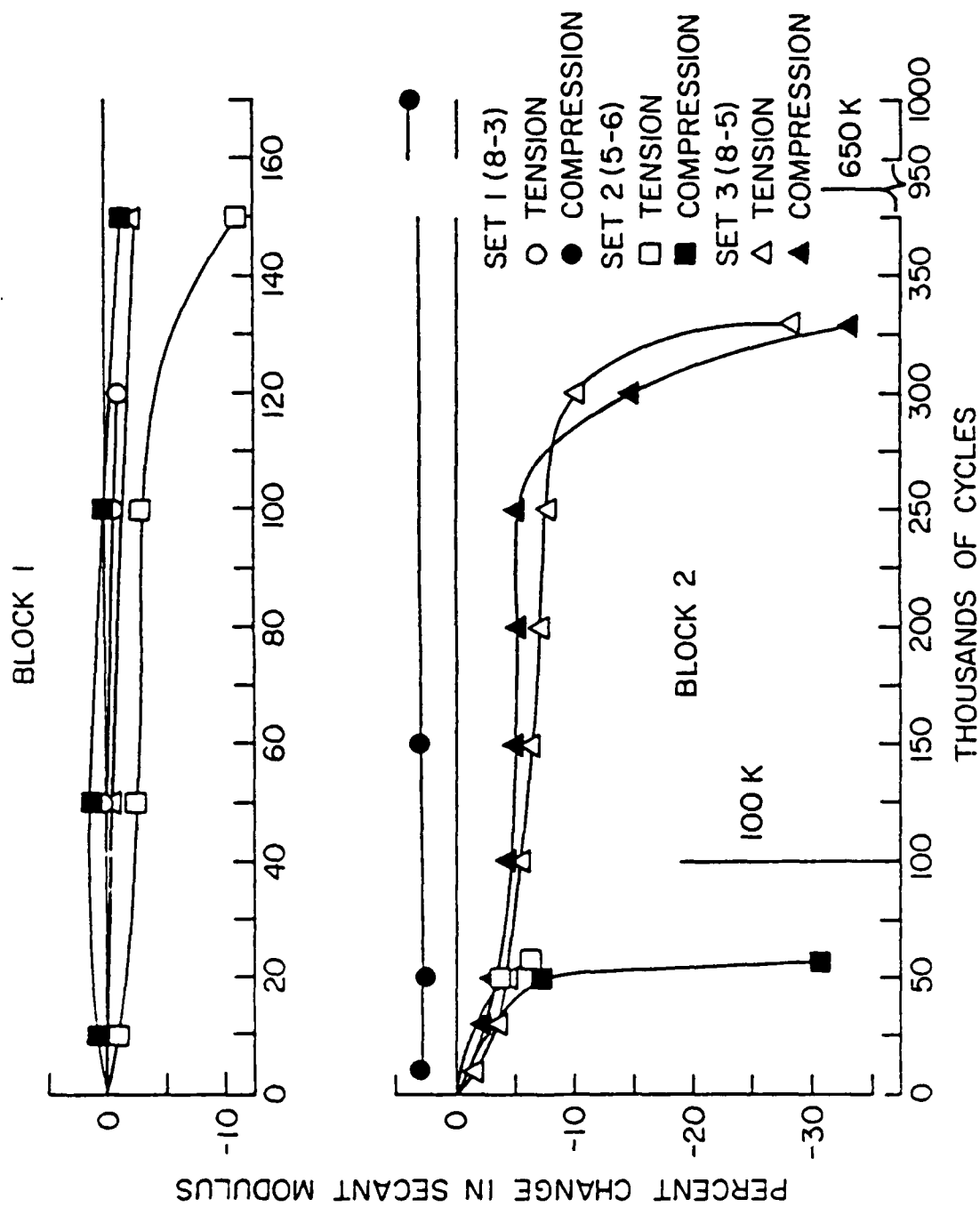


Figure 31. Stiffness Change During Block Loading of Three Specimens.

crack length is very small, it is, nevertheless, an initial crack when Block 2 loading begins. It should also be remembered that there has been a 1.5% stiffness change during Block 1 loading, which influences the laminate strain values that occur during Block 2 loading. Block 2 consists of fully reversed constant amplitude fatigue loading which corresponds to an initial value of about 4,500  $\mu$ e in amplitude. Block 2 loading is continued until specimen failure, an event that is defined by compressive instability at the value of applied load amplitude. A 7% change in the stiffness of the specimen is observed during Block 2 loading. The delamination model is used to calculate the life of the specimen (assumed to be coincident with the propagation of a delamination interface across the total width of the specimen) using the stiffness change and calculated crack length from Block 1 as initial values to the calculation for Block 2 loading. The Block 2 calculation then gives a life of 72,000 cycles compared to an observed life of about 57,000 cycles. If the change in stiffness in Block 1 is about 6%, then a predicted crack length of  $8.5 \times 10^{-5}$  is obtained, and a predicted life of 45,000 cycles for Block 2 loading is obtained from the model. If the Block 1 initial change in stiffness and crack length are ignored during the Block 2 calculation (to completely remove the influence of a prior loading history), the Block 2 calculation yields a predicted life of 71,500 cycles. The prediction of 45,000 cycles of life for the block loading results is to be compared with the average value of 33,000 cycles observed for three tests, as recorded in Table 6, and a predicted life of 71,500 cycles when Block 1 loading is ignored is to be compared with an observed

value of about 100,000 cycles for that loading applied alone. Hence, as indicated in Table 5, the block loading results are within about 7% of the observed data and the predictions for Block 2 alone differ by about 11% from the observations. This is thought to be reasonable agreement, quite similar to the accuracy of results obtained by using the delamination model that calculates the stiffness change rather than using observed values described earlier. It is also apparent that the model is very sensitive to the details of the block loading spectrum. Similar results are also shown for "Block 3" loading in Table 6.

As we mentioned before, when a model such as the present one is used which depends on measured values of stiffness change, it has the general major advantage of being highly accurate as a predictor of residual strength and life for the individual specimen for which the measurement was made. When that type of model is used for a prediction of residual properties for an arbitrary specimen for which no measurements are available, some reasonable means of estimating the stiffness changes must be used. For the T-T model, a rationale has been established for that estimation process. For T-C loading, no well-established rationale is yet available, partly because of the large increases in stiffness that are caused by combined modes of damage development, specifically combinations of matrix cracking and edge delamination.

As a final demonstration of how the model can be used for more generally loading situations, we consider cases for which the stress ratio may have a range of values rather than just  $R=1$ , 10 or 0.1 as above. First, it must be determined if the fatigue loadings corresponding to other  $R$  values have a similar

affect on material behavior as the classical cases already considered, or if the behavior can easily be extrapolated from the familiar results. And second, it must be determined if the models used to describe that behavior, which are based on mechanisms peculiar to situations where either tensile or compressive damage modes dominate, can be applied to intermediate situations. We have mentioned earlier that the  $R=-1$  situation (T-C) is especially severe in the sense that tensile loading alone or compressive loading alone, with the same stress range as the fully reversed stress amplitude, produces dramatically less damage over the same number of cycles compared to the fully reversed case. It is reasonable to suspect that there is a transition range over which this synergism disappears. Finally, the present model depends on two different analytical formulations, one for the situation where tensile failure dominates, and one for the situation where there are compressive failures. Is it appropriate to switch from the tensile model to the T-C model when only a small amount of compressive loading is present? All of these considerations have not been examined completely, but some of them will be considered below. Before examining these results, it is important to emphasize that a basic research investigation is needed to examine the actual processes of interaction between tensile and compressive damage modes so that a more rational approach to mechanistic modeling could be taken.

Based on the present experimental observations, we have taken the following approach. Figure 32 presents a series of fatigue life data for five different  $R$  values. These data have been plotted as a function of the total strain range (actually

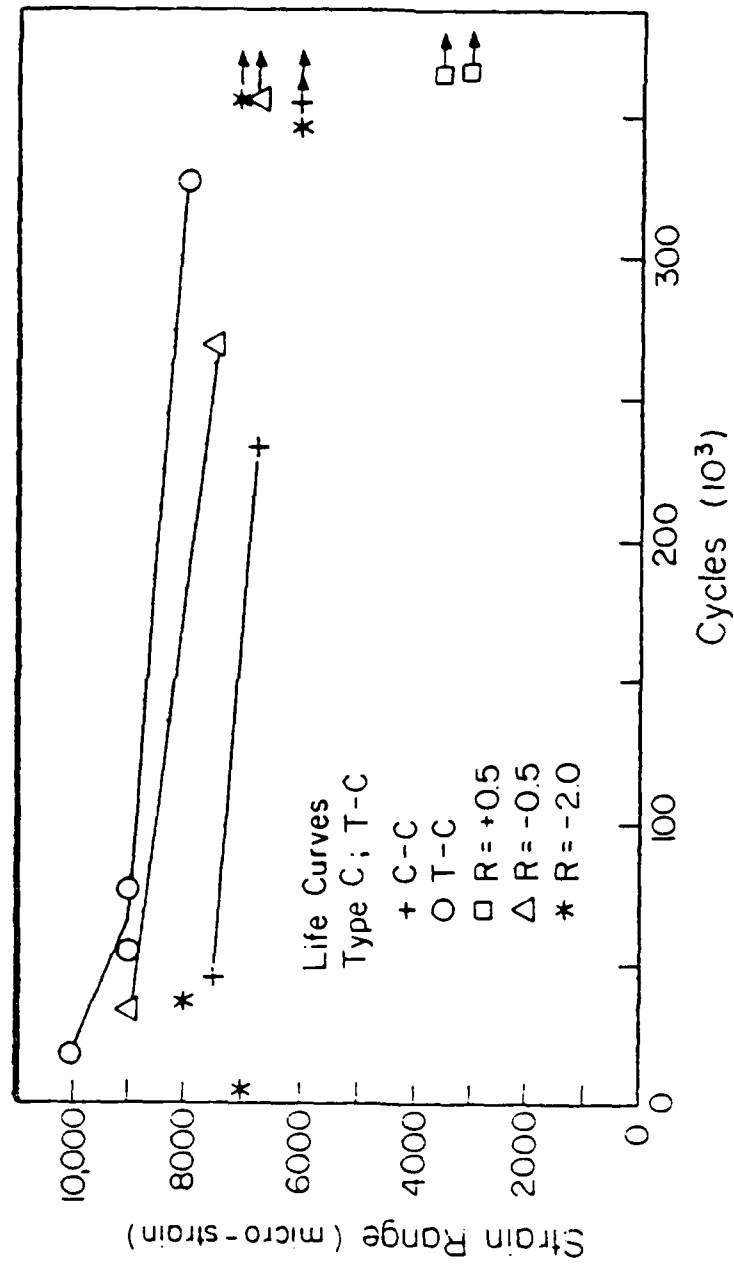


Figure 32. Fatigue Life Observations for Five Different R Values.

total stress range), i.e., the absolute value of the maximum stress minus the minimum stress in the test. While it is true that plotting the results against the total strain range does not completely coalesce the data, it is also very clear that the results are closely grouped for such a plot, more closely grouped than any other portrayal that the authors were able to find. Another striking feature of the curves is the fact that they appear to be parallel to one another, that is, they appear to have a quite similar slope. Hence, it was decided to use the total strain range (or total stress range) in the model that we have been using for loading which includes compressive load excursions as we have done in earlier applications of that model, and to introduce a dependence on the stress ratio,  $R$ , by incorporating into the model a function of  $R$  which multiplies the strain range by a factor which is equal to the vertical separation of the curves in Figure 32. Since our model has been applied earlier to the fully reversed  $R=-1$  case (for the Type C laminate), the data for that situation will be used as a baseline, and all other strain amplitudes will be adjusted accordingly. For the test data shown in Figure 32, the correction factors become the values shown below.

$R = -\text{infinity}$	Correction factor = 1.188
$R = -1$	Correction factor = 1
$R = -0.5$	Correction factor = 1.093
$R = -2$	Correction factor = 1.227

A polynomial curve was fit to those points and used as the function of  $R$  which corrects the strain range input into the T-C model described in the previous section. To illustrate the

nature of the results, two different types of calculations will be demonstrated below. We will discuss calculations for cyclic loading which includes some compressive load excursions, namely  $R=-1$ ,  $R=-2$ , and  $R=-0.5$ . The two situations to be examined are the calculations for the T-C model in the two forms discussed earlier, namely, the form which uses the delamination propagation power law equation and calculated values of stiffness change to adjust the strain as a function of cycles, and the second form of the model which uses the measured stiffness change data as an input to adjust the strain level as a function of cycles. We will refer to the second form of the model as a "data-driven model". Figure 33 shows the residual strength predictions from the data-driven model as a function of cycles for three specimens, as well as the life predictions and observations for those three specimens. Since the  $R=-1$  case was used as a baseline, and since the data driven model is strongly (and positively) influenced by the stiffness changes measured in a given test, the predicted results are very close to the observed values.

Figure 34 shows predicted and observed results for  $R=-0.5$ . Results predicted from the data-driven model as well as the model which requires only the delamination equations are shown. It is interesting to note that the observed life values fall within the bracket formed by the two predicted values for each of the specimens analyzed. Moreover, the two predicted values and the observed value are quite close together. For specimen C8-12 the test was terminated at 350,000 cycles and a residual strength was measured. The strength of that specimen was observed to have been reduced by 4%. The predicted strength reduction using the

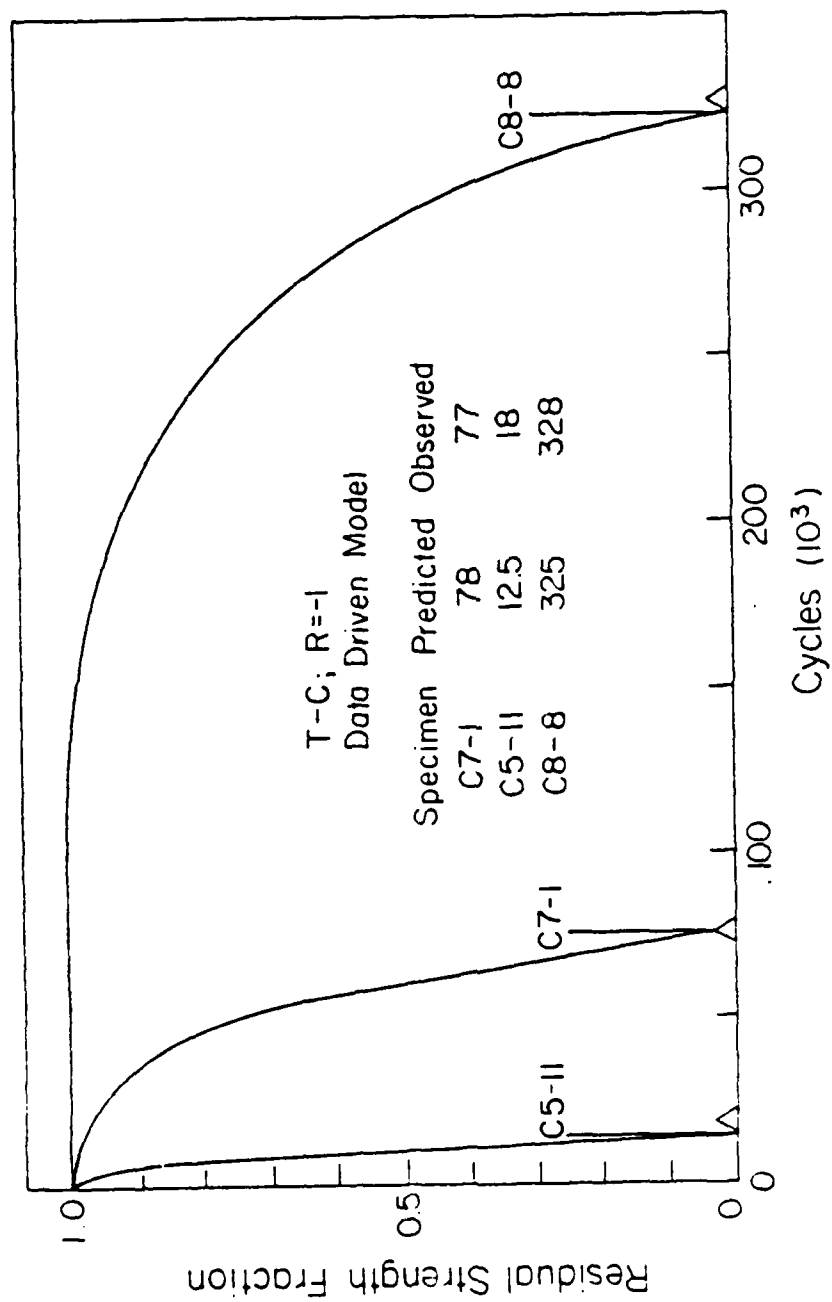


Figure 33. Residual Strength Prediction for  $R=-1$ , Type C Specimen.



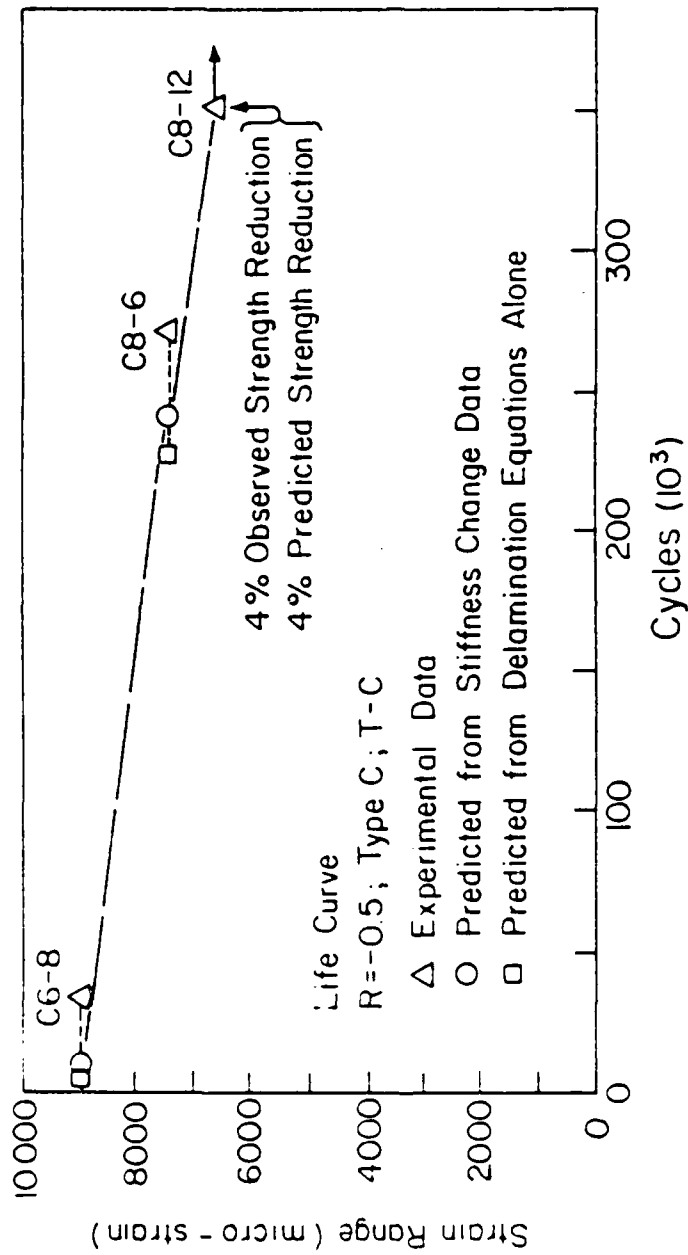


Figure 34. Life Predictions and Observations for  $R = -0.5$  Tests.

data driven model was also 4%, an agreement that is certainly fortuitously close.

The results for the  $R=-2$  tests are shown in Figure 35. These tests are, of course, the counterpart to the  $R=-0.5$  tests in the sense that for  $R=-2$  the tensile component of loading is half as large as the magnitude of the compressive component, while for  $R=-0.5$  the compressive component of loading is half as large in magnitude as the tensile component. However, the experimental results for the  $R=-2$  situation were somewhat strange, as can be seen from the data plotted in Figure 32. Figure 35 shows predicted and observed results for three specimens tested with  $R=-2$ . The observed stiffness changes were small for these tests, about 1% for specimen C8-10 and about 7% for specimen C7-9. Hence, the data driven model predicts values of life that are noticeably larger than the observed values. The model which uses the delamination equations alone is conservative as before. Hence, the observed results fall between the predicted ones. For the lowest strain range in Figure 35, the specimen did not fail in one million cycles, and was pulled to failure after the test to determine the residual strength at that point. The residual strength was essentially identical to the quasi-static baseline strengths measured earlier. Neither of the models predicted any strength loss for those amplitudes. While the life predictions in Figure 35 are rather widely spaced, they are all within a factor of 2 or 3 of the observed data, a level of agreement that is generally tolerable in the context of fatigue behavior.

Table 7 is a summary of the results for the variable  $R$  series of tests and predictions. The life predictions and re-

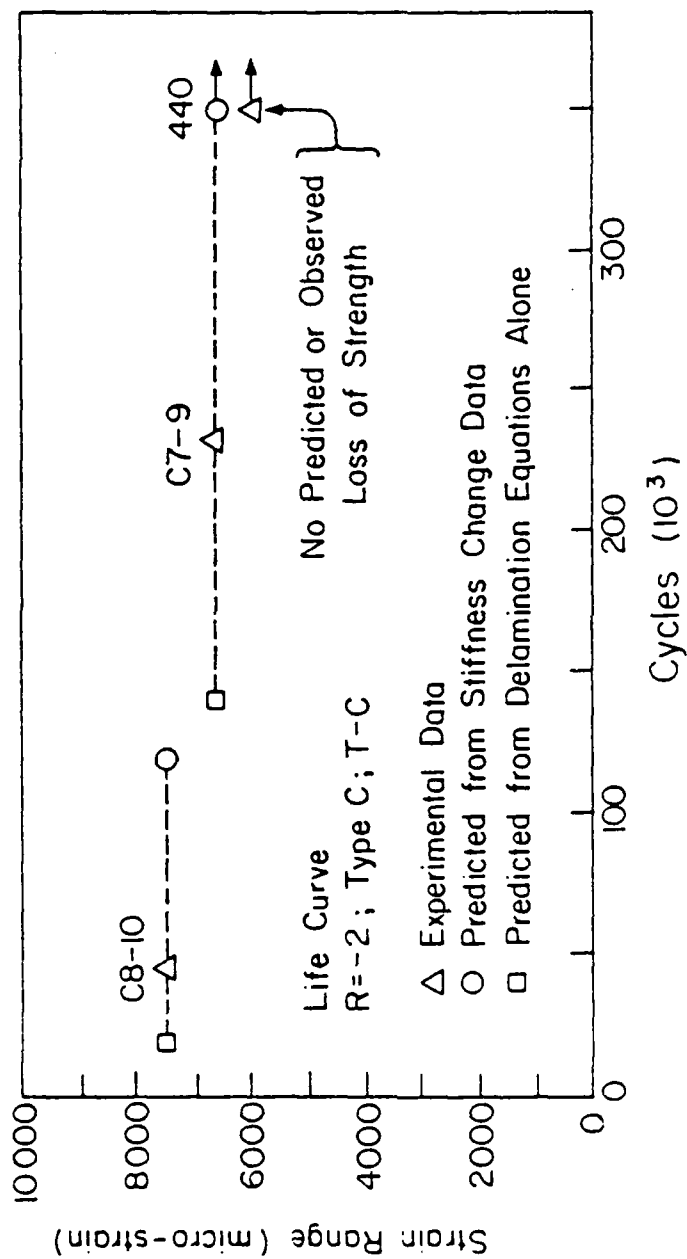


Figure 35. Predicted and Observed Life for R=-2 Tests.

TABLE 7.

## SUMMARY RESULTS FOR VARIABLE R SERIES

R	Specimen	Max e	Min e	Observed	Life ( $10^3$ )		Strength (%)	
					Predicted <sup>1</sup>	Predicted <sup>2</sup>	Observed	Predicted
-0.5	C6-8	6000	-3000	34	9.8	4.6		
-0.5	C8-6	5000	-2500	269	240	226		
-0.5	C8-12	4500	-2250	1000+			0.96	0.96
-1	C7-1	5000	-5000	18	12.5			
-1	C6-2	4500	-4500	56	77.4			
-1	C5-11	4500	-4500	77	77.4			
-1	C8-8	4000	-4000	328	325			
-2	C8-10	2500	-5000	45.6	120	19		
-2	C7-5	2250	-4500	232	440	139		
-2	C5-3	2000	-4000	1000+			1.0	1.0

<sup>1</sup> Predicted from stiffness change data

<sup>2</sup> Predicted from delamination equations alone

sidual strength prediction are shown along with the observed data for the tests analyzed. It appears that engineering accuracy can be obtained with this rather simple approach to the modeling of fatigue loading spectra which involve compressive load excursions. However, it should be re-emphasized that the basic mechanisms involved in these tests, the interaction of those mechanisms, the micro-damage states, and the micro-stress states have not been addressed in any detail here. Hence, it is not possible to define the boundaries of applicability of this model nor is it possible to imply that the cumulative damage behavior for all R values involving compressive load excursions can be predicted from this scheme.

### SECTION III PHASE III PREDICTIONS AND RESULTS

#### 1. PREDICTIONS AND RESULTS

Phase III of the present program was concerned with model verification. This part of the program consisted of two major tasks. The first task involved use of the model to obtain predicted responses for specified testing conditions. The second major task was to conduct those tests to compare the predictions with the experimental results. The performance to be considered in Phase III is summarized in Table 8. Four major categories were selected to provide information that could be used to verify most of the major aspects of the cumulative damage model and reveal any limitations of that model. Two of the categories involved variations on specimen geometry, one on specimen material, and one on fatigue loading conditions. The baseline material system of the previous phases, AS1/3502, and the Type C stacking sequence was used for most of the tests. However, a series of tests with an entirely new material (Gr/BMI) and an entirely new stacking sequence (the Type E laminate as defined earlier) were also included. Details of the model predictions for these situations are described below.

One of the model refinement activities conducted under Phase II of this investigation was the development and application of the methodology to use the model to describe self-similar damage growth such as edge delamination. Since the failure (and life) of

TABLE 8.  
PHASE III TEST MATRIX

	Stacking Sequence	Width	Material	Loading Conditions	Number of Specimens
Stacking Sequence	"E"	1"	AS/3502	T-T T-C Block	9
Width	"C"	2"	AS/3502	T-C	3
Material	"C"	1"	Gr/BMI	T-C Block	6
Loading Condition	"C"	1"	AS/3502	Block 1 Block 2 Block 3	9

the laminates considered in this program was generally controlled by the growth of delamination, one method of testing the model was to vary the specimen width. To this end, predictions were made and tests were conducted for 2-inch wide specimens to contrast with the 1-inch wide specimens used for the remainder of the program. The geometry of the specimens was otherwise identical. The load condition was fully reversed ( $R=-1$ ) constant amplitude tension-compression cycling at a strain amplitude of 4,500  $\mu\epsilon$ . Since these predictions were being made before experimental tests were run, no experimental data was available to indicate the amount of stiffness change that could be expected over the life of the specimen. As we have described earlier, it is possible to estimate such a stiffness change based on the damage that is predicted by quasi-static failure analysis of the individual plies of the laminate, and the laminate stiffness change that corresponds to an appropriate discount of the ply level stiffnesses as that damage develops. For the present situation, this process produced an estimate of 12.7% change in laminate stiffness over 50,000 cycles. Given the specified initial conditions, an estimated strain range given by Equation 21 was used for the computation.

$$\Delta\epsilon = 0.009 + 0.00234 * (n/10^5) \quad (21)$$

It should be noted that this equation is linear, an approximation used only for convenience since actual stiffness change data for the laminate were not available as an indicator of the nonlinear-



ity in that equation. With that input, and the delamination propagation relationships described earlier, the model was used to calculate the number of cycles required to propagate the delamination across the total width of the specimen. The model predicted that the life of the specimen defined in that manner would be between 45,000 and 62,000 cycles. This value is shown in Table 9 along with the experimental results to be discussed in a later section. If the specimen had been 1-inch wide, the model would have predicted a life of about 23,000 cycles. The residual strength estimate is shown in Figure 36.

These results are reassuring in several ways. First, and most important, since all of the predictions of life by the model for combined tension-compression loading were made based on the number of cycles required to propagate the delamination through the entire width of the specimen, and since instability generally caused failure of the specimen in compression before delamination had propagated to that extent during testing, one would expect the predictions of the model to be consistently high by some fairly constant margin. In fact, it should be physically impossible for the lives predicted by the model to be lower than those measured in the laboratory. We will see that this is indeed the case all results reported. Second, since the model is very sensitive to a variety of parameters, and no physical measurements from the specimens (such as the area of the specimens, their initial stiffness, or any peculiarities of their geometry or response) were available when the calculations were made, the order of magnitude agreement between measurements and predicted results is satisfactory, especially in the context of the varia-

TABLE 9.

## CUMULATIVE DAMAGE MODEL PHASE III RESULTS

Laminate	Test	Loading	Specimens	Observed Life (Cycles)	R.S.	Predicted Life (Cycles)
C	Width	T-C	C10-7	34600	--	45- 62Kc
		R=-1	C10-3	16740	--	45- 62Kc
		4500 $\mu\epsilon$	C10-5	25220	--	45- 62Kc
C	Load	Block 1 note (1)	C10-22	105890	--	268-410Kc
			C10-10	162660	--	268-410Kc
			C10-15	102170	--	268-410Kc
		Block 2 note (2)	C10-13	39160	--	226-341Kc
			C10-23	60980	--	226-341Kc
			C10-19	192940	--	226-341Kc
		Block 3 note (3)	C10-18	200210	--	200-210Kc
			C10-21	205370	--	200-210Kc
			C10-11	145610	--	200-210Kc
E	Lam.	T-T	E1-2	1M+	27900	1M/20000 (4):3-33Kc (5)
		R=0.1	E1-17	1M+	25250	1M/20000 :3-33Kc
		7000 $\mu\epsilon$	E1-8	1M+	26950	1M/20000 :3-33Kc
		T-C	E1-15	543340	--	50-350Kc :15-150Kc
		R=-1	E1-12	595270	--	50-350Kc :15-150Kc
		3000 $\mu\epsilon$	E1-5	285830	--	50-350Kc :15-150Kc
		Block note (6)	E1-1	1M+	27150	175K-1Mc :103-205K
			E1-11	1M+	28550	175K-1Mc :103-205K
			E1-19	1M+	27300	175K-1Mc :103-205K
C	Material	R-1 $\pm 4000 \mu\epsilon$		6420		23441-35000
				6400		
				7760		
C	Material	Block R=0.1(150K) $\epsilon_{max}=5000 \mu\epsilon$ R=-1 $\pm 4000 \mu\epsilon$		155000		262500-437000
				166000		
				172000		

## Loading Condition

- Notes:
- (1) 100Kc TC @ R=-.5 (5000  $\mu\epsilon$ ) : TC @ R=-1 (4000  $\mu\epsilon$ ) to Failure
  - (2) 100Kc TC @ R=-1 (4000  $\mu\epsilon$ ) : TC @ R=-.5 (5000  $\mu\epsilon$ ) to Failure
  - (3) 100Kc TT @ R=.1 (6000  $\mu\epsilon$ ) :
  - 100Kc TC @ R=-.2 (6000  $\mu\epsilon$ ) :
  - 100Kc TC @ R=-.5 (6000  $\mu\epsilon$ ) :
  - 100Kc TC @ R=-.7 (6000  $\mu\epsilon$ ) :
  - 100Kc TC @ R=-1 (6000  $\mu\epsilon$ ) : to Failure
  - (6) 100Kc TC @ R=-.5 (3200  $\mu\epsilon$ ) : TC @ R=-1 (3000  $\mu\epsilon$ ) to Failure
  - (4) Tension-controlled failure mode prediction
  - (5) Delamination-controlled failure mode prediction

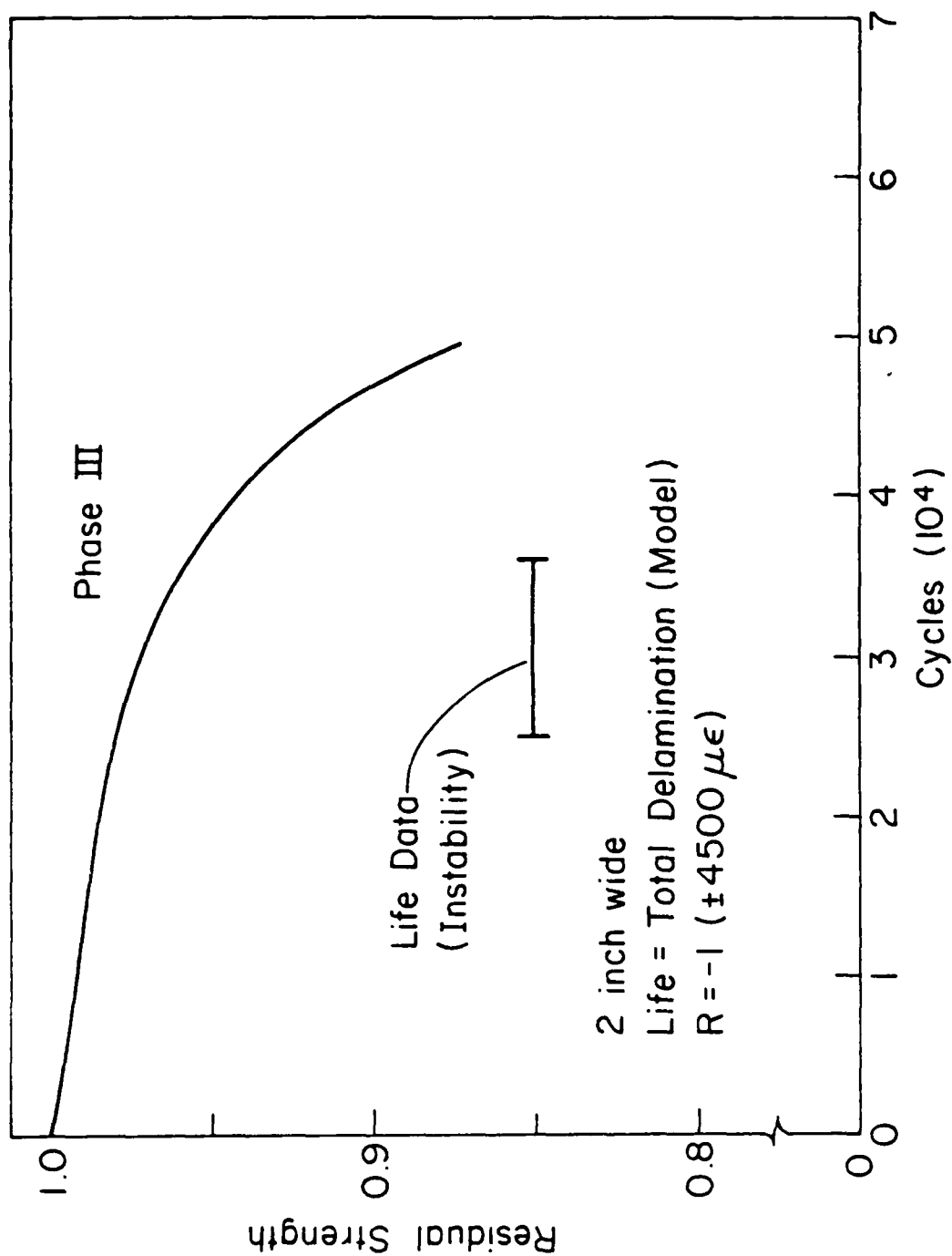


Figure 36. Predicted and Observed Results for Two Inch Wide Specimens

tion commonly observed in fatigue performance.

Another aspect of the model to be tested in Phase III was its ability to accurately predict the fatigue response of a composite laminate subjected to complex load histories. To this end, three block loading sequences were applied to a Type C laminate as suggested in Table 8 under the topic of "Loading Condition". The first two of the load histories (Block 1 and Block 2) were performed to determine the ability of the model to identify differences in laminate response and life due to the order of load application. Block 1 consisted of 100,000 cycles of constant amplitude loading at  $R=-0.5$  followed by fully reversed ( $R=-1$ ) constant amplitude loading to failure. The second load history, Block 2, consisted of 100,000 cycles of fully reversed loading followed by the  $R=-0.5$  loading sequence to failure. The constant amplitude load levels used for each of the  $R$  values in the two blocks were identical. The load levels were determined from the model on the basis of a combination that was predicted to give approximately 500,000 cycles of life. This aspect of the predictions should be emphasized, because it is quite similar to the exercise that an engineer would conduct to determine the acceptable load levels for a desired lifetime of service for the component in question. There is little doubt that the model has its greatest utility for this type of calculation. Hence, in the present situation as would have been done for the design of a structure, the load levels subsequently used for physical testing (or design proportioning) were determined from model predictions. This is true for all of the block loading calculations in Phase III.

For Block 1, a maximum strain of 5,000  $\mu\epsilon$  (with  $R=-0.5$ ) applied for 100,000 cycles was used for the first step of the prediction. The strain range, given by Equation 22, was estimated from an earlier test.

$$\Delta\epsilon = 0.00755 + (2.105 \times 10^{-8}) n - (1.938 \times 10^{-13}) n^2 + (5.695 \times 10^{-19}) n^3 \quad (22)$$

At the end of 100,000 cycles, the two estimation schemes used by the model predicted crack length of 0.185 and 0.054 inches, respectively. These values were used as initial crack lengths for step 2 of Block 1 loading. Also, the laminate modulus was reduced by about 5% by step 1 loading, a value which was also accounted for in the step 2 analysis.

Step 2 consisted of loading with  $R=-1$  with a strain amplitude of 4,000  $\mu\epsilon$ . A linear approximation for the strain polynomials, given in Equation 23, was used for this part of the analysis.

$$\Delta\epsilon = 0.0078 + (6.3 \times 10^{-9}) n \quad (23)$$

Results of the computation are listed in Table 10 under the heading "Sequence 1". The range of predicted life was 268 to 410,000 cycles.

For Block 2 loading, the sequence of load application was reversed so that the predictions began with an  $R=-1$  application of a strain amplitude of 4,000  $\mu\epsilon$  for 100,000 cycles, followed by

the  $R=-0.5$  loading to failure. A stiffness reduction of about 7% resulted from the first step of that loading sequence. Initial crack lengths for step 2 of that sequence were 0.11 and 0.0044 inches, respectively. A total range of life prediction for the Block 2 loading sequence was 181 to 324,000 cycles as shown in Table 10. Figure 37 shows a part of the results of these computations. It should be remembered that the residual strength curves are only indicators of behavior since a failure criterion for compression in the damage state has not been established. Nevertheless, from a comparison standpoint, it is clear that reversing the sequence of application of the two steps of loading changes the predicted residual strength and life significantly. A second sequence of application ( $R=-1$  followed by  $R=-0.5$ ) produces a significantly smaller life than the reverse sequence of loading. Also, the residual strength curves cross each other according to Figure 37. Finally, the residual strength curves are continuous, highly nonlinear, and not entirely reliable since they are based on total stiffness reductions in the tensile condition. A look at Table 9 indicates that these predictions are indeed consistent with the experimental results, in the sense that they are consistently higher than the experimental observations for reasons explained earlier, and the lower life predicted for sequence 2 loading is observed. The model predicts that the life should be reduced by sequence 2 loading by about 17% while the observations suggest that a reduction of 23% is to be expected.

The final sequence in the load history study consists of Block 3 in Table 8. That block consists of several steps of constant amplitude loading. The first step consists of 100,000

TABLE 10.  
PHASE III -- BLOCK SEQUENCE ESTIMATES

	Sequence 1 (10 <sup>3</sup> cycles)	Sequence 2 (10 <sup>3</sup> cycles)
Block 1 R=-0.5 $\epsilon_{\max}=5000\mu\epsilon$	100	81/213 110/224
Block 2 R=-1 $\epsilon_{\max}=4000\mu\epsilon$	168/293 <sup>(1)</sup> 241/310 <sup>(2)</sup>	100
Total life * 10 <sup>3</sup> cycles)	268-410	181-324

- (1) Calculated using crack length estimated from growth law for delamination alone.
- (2) Calculated using effective crack length for all damage suggested by stiffness changes.

\* Life at R=-0.5, 5000  $\mu\epsilon=G_{\max}$   $\approx$  226-240 k cycles  
(comparison data 269 k).

Life at R=-1, 4000  $\mu\epsilon=G_{\max}$   $\approx$  324-440k  
(comparison data, 328 k)

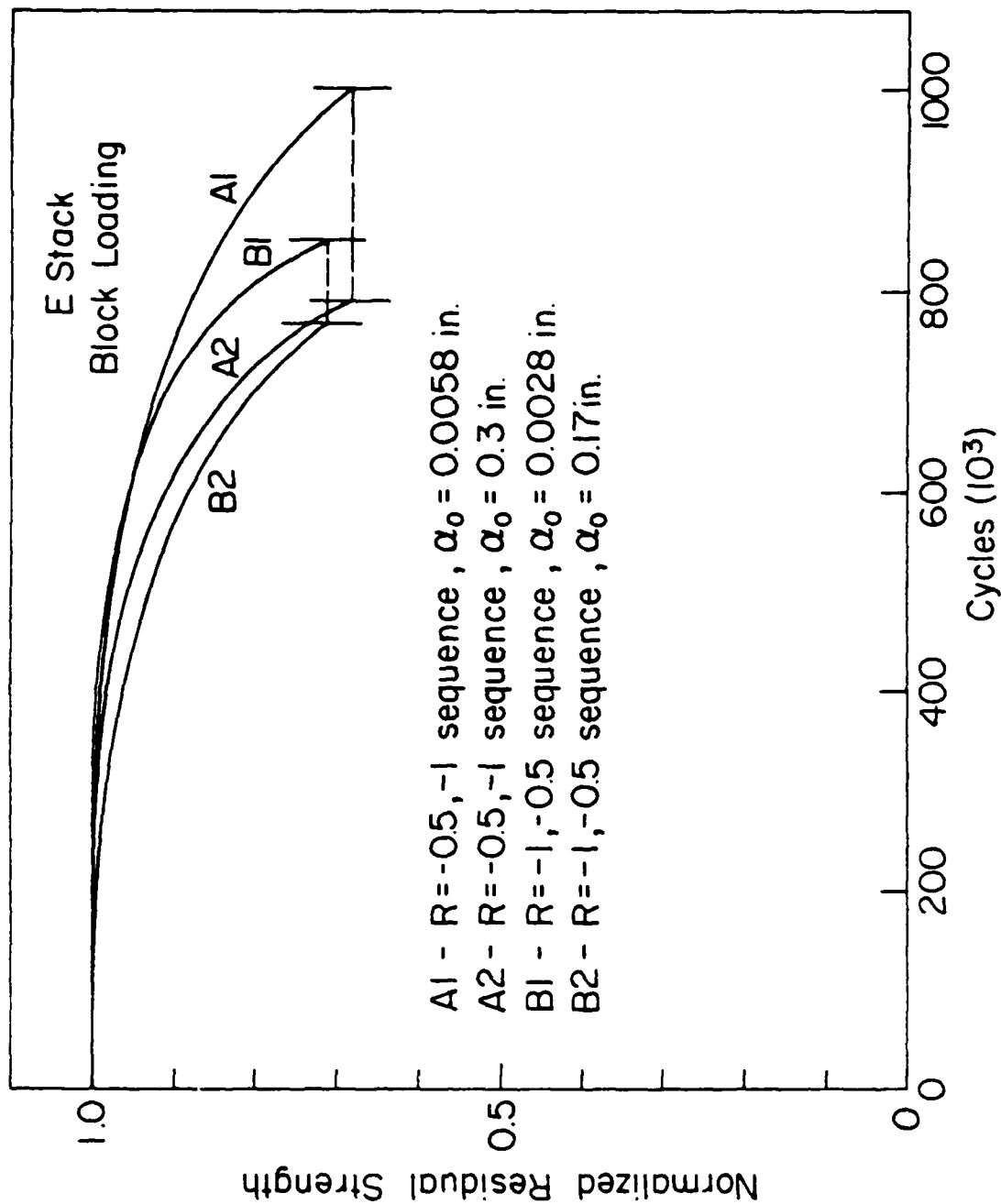


Figure 37. Estimated Lives for Block Loading with Reversed Sequences



cycles of tension-tension  $R=0.1$  fatigue loading at an initial strain level of 6,000  $\mu\epsilon$ . The following blocks, each of 100,000 cycle duration, consisted of tension-compression loading with each succeeding block having an increasing absolute value maximum compressive load while maintaining a constant maximum tensile load. The corresponding  $R$  values for those blocks was -0.2, -0.5, -0.7, and -1.

It was estimated that for step 1 of the loading sequence, a 3.2% change in the laminate modulus would be observed. The tensile model was used for the calculation with the local normalized stress amplitude (and the local failure function) equal to the expression shown in Equation 24.

$$\begin{aligned} S/S_u = & 0.4714 + (1.9864 \times 10^{-7}) n - (7.77 \times 10^{-10}) n^2 \\ & + (1.15 \times 10^{-18}) n^3 - (5.484 \times 10^{-25}) n^4 \end{aligned} \quad (24)$$

The 100,000 cycles of loading at this amplitude produced less than 1% predicted change in the residual strength of the laminate. Hence, the main influence on the subsequent steps of loading of the first step of loading was the reduction in modulus. Since the experimental tests were actually run at constant load amplitudes, a reduction in modulus is treated in the modeling process as a reduced range of strain compared to the range specified on the basis of the initial laminate modulus. However, it should be noted that the incremental change in stiffness due to delamination used for computation of the strain energy release

rate in that damage mode was kept constant throughout all calculations, reflecting the assumption that the driving force for delamination was uninfluenced by the initial step of loading. As mentioned before, step 2 loading produced initial crack lengths which were used as starting points for step 3 calculations. The results of the first three steps of loading are shown in Figure 38. It can be seen that virtually no change in residual strength occurs until step 3 loading begins. At that point the model predicts a precipitous reduction with rapid failure after the initiation of that step of loading. The model predicts a total life which ranges between 200 and 210,000 cycles. Table 9 indicates that the observed results are virtually identical with these predictions.

This last result appears to be a particularly important test of the model. Since the tension-compression form of the model depends on the strain energy release rate which, in turn, depends on the square of the strain range, step 2 causes very little to happen while step 3 is precipitous. Hence, the model predicts that a dramatically different physical response will result from a relatively small change in the strain range, a definitive test of the model. The next set of predictions to be considered will be those associated with the change in the stacking sequence of the laminate. One of the most important (and demanding) predictions that any model can attempt is to estimate the influence of changing the stacking sequence of a laminate on the residual strength and life of the composite component. Changing the stacking sequence of a laminate is a common event, motivated by attempts to control edge or surface behavior in most cases. In the

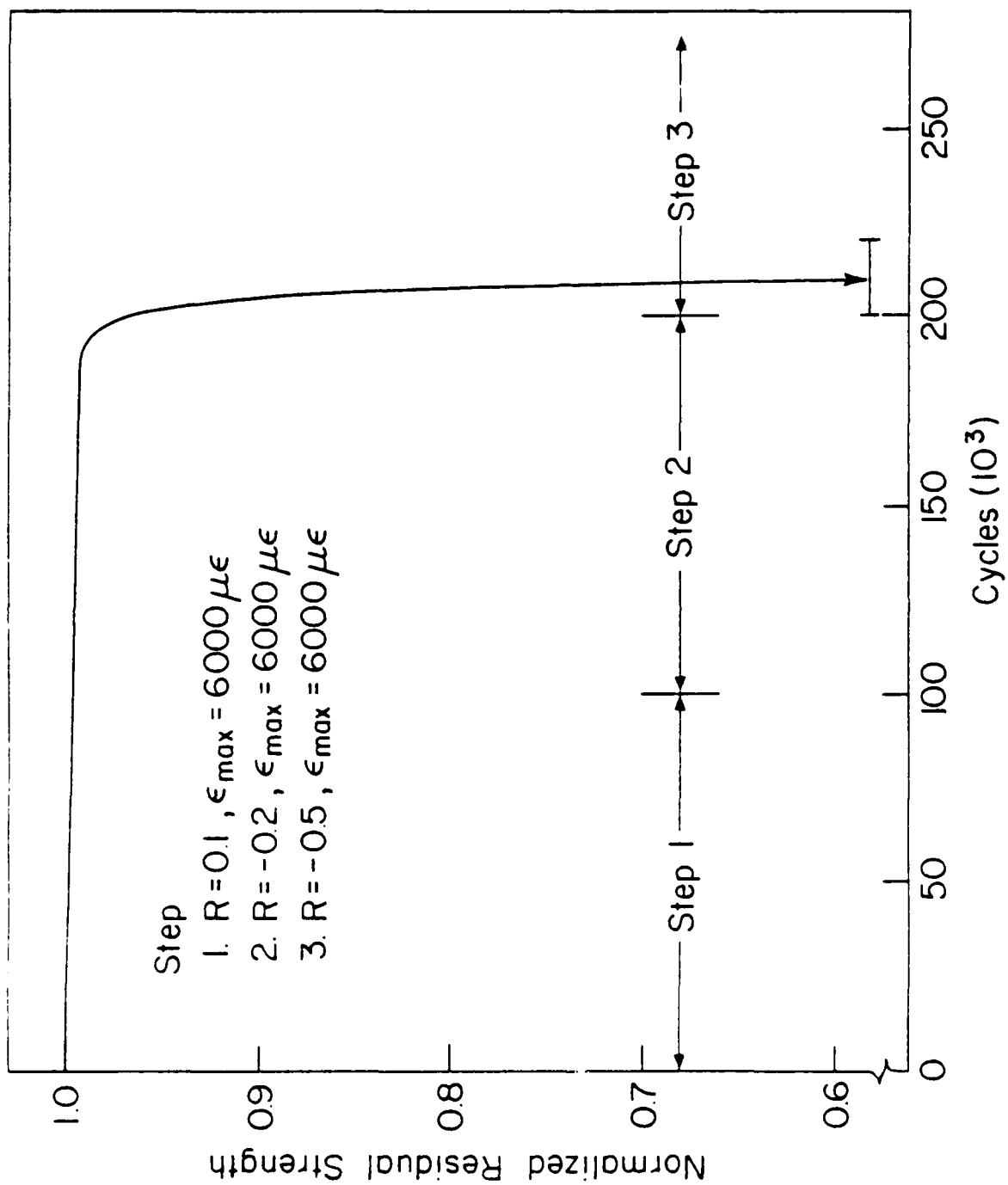


Figure 38. Predicted Life for Three Blocks of Widely Different Loading

present case, it is anticipated that the model would be used to find an optimum laminate stacking sequence for fatigue resistance. This process is simulated in the Phase III predictions by picking situations for which the response of the Type C laminate were previously established and attempt to predict that response for a new Type E laminate having a stacking sequence given in Equation 25.

$$[(0/45/90/-45)_S / (0/45/-45/90)_S / (0/45/-45/0)_S]_S \quad (25)$$

The Type E laminate has 31.7% 0 degree plies, 50% 45 degree plies, and 8.3% 90 degree plies; hence, it is dominated by 0's and 45's. The initial ratio of the fiber direction stress in the zero degree plies (the critical elements) to the applied stress in that direction is 1.9. When the 90 degree plies crack, laminate analysis with discount schemes indicates only a 0.8% change in the laminate modulus, and a change in the local ratio of critical element stress to applied stress of a comparable amount to a value of 1.92. If all off-axis plies crack, a change of 10% in the modulus of the laminate is predicted, and a local value of 2.12 for the critical element stress ratio is predicted by laminate analysis. Laminate analysis also predicts that the 90 degree plies will crack at about 61 ksi, the 45's at about 89 ksi, and the laminate will break at about 114 ksi or about 1.18% strain.

Two items are of special interest to the computations for this laminate. The first of these is the affect of the biaxial stress state which occurs in the zero degree plies. In our ear-

lier work, we had found that when the first term in the Tsai-Hill failure theory was reduced to about 0.9 at failure, it suggested that the biaxiality in the zero degree plies had an influence on the calculation (which is otherwise one-dimensional) and must be accounted for. For the Type F laminate that term had an initial value of 0.943 and a final value of 0.894 when all the off-axis plies had cracked. For the Type E laminate those values are 0.983 initially and 0.971 in the final condition. While it was decided to use the biaxial reduction in the local ratio of stress in the critical elements to the applied stress for the present calculations, this is strictly a discretionary choice, and tends to make the predicted lives longer than they would have been otherwise. If one was doing this for an engineering calculation instead of as a verification of the model, a more conservative estimate would have been obtained by not using the biaxiality factor.

The second issue had to do with delamination. An approximate calculation of the interlaminar normal stress,  $\sigma_z$ , (including the effect of thermal stresses) indicated that these values could be significant, about 1,300 psi for an applied axial strain of 3,000  $\mu\epsilon$ , for example. This suggested that it was possible for delamination to become a major damage mode in both tension and compression loading. Of course, delamination was assumed to occur under combined tension-compression loading, but the tension part of the model does not account for the affect of delamination on such things as the stiffness change. Because of that, predictions were made for situations where the stiffness change was consistent with small to moderate delamination and additional calculations were made for situations where moderate to large delamination

occurred. The calculations for matrix cracking only are shown in Figure 39. Linear estimates were used for both the local stress ratio and the failure function. It should also be noted, as indicated earlier, that the calculations are actually done on the basis of the applied stress that is implied by the assumed modulus multiplied times the strain range that one wishes to use for the test. Hence, any changes in area or modulus of the specimen from those assumed in the calculation could cause significant differences between the observed values and the calculated ones. Nevertheless, the plots in Figure 39 are extremely useful for the applications person since a quick check of those results will provide a good estimate of the values at which the laminate can be expected to serve for a given life range. Of course, if delamination enters the picture, these lives must be shortened because the change in stiffness will be significantly larger than that assumed in those calculations. If delamination does enter the picture, calculations can be made by increasing the stiffness change in the tension-tension model or by running the calculation using the delamination model normally used only for combined tension-compression. We have conducted a set of calculations for the latter case for comparison purposes and obtained the results shown in Table 11. One can see that the results differ from the previous calculations by nearly an order of magnitude. In order to make these calculations it was necessary to compute the strain energy release rate associated with delamination. This is a demanding task. As we noted earlier, the model uses the expressions for strain energy release rate suggested by O'Brien, which depend on the applied strain range and the difference between the

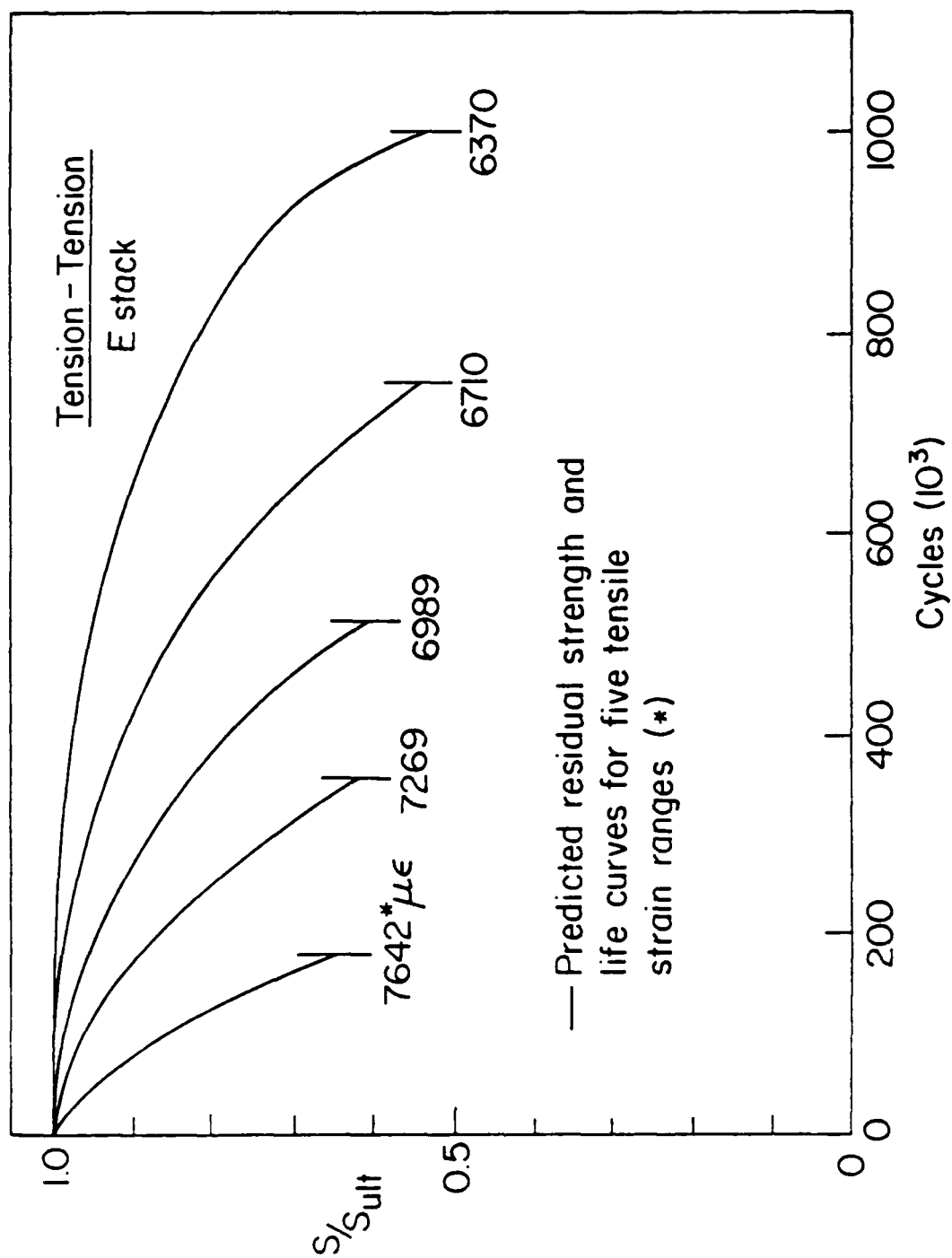


Figure 39. Predicted Residual Strength and Life for Tension-Tension Loading Assuming Only Matrix Cracking

TABLE 11.

LIVES PREDICTED ASSUMING DELAMINATION DOMINATES E-STACK

<u>Strain Range</u> ( $\mu\epsilon$ )	<u>Life Range</u> * (k cycles)
5600	50-450
6000	15-150
6370	3-33

\* R=-0.1



delaminated and undelaminated modulus of the laminate. Calculation of the delaminated modulus requires that one estimate the location and extent of the delaminations that can be expected for a given strain range. Guidance in this process can be obtained from quasi-static testing, but some decisions regarding apportionment must be made on the basis of experience, and will be approximate in any case. The laminate analysis indicates that delamination should occur near the 90 degree plies about midway through the half-thickness of the laminate. If total delamination of that interface were to occur, a change in modulus of about 1.1% would be expected. This is a large value compared to the amount observed in the Type C laminates where a change of about 0.65% was predicted. Of course, if the laminate does not completely delaminate, a smaller change in modulus would occur. The question is one of extent. In a realistic situation for an actual composite laminate or component, one would expect to have non-destructive testing information to provide guidance about the extent and type of delamination. For the present case, it was decided to make calculations for a change in modulus of 1.1% and about 6% for comparison purposes, corresponding to severe delamination and moderate delamination in this laminate. The calculations in Table 11 were conducted using a change in modulus of about .6%. An indication of the sensitivity of the calculations to the assumed value of the change in stiffness due to delamination is provided by Table 12. As indicated earlier, one can see that the model is very sensitive to the type and extent of delamination that occurs. It should also be noted that by "extent", we refer only to the number of interfaces which delaminate in a

TABLE 12.

E-STACK CALCULATIONS FOR  $\pm 4000 \mu\epsilon$ 

$\Delta E$ (msi)	Life prediction *
0.048	300-1066 E3
0.06	25- 333 E3
0.1	110- 600
0.12	14- 24

\* delamination-driven calculation

thick laminate, not the length of the delaminations which does not influence the calculations of strain energy release rate. Figure 40 shows the results for the calculations indicated by the first two cases in Table 12.

Since it was desired to have a life of about half a million cycles, it was decided to use the model to estimate an appropriate strain range for that test. It was found that for an  $R$  value of  $-1$ , a strain range of about  $3,000 \mu\epsilon$  should provide a life of about half a million cycles. For that situation, an estimate of life for the severe delamination case (a change in modulus of  $0.12 \text{ msi}$ ) provided estimates of life in the range of 15 to 150,000 cycles. For moderate delamination (a change in modulus of  $0.06 \text{ msi}$ ), lifetimes of over 2.5 million cycles were predicted. If it is assumed that the actual laminate behavior is somewhere in between those extremes, then one might expect 500,000 cycle life to correspond to about  $3,000 \mu\epsilon$  in fully reversed loading. Table 9 shows that that is exactly the case. The value of  $3,000 \mu\epsilon$  was picked entirely on the basis of the model which was used to estimate a strain range that would correspond to 500,000 cycles of life. The experimental values are quite close to that estimate.

As final test of the theory for the new stacking sequence, a block loading with two steps was considered. The first step was applied with  $R=-0.5$  with a  $3,200 \mu\epsilon$  amplitude in the tension direction. The second step was applied with  $R=-1$  with a  $3,000 \mu\epsilon$  amplitude to failure. Again, it should be mentioned that these strain levels were picked based on model predictions as levels that would correspond to lifetimes of about 500,000 cycles. The

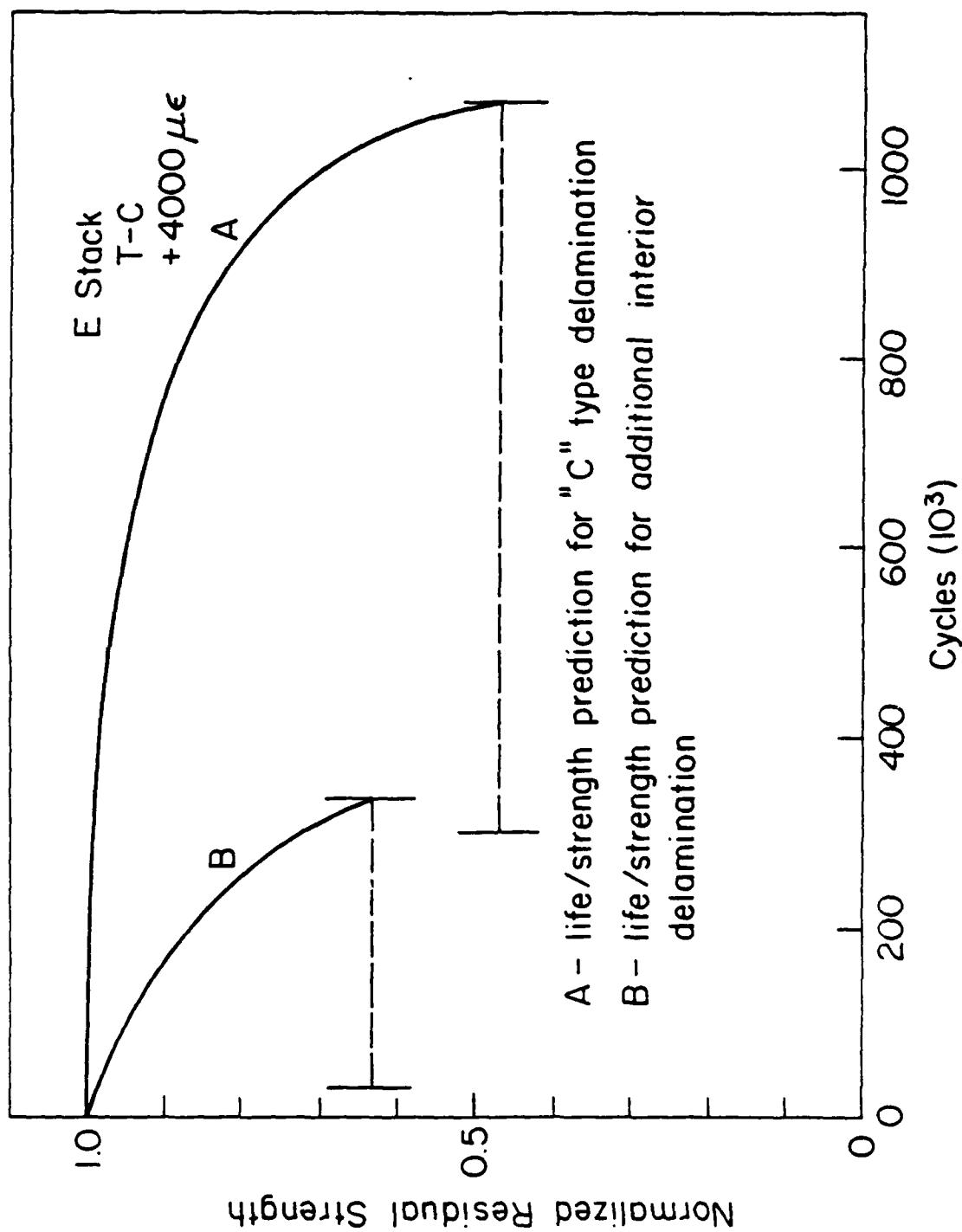


Figure 40. Results for Different Stacking Sequence under T-C Loading

TABLE 13.  
BLOCK LOADING OF E-STACK FOR SEVERE DELAMINATION

$\Delta E=0.12$ msi	<u>Sequence 1</u>		<u>Sequence 2</u>	
	$a_0(\text{in.})$	life(cycles)	$a_0(\text{in.})$	life(cycles)
Block 1 R=-0.5 +3200-1600	0.0052 0.3	100 k		40-540 k
Block 2 R=-1 $\pm 3000$		3-105 k 4- 48	>0.5 0.33	100 k
Total life		103-205 k		140-640 k

predictions for the sequence just described are shown in Table 13. Lifetimes of between 103 to 205,000 cycles were predicted using the strain levels indicated to obtain those results. If the sequence of loading is reversed, a significantly longer life is predicted as shown in Table 13. The second sequence was not tested experimentally. However the first sequence was subjected to several specimens and the results are indicated in Table 9. It can be seen that the severe delamination case is again too conservative compared to the data. Moderate delamination calculations are more nearly correct.

In summary, for the different stacking sequence, the model seems to provide excellent guidance in the choice of strain ranges to produce the desired life. In fact, for the present case, when a desired lifetime of 500,000 cycles was used in the model to set strain levels, the predictions were consistently conservative in the sense that a lifetime of 500,000 cycles or more was observed in every case. This is true despite the fact that there are a large number of unknowns that enter the calculations, some of which (such as the nature of the delamination) would be available if a component made from this material were actually in service. It should be emphasized that none of the constants in the power law equation that relates the strain energy release rate to the rate of crack propagation were changed for these calculations. It may well be that better predictions could be obtained if those constants were modified based on careful delamination rate experiments.

The final test of the model was conducted by introducing a new material system, for this purpose, a graphite-bismaleimide

material system was used; a T300/V378A system was chosen. The damage modes observed in the quasi-static loading of these specimens was essentially the same as that in the AS1/3502 system although the damage rates seemed to be accelerated. The unidirectional S-N curve for the BMI system fell consistently below those of the epoxy system, indicating a shorter life and more rapid damage accumulation process for the critical elements in the new material system. As indicated in Table 8, two types of loading were considered for the new laminate. The first of these was a tension-compression loading with an amplitude of 4,500  $\mu$ e.

A quasi-static laminate analysis indicates that a total change of 18% in the laminate modulus would be expected when all off-axis plies had cracked. This is somewhat larger than was observed for the Type C laminate. However, because of the observations regarding accelerated damage in this matrix material, 18% stiffness change was used for the calculations. Since, in the quasi-static tests, the delamination observed was essentially the same as the Type C material, a change in modulus due to the delamination of 0.048 msi (the same as the Type C laminate) was used. This value was thought to be on the low side since the rate of growth of damage in the BMI material was known to be somewhat higher than the epoxy. However, no specific basis for a higher value was available. The results of the calculation are shown in Figure 41 which indicates that a predicted lifetime of between 23 and 35,000 cycles is higher than the observed range of values as expected. However, the predictions are by no means unreasonable, since life determined from the model was assumed to be equal to the number of cycles required to propagate the delamination

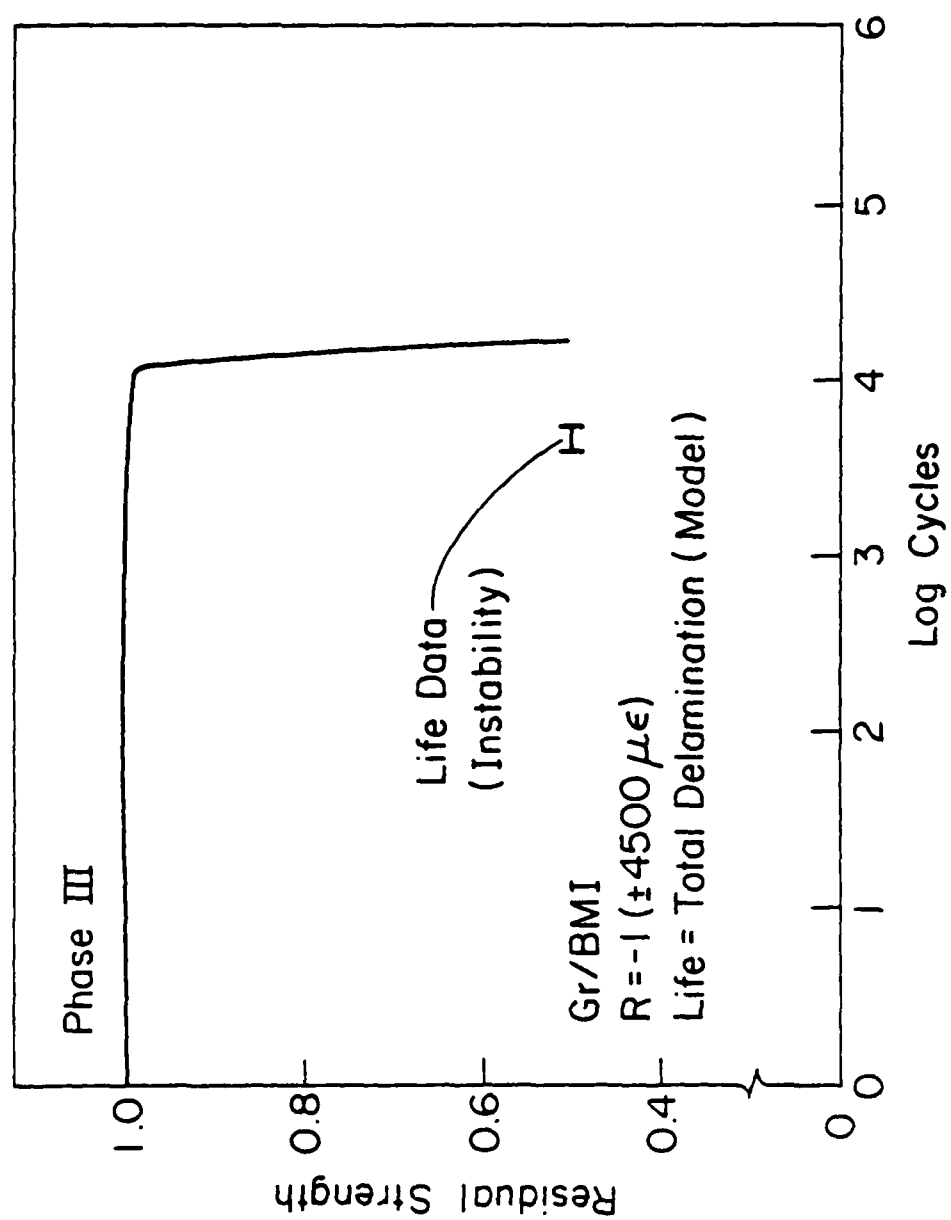


Figure 41. Predictions and Data for Reversed Loading of Graphite BMI Specimens



totally through the specimen while the experimental life was determined by the number of cycles before instability occurred prior to total delamination.

The final set of predictions were for block loading of the new material system with an initial step of tension-tension with a maximum strain level of 5,000  $\mu\epsilon$  followed by a  $R=-1$  step of loading with an amplitude of 4,000  $\mu\epsilon$ . Based on the laminate analysis and the quasi-static test, a total change in stiffness of 5% was assumed over the first step of loading in tension. The resulting change in residual strength was essentially negligible due to the first step of loading.

For the second step of loading, we were faced, again, with the question of what to assume for a stiffness change associated with total damage and with delamination alone. The lower bound value of 0.048 msi was assumed for the delamination change of modulus, and a total change of 18% over 300,000 cycles was assumed for the total damage state. The results of the calculation are shown in Figure 42 along with the data from Table 9. The predictions are higher than the data as one would expect given the nature of the calculations and the criteria for failure. However, the two magnitudes are quite satisfactorily comparable.

In summary, Phase III has provided an opportunity to verify recent refinements of the model, to study the ability of the model to extend to other materials of engineering interest, to verify the geometry independence of the model, and finally to demonstrate the ability of the model to predict residual strength and life under complex, competing damage modes applied in block-histories of loading. Throughout these verification activities,

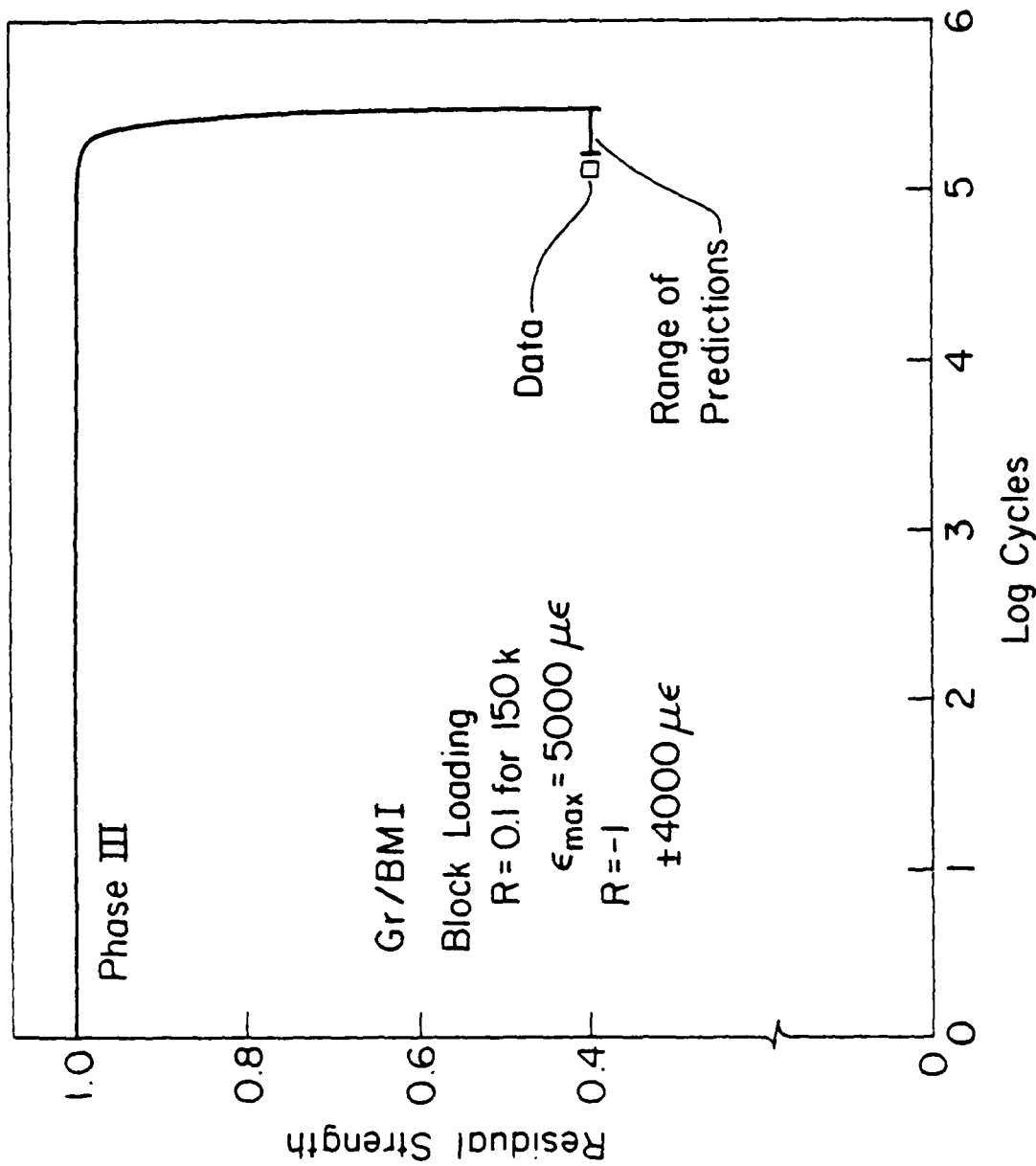


Figure 42. Block Loading Results for Graphite BMI Specimens

the model showed surprising consistency; it produced useful engineering estimates that were reasonable in every case. Considering the simplicity of the highly idealized inputs that are being used for the model at this time, this is a somewhat surprising result.

## SECTION IV

### SUMMARY AND CONCLUSIONS

#### 1. Experimental Procedures for Cumulative Damage Model Input

The overall objective of the experimental portion of this program has been to quantify material responses for the specific purpose of model development, refinement, and verification. Damages induced in selected laminates under the fundamental loading conditions of quasi-static tension and compression, constant amplitude fatigue at various R-ratios, and simple spectrum fatigue were thoroughly investigated. In addition to establishing the chronology and location of damage development, changes in specimen stiffness and strength were also established. These material responses were related to the damage state existing in the subject specimen at the time of measurement. Both nondestructive and destructive test techniques were employed to monitor the damage development and property changes. The nondestructive techniques applied included surface replication, enhanced x-ray radiography, and stiffness measurements. All data was input to the cumulative damage model development, refinement, and verification activities, as described in the previous section.

The following sections describe the laminates, specimens, and test methods employed. The experimental results were presented in the previous sections or in References 1 and/or 2.

## **A. Specimen Description**

The basic specimen geometry used throughout this program consisted of a 48 ply, one inch wide laminate with a four inch unsupported gage length between the test machine grips. The same material system, AS1/3502, was used throughout all program Phases with the exception of the T300/V378A system used for one series of Phase III testing.

The selection and use of six laminate stacking sequences provided the modelling effort with different damage developments. The difference in the number of 0 degree plies, off-axis plies, and 90 degree plies between the various laminates, combined with differences in the interlaminar normal stress distribution, served to generalize the cumulative damage model.

Each panel fabricated has been labeled according to stacking sequence and panel number. For example, Panel C5 refers to the fifth panel of Type C configuration. Each of the 12 specimens cut from each panel were labeled continuously one through twelve. Thus specimen labeled C5-10 is the tenth specimen cut from the fifth Type C panel. References to specific test results in this and previous reports has followed this numbering convention.

## **B. Nondestructive Test Techniques**

Surface replication is a well-established metallographic procedure applied to optical and electron microscopy. This technique has only recently been applied to composite materials. The basic procedure is quite straightforward. A thin strip of 0.005"-thick cellulose acetate tape is anchored to the polished surface of the specimen by adhesive tape. A small amount of

acetone is then injected between the specimen and the replicating tape. The acetone locally dissolves the replicating tape which flows into cracks in the composite laminate. The cellulose acetate hardens in a few minutes and is peeled from the specimen bearing an imprint of the specimen edge.

Edge replicas provide a permanent record of the damage state over the entire length of the specimen at the instant that a certain load level is reached. This technique can be applied while the specimen is in the test machine under load so that the recordings will capture the damage state in its most enlarged or open state. If the inspection is made after the load is removed from the specimen, many smaller cracks may close and not be detected. The replicas are easily stored for reexamination and future reference. Furthermore, replication is a simple technique that does not require complicated or extensive equipment.

Surface preparation is an important step in applying this technique. The entire specimen edge is metallurgically polished on a polishing wheel using a 3 micron aluminum oxide/water suspension system on a felt polishing cloth.

Edge replication was extensively employed throughout this program. In the fatigue testing, the test machine was periodically halted during the test, allowing the development of replica records of damage progression as a function of cycles. For each specimen so tested, the replicas were mounted between glass slides for viewing using a standard microfiche reader. Figure 43 is a typical view of the damage observed using this system. Transverse cracks and delaminations are clearly visible as darkened lines on the cross section view.

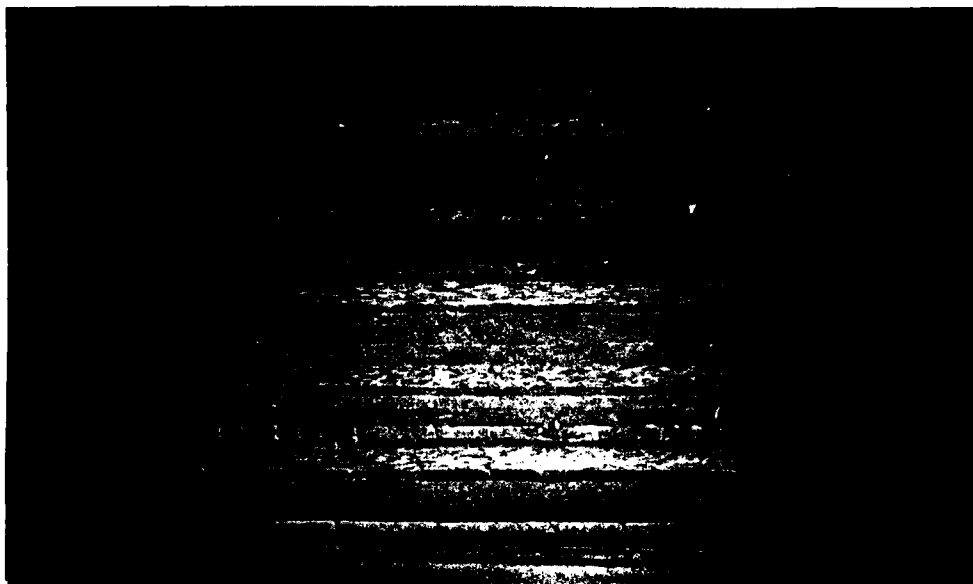


Figure 43. Typical View of Damage State Using Edge Replica

As a second NDE technique employed during the testing, a low voltage (25 kv and 20 ma) X-ray NDE technique modified for composite material application was used to monitor damage development through the specimen width. An opaque additive, zinc iodide, is introduced to the composite through the specimen edge. The  $ZnI_2$  enters the cracks and delaminations which develop in the specimens by capillary action. The images of the voids and delaminations are greatly enhanced by the highly attenuating characteristics of the opaque additive.

A 110 kv Picker portable X-ray unit was used in this study. It has a 2.25mm beryllium window and a focal spot of 0.5mm. Kodak Type M industrial X-ray film was employed. A 65-second exposure time was required for each exposure.

X-ray records of the damage growth in the composite specimens were enlarged when prints were made from the exposed film. Figure 44 is a representative example of such a record for a Type E specimen, where both transverse cracks and edge delaminations are clearly visible. The darkened areas on the prints represented flawed areas where the opaque additive had penetrated. The actual length and area of the damage zones were obtained from the prints using the appropriate scaling factor.

Changes in specimen stiffness were also monitored during the mechanical testing. An extensometer was employed in the measurement of axial strain. It has a two inch gage length and was seated in aluminum blocks which were bonded to the specimens prior to testing. The two inch gage length provided for an averaging of the damage so as to eliminate the effects of any local material variations. The aluminum blocks provided for





Figure 44. Typical View of Damage State Using X-Radiography

reproducible seating of the extensometer which was removed during fatigue testing and mounted at discrete inspection times. The transverse strain was monitored through the use of a strain gage with a quarter-inch gage length mounted in the center of the specimen span.

### C. Test Procedures

#### 1) Monotonic Tension and Compression

To determine the initial moduli of the laminates in this study, a series of ramp to failure tests was employed. In these tests, specimens having two longitudinal strain gages (front and back) and one transverse gage were mounted in the MTS machine. The specimens were then continuously loaded to failure at a load rate calculated to correspond to a typical load rate to be encountered in the constant amplitude fatigue tests. These tests were performed under computer control with load and strain channels being continuously recorded. Moduli were obtained by post-processing the data using a regression fit of the load (stress) and strain data.

#### 2) Quasi-Static Tension and Compression

A series of tests was performed to determine the damage development and property changes of the laminates in this study under static loading conditions. Since real-time methods of damage documentation of the type necessary in this program do not exist, these tests consisted of monotonic loadings by stages with load interruptions for the NDE evaluations.

The experimental procedure employed in both the quasi-static

tension and compression tests was quite straightforward. The specimen was installed in the MTS hydraulic grips, a nominal initial tensile load was applied, and initial NDE evaluations were made. Once this initial examination was completed, the tensile load was removed, the extensometer was mounted on the specimen, and the initial specimen modulus determined by monotonically loading the specimen to a small predetermined load. The load was then returned to zero and the extensometer removed.

The specimen was then monotonically loaded (in either tension or compression, as appropriate) to a predetermined load value. The load was returned to zero and the NDE and stiffness procedures again employed. This process was repeated, with increasing load values in each step, until the specimen failed. The load reductions for each inspection were deemed necessary because the hold-at-load times required for the inspections were long which could adversely affect the results, especially at high loads.

### 3) Fatigue Testing

Three types of fatigue tests were conducted in this program: tension-tension, compression-compression, and tension-compression at several R-ratios. All fatigue tests featured constant amplitude sinusoidal waveform loading, run under load control. A series of simplified spectrum tests, consisting of blocks of constant amplitude fatigue, were also performed.

The fatigue load level for a particular specimen was predetermined to satisfy the modelling needs. In most cases, the target specimen initial loading was expressed in strain or strain

range. The load level corresponding to the target initial strain was determined by monotonically loading each specimen to the NDE load level, generally 5000 pounds or approximately 1.3 ksi. This procedure allowed the accurate determination of the initial modulus of each specimen, in turn allowing the calculation of the applied load required to achieve the target strains. It is important to note that all references to specimen strain levels in this and previous reports imply initial strains only. As documented, as damage develops stiffness decreases. Under a load controlled test, specimen strain must therefore increase. Within the present modelling effort, only specification of the initial strain level is required.

The experimental procedure employed in the fatigue tests was identical to that used in the quasi-static testing, with the obvious exception that the loading between successive NDE evaluations was a predetermined number of fatigue cycles. This procedure thus results in a documentation of damage development and property changes as a function of fatigue cycles.

Each specimen was loaded in this manner until either a predetermined number of cycles, failure, or one million cycles. Those specimens which survived one million cycles and those where testing was halted at a predetermined cycle count were monotonically loaded to determine their residual strength. Thus data on life and strength reduction was obtained.

## 2. CLOSURE

The cumulative damage model that we have presented above has the following salient features:

The model predicts the strength and life of engineering composite laminates under tension-tension, tension-compression, compression-compression, block-spectrum loading, and constant amplitude loading with R values between 0 and minus infinity.

The model replaces Miner's Rule with an engineering model which is based on the physical mechanisms of damage and failure.

Among other things, the model is able to account for the following features:

- (a) Sequence effects in block loading.
- (b) The effects of unknown load histories. (The model is able to predict the residual strength and life from the results of inspections, vis-avis, from measurements of stiffness changes for individual specimens, a critically unique feature.)
- (c) Biaxial stress effects on the degradation of the 0 degree plies.
- (d) Different changes in stiffness under the tensile load excursions compared to compressive load excursions for variable R value T-C loading.
- (e) Different baseline quasi-static strength and stiffness (which enter as normalization factors).

- (f) Different laminate types, i.e., different combinations of ply orientations, physical dimensions, ply properties, stacking sequences, etc.

While the authors believe that this modeling effort has provided a firm foundation for continued work, it is only a first attempt to construct a mechanistic model of damage accumulation. During the course of the work it has become apparent that additional research and synthesis is needed in several areas. A few are listed below.

Mechanistic models are only as good as our understanding of the damage events induced by fatigue loading in composite laminates. If progress is to continue in the area of mechanistic modeling of cumulative damage, progress must continue in the area of understanding these events. Perhaps the greatest need for investigation is associated with damage development that is induced by combined tension and compression load excursions, a process which is poorly documented and not well understood. A variety of other situations which involve combined damage modes also are in great need of further investigation.

There is a need for a more thorough and complete analysis of the internal stress states that exist in the neighborhood of damage events. This is especially true of damage events which involve or induce three-dimensional stress states, such as transverse cracks which cross at

the interface of two plies having different orientations.

Mechanistic modeling to date has concentrated on the development of damage. The coalescence and localization of damage has not received sufficient attention. If accurate predictions of the fracture strength (or residual fracture strength) of laminates is to be obtained from mechanistic modeling, it is essential that additional attention be given to the development and precise nature of the fracture event, and to those events which precipitate the fracture process.

The present investigation has been concerned with block loading or constant amplitude fatigue cycling. The modeling approach that has been used is, however, applicable in theory to spectrum loading. A logical next step in this investigative process would be to attempt to apply the present model or refinements thereof to a more general spectral loading.

The present investigation has been concerned with coupon specimens for which the nominal stress state is uniform. The present approach could be, and should be, applied to nonuniform stress states such as those found in notched specimens.

There is a continuing need to develop a nondestructive testing technique and associated damage parameter that can be used for mechanistic modeling purposes as well as for

field interrogations for routine inspection purposes. For our present purposes, we have used stiffness change as a damage parameter with considerable success. However, a development effort is needed if that damage parameter or other ones are to be applied to engineering components in field service.

Another logical area of investigation as a follow on to this effort is the study of various environmental effects including temperature and moisture.

There is a great need for an experimental investigation of the internal stress states associated with damage events and combination of damage events. In the past few years, a number of experimental techniques such as moire' diffraction have been perfected which are capable of measuring the very small displacements and displacement gradients associated with small damage events such as matrix cracks, fiber fractures, and local debondings or delaminations. It is essential that these techniques be further developed and applied to fatigue damage development in composite laminates, not only for the purpose of validating various analysis methods, but also for the purpose of guiding the development of those methods and, most importantly, for the purpose of providing the physical information necessary for investigators to develop an understanding of the damage development processes.



The philosophical, analytical, and conceptual generalities that investigators are able to make are always limited by experience. One of the greatest needs for further work is the need for improved and more complete characterization of the fatigue behavior and damage development in various laminates and material systems.

The transfer of techniques, understanding, and technology from the laboratory to the practitioner is always a challenge, but it is an extremely demanding challenge in the present case. A development program is needed which will address this transfer. A first step might be to generate interactive computer codes that can be used for design and analysis by practicing engineers without the continuous service of specialist scientists.

The ten areas of need above are only a few of the major topics that come to mind. The present investigation suggests that progress can be made when opportunities are provided.

## REFERENCES

1. K.M. Liechti, K.L. Reifsnider, W.W. Stinchcomb, and D.A. Ulman, Cumulative Damage Model for Advanced Composite Materials: Phase I Final Report, AFWAL-TR-82-4094, July 1982.
2. H.R. Miller, K.L. Reifsnider, W.W. Stinchcomb, and D.A. Ulman, Cumulative Damage Model for Advanced Composite Materials: Phase II Final Report, AFWAL-TR-84-4007, March 1984.
3. A. Highsmith and K.L. Reifsnider, "Stiffness Reduction Mechanisms in Composite Laminates", Proc. ASTM Conf. on Damage in Composite Laminates, STP 775, K. L. Reifsnider, Ed., Bal Harbour, F., Nov. 12-14, 1980, pp. 103-117.
4. Damage in Composite Materials, ASTM STP 775, K.L. Reifsnider, Editor, (American Society for Testing and Materials, 1982).
5. K.L. Reifsnider, E.G. Henneke II and W. W. Stinchcomb, Defect-Property Relationships in Composite Materials, AFML-TR-76-81, Part IV, Air Force Materials Laboratory, June 1979.
6. K.L. Reifsnider, "Some Fundamental Aspects of the Fatigue and Fracture Response of Composite Materials", Proceedings, 14th Annual Meeting of Society of Engineering Science, Lehigh Univ., Bethlehem, PA. p. 373-384, Nov. 14-16, 1977.
7. J.E. Masters and K.L. Reifsnider, "An Investigation of Cumulative Damage Development in Quasi-Isotropic Graphite-Epoxy Laminates", in Damage in Composite Materials, K. L. Reifsnider, Ed., STP 775, American Society for Testing and Materials, 1982, pp. 40-62.
8. K.L. Reifsnider and A.L. Highsmith, "Characteristic Damage States: A New Approach to Representing Fatigue Damage in Composite Materials", in Materials, Experimentation and Design in Fatigue, (Westbury House, Guildford, U.K., 1981) pp 246-260.
9. T.K. O'Brien, "Stiffness Change as a Nondestructive Damage Measurement", in Mechanics of Nondestructive Testing, W.W. Stinchcomb, Ed., (Plenum Press, New York, 1980) pp. 101-121.
10. R.D. Kriz, W.W. Stinchcomb and D.R. Tenney, Effects of Moisture, Residual Thermal Curing Stresses and Mechanical Load on the Damage Development in Quasi-Isotropic Laminates, VPI-E-80-5, College of Engineering, Virginia Polytechnic Institute and State University, Feb. 1980.

#### REFERENCES (CONCLUDED)

11. K.L. Reifsnider, W.W. Stinchcomb and E.G. Henneke II, Defect-Property Relationships in Composite Laminates, AFML-76-81, Part III, Apr. 1979.
12. P.C. Yeurg, W.W. Stinchcomb and K.L. Reifsnider, "Characterization of Constraining Effects on Flaw Growth", Nondestructive Evaluation and Flaw Criticality for Composite Materials, STP 696, P.B. Pipes, Ed., American Society for Testing and Materials, 1979.
13. R.D. Jamison, A.L. Highsmith and K.L. Reifsnider, "Strain Field Response of 0 degree Glass/Epoxy Composites Under Tension", Composites Technology Review, Vol. 3, No. 4 (1981) pp. 158-159.
14. A.L. Highsmith and K.L. Reifsnider, "Non-uniform Microstrain in Composite Laminates", Composites Technology Review, Vol. 4, No. 1 (1982) pp. 20-22.
15. A.L. Highsmith, "Damage Induced Stress Redistribution in Composite Laminates", Dissertation, Doctor of Philosophy, College of Engineering, Virginia Polytechnic Institute and State University, Blacksburg, Virginia 24061, Dec. 1984.
16. T.K. O'Brien, "Characterization of Delamination Onset and Growth in a Composite Laminate", Damage in Composite Materials, ASTM STP-775 (1982), American Society for Testing and Materials.
17. D.J. Wilkins, A Comparison of the Delamination and Environmental Resistance of a Graphite/Epoxy and a Graphite/Bismaleimide, NAV-GD-0037, NASC (1981).
18. T.K. O'Brien, "Tension Fatigue Behavior of Quasi-Isotropic Graphite Epoxy Laminates", Fatigue and Creep of Composite Materials, H. Lilholt and R. Talreja, Eds., Riso National Laboratory, Roskilde, Denmark (1982).

END  
FILMED

4-86

DTIC